EFFECTIVE MODEL PREDICTIVE CURRENT CONTROL SCHEMES FOR PERMANENT MAGNET SYNCHRONOUS MOTOR DRIVE

Submitted in the partial fulfillment of the
requirementsfor the award of the degree of

DOCTOR OF PHILOSOPHY

By
Parvathy M. L.
(Roll No. 719039)

Supervisor:
Dr. T. Vinay Kumar
Assistant Professor

DEPARTMENT OF ELECTRICAL ENGINEERING NATIONAL INSTITUTE OF TECHNOLOGY WARANGAL – 506004, TELANGANA STATE, INDIA
June-2023

APPROVAL SHEET

This Thesis entitled "**Effective Model Predictive Current Control Schemes for Permanent Magnet Synchronous Motor Drive**" by **Parvathy M.L.** is approved for the degree of Doctor of Philosophy.

Examiners

_____

_____

_____

Supervisor
Dr. T. Vinay Kumar
Assistant Professor
EED, NIT Warangal

Chairman
Dr. N. Vishwanathan
Professor,
EED, NIT Warangal

Date: _____

DEPARTMENT OF ELECTRICAL ENGINEERING
NATIONAL INSTITUTE OF TECHNOLOGY
WARANGAL – 506 004

DEPARTMENT OF ELECTRICAL ENGINEERING
NATIONAL INSTITUTE OF TECHNOLOGY WARANGAL

CERTIFICATE

This is to certify that the thesis entitled **"Effective Model Predictive Current Control Schemes for Permanent Magnet Synchronous Motor Drive"**, which is being submitted by **Mrs. Parvathy M.L.** (Roll No. 719039), is a bonafide work submitted to the National Institute of Technology, Warangal in the partial fulfillment of the requirement for the award of the degree of **Doctor of Philosophy** in the Department of Electrical Engineering. To the best of my knowledge, the work incorporated in this thesis has not been submitted elsewhere for the award of any degree.

Dr. T. Vinay Kumar(Supervisor)
Assistant Professor
Department of Electrical Engineering
National Institute of Technology Warangal
Warangal – 506004

Place:

Date:

DECLARATION

This is to certify that the work presented in the thesis entitled "**Effective Model Predictive Current Control Schemes for Permanent Magnet Synchronous Motor Drive"** is a bonafide work done by me under the supervision of **Dr. T. Vinay Kumar**, Department of Electrical Engineering, National Institute of Technology, Warangal, India and was not submitted elsewhere for the award of any degree.

I declare that this written submission represents my ideas in my own words and where others' ideas or words have been included; I have adequately cited and referenced the original sources. I also declare that I have adhered to all principles of academic honesty and integrity and have not misrepresented or fabricated or falsified any idea/data/fact/source inmy submission. I understand that any violation of the above will be a cause for disciplinary action by the institute and can also evoke penal action from the sources which have thus not been properly cited or from whom proper permission has not been taken when needed.

Parvathy M.L.

(Roll. No:719039)

Date:

Place: Warangal

ACKNOWLEDGEMENTS

Words cannot express the immense gratitude that I feel towards my supervisor *Dr. T. Vinay Kumar***,** Assistant Professor, Department of Electrical Engineering, National Institute of Technology, Warangal**.** It has been a great experience learning from him and his constant support and guidance have always motivated me to do productive work. I appreciate his kindness in patiently listening to my problems and I am deeply indebted for all the efforts he took to support me during the most difficult days of my Ph.D. He taught me to be determined, dedicated, and patient towards work and this is something I would persevere in my future endeavors.

I am thankful for the support and cooperation offered by *Prof. B. L. Narasimharaj*u, Head of the Department of Electrical Engineering.

I am very grateful to my Doctoral Scrutiny Committee chairman *Prof. N. Vishwanathan* and other Doctoral Scrutiny Committee members, *Dr. Chintham Venkaiah*, Professor, Department of Electrical Engineering, *Dr. G. Siva Kumar*, Associate Professor, Department of Electrical Engineering and *Dr. U.S.N. Raju***,** Associate Professor, Department of Computer Science and Engineering for their constructive suggestions and advice for the progress of my research work.

I am grateful to *Prof. M. Sailaja Kumari* and *Prof. S. Srinivasa Rao,* Professors and former Head of the Department of Electrical Engineering, for their constant motivation, support, and cooperation during the course of my work. I also appreciate the technical aid offered by other teaching and non-teaching members of the Department of Electrical Engineering, NIT Warangal.

I would like to express my deepest gratitude to our team including *Dr. Kusuma Eshwar*, *Dr. Sagar Petkar*, *Mr. Puli Rajanikanth,* and *Dr. K.M. Ravi Eswar* for all the useful insights and assistance offered during the course of work. I am sincerely thankful to my friends *Miss. Bella K*, *Mr. Ashok Kumar Kanithi*, *Mr. M.F. Baba,* and *Dr. Chinmay Kumar Das* for supporting me throughout this journey. I am also thankful to *Dr. Patnana Hema Kumar, Mr. Chinna Karasala, Mr. Bhavin Salvi, Mr. Koyyana Srinivasa Rao, Mr. Dinesh Kumar, Miss Pitcha Sai Nandini, Miss Anusha Dharavath, Miss Swecha Tadepalli, Dr. Seenu P.Z.,* and *Dr. Nikhil Thoppil* for their

constant support.

I would not have undertaken this journey without the encouragement and support provided by my father *Mr. A. M. Mohanan Nair*, mother *Mrs. S. Leela*, and brother *Mr. Arun M.L.* I am eternally grateful for their endless motivation and acknowledge all the efforts they have put in to support me throughout this journey. I am also thankful to my in-laws, *Mr. A. P. Narayanan* and *Mrs. Rajamoni K* for their unceasing support and prayers. They have always encouraged me to do better in life and chase my dreams. I also thank my sister-in-law *Mrs. Jini Rengith* and brother-in-law *Mr. Rengith Menon* for their motivation and support during the course of my research. I wholeheartedly thank my friends, *Miss. Sairah Jacob*, *Miss. Kavitha P*, *Miss. Sharon D.K.* and *Miss. Sunayna Anwa*r for supporting me throughout the tough days of this journey.

Last, but not least, this journey would not have been accomplished without my partner, *Dr. Jinoop A. N.*, who whole-heartedly stood by my side, bearing my absence during this period. I appreciate all the efforts he took to support me to pursue my Ph.D. and thank him for guiding me through all the challenges. From being my biggest cheerleader to my critic, I am forever grateful to my husband for his relentless support during the best and worst days of my professional and personal life. Furthermore, I am grateful to the almighty for guiding me to seek paths that could evoke my knowledge and compassion.

Parvathy M L

ABSTRACT

KEYWORDS: Model Predictive Current Control, Duty modulation, Computational burden, dual voltage vectors, multiple voltage vectors, steady-state performance, Permanent magnet motors.

Out of the total electrical energy generated worldwide, 46% is consumed by electrical machines leading to the emission of 6040 megatons of carbon dioxide gas. Therefore, it is essential to use motors with higher efficiency for the conservation of energy, protection of the environment, and sustainable development. Permanent Magnet Synchronous Motor (PMSM) is favorable for industrial and transportation applications due to its compact size, higher torque to weight ratio, efficiency, and reliability.

In recent years, with the progression in digital signal processing technology, an effective and advanced control strategy like Model Predictive Control (MPC) which is computationally exhaustive has received wider attention. It offers the feasibility to use multiple constraints, multiple objectives, and multiple variables while maintaining its simplicity and intuitiveness. The most prominent MPC schemes are Model Predictive Torque Control (MPTC) and Model Predictive Current Control (MPCC). The MPTC scheme has the objective function defined using the torque and flux variables. However, in MPCC, the cost function is defined using stator currents as control variables. This eliminates the problem of tedious tuning of the weighting factor.

The MPCC scheme offers excellent dynamic performance through the indirect control of torque and flux variables using the stator currents. However, the main challenges observed in the MPCC scheme are larger ripples in torque and flux ripples under steady-state conditions. To overcome this, the application of two or more voltage vectors is widely researched. However, the main challenge for the real-time application of multiple voltage vector-based control schemes is the increased computational burden. Thus, the wider application of the MPC scheme is still under the radar due to its higher computational complexity. This thesis proposes control strategies to improve the steady-state performance of the MPCC-controlled PMSM drive and addresses the limitation of increased computational complexity.

To improve the steady-state torque and flux performance of the MPCC-controlled PMSM drive, a dual voltage vector concept is implemented. The cause of increased ripples in torque and flux is identified to be the application of a single voltage vector for the entire control period irrespective of the magnitude of the error between control variables. Thus, to control the magnitude of the optimum voltage vector, a null vector is added to it. The duration for which the optimum vector is applied is determined based on the deadbeat principle. The duty ratio calculation used is simple and less sensitive to parameter variations. The application of dual voltage vectors undeniably improves the performance of the drive at the expense of increased computational time. Thus, a low complex dual voltage vector application scheme is evaluated in this research, which reduces the number of voltage vectors used for prediction, cost function evaluation, and optimization to three. The voltage vector preselection does not require additional determination of sector or reference vectors. This reduces the computational time and with the application of an active and null voltage vector, the steady-state drive performance is improved. The duration of application of the active vector is determined using the rms ripple minimization technique.

In certain operating conditions where the error magnitude is large, it is required to apply more than two voltage vectors in a control period. Thus, multiple voltage vector application strategies are investigated using the virtual voltage vector concept. However, with the augmentation of the control set using the virtual voltage vectors, there would be a catalyzed increase in the computational burden. To limit the increase in the computational complexity, a voltage vector preselection scheme is employed which effectively locates the optimum voltage vector that minimizes the error. The duration of application of voltage vectors is determined using the average error minimization technique.

The application of two or more voltage vectors in a sample time can provide a better steady-state response with an increase in computational complexity. To address this, a simplified voltage vector selection-based MPCC is proposed which directly evaluates the optimum voltage vector without prediction, cost function evaluation, and optimization. The multiple voltage vector application is then achieved by determining the position of the first optimum voltage vector using a modified position determination approach. The proposed MPCC improves the

steady-state performance with reduced computational complexity. The duration of active voltage vectors is directly evaluated using the cost function ratios. This reduces the parameter sensitivity of the calculation.

The proposed MPCC schemes are developed using MATLAB/Simulink. The real-time implementation of the control schemes is achieved using the dSPACE-1104 control platform. The effectiveness of the control techniques is evaluated using comprehensive comparisons with the existing scheme.

Table of Contents

List of Figures

List of Tables

Abbreviations

AC	Alternating Current
ADC	Analog to Digital Converter
BLDC	Brushless DC
CCS-MPC	Continuous Control Set Model Predictive Control
CS	Control Set
C-MPCC	Conventional Model Predictive Current Control
DSP	Digital Signal Processor
DSO	Digital Storage Oscilloscope
DC	Direct Current
DTC	Direct Torque control
ECS	Extended Control Set
FOC	Field Oriented Control
FPGA	Field Programmable Gate Array
FCS-MPC	Finite Control Set Model Predictive Control
IPMSM	Interior Permanent Magnet Synchronous Motor
MPC	Model Predictive Control
MPCC	Model Predictive Current Control
MPTC	Model Predictive Torque Control
PMSM	Permanent Magnet Synchronous Motor

PI	Proportional and Integral
PWM	Pulse Width Modulation
SVPWM	Space Vector Pulse Width Modulation
SMPMSM	Surface mounted Permanent Magnet Synchronous Motor
SRM	Switched Reluctance Motor
THD	Total Harmonic Distortion
VG	Vector Group
VSI	Voltage Source Inverter
VV	Voltage Vector
V/f	Voltage/frequency

List of Symbols

T_e	Electromagnetic torque (Nm)
B	Frictional co-efficient
p	Number of pole pairs
ψ_f	Flux produced by permanent magnets (Wb)
R_s	Stator resistance (Ω)
L_s	Stator inductance (H)
T_s	Sampling time (s)
$i_{\alpha s}$	α-axis stator current (A)
$i_{\beta s}$	β-axis stator current (A)
i_{ds}	direct-axis stator current (A)
i_{qs}	quadrature-axis stator current (A)
u_s	Stator voltage vector (V)
i_s	Stator current vector (A)
θ_r	Rotor position (rad)
J	Moment of inertia (kg-m^2)
T_l	Load torque (Nm)
e	Back emf in the PMSM (V)
ω_r	Rotor speed (electrical rad/s)
ω_{ref}	Reference speed (electrical rad/s)
G	Cost function (A)
C	Proposed current constant (A)
k	Proposed current constant (A)
i_s^*	Reference current vector (A)
Δi_s	Stator current error (A)

$\Delta \Psi_s$	Stator flux error (Wb)
Δi_{s_grad}	Gradient of stator current error (A/s)
U_s^*	Reference voltage vector (V)
V_{opt}	Optimal voltage vector (V)
V_{prin}	Principal voltage vector (V)
V_α	α-axis stator voltage (V)
V_β	β-axis stator voltage (V)
ψ_s	Stator flux (Wb)

Chapter 1

Introduction

1. Introduction

1.1 Background

Out of the total electrical energy generated worldwide, 46% is consumed by electrical machines leading to the emission of 6040 megatons of carbon dioxide gas [1]. At least half of the electrical energy generated globally is converted into mechanical energy for agricultural, transportation, domestic, and industrial applications. In industries, electric motors act as the major load and utilize around 70% of the generated electricity. The groundbreaking invention of alternating current (AC) motors by Nikola Tesla in 1888 paved the way for the commercialized application of a three-phase Induction motor. It has the advantages of low cost and rugged construction to withstand harsh environments [2]. The progression in semiconductor technology has aided in the regulation of power as well as better electrical energy utilization, which plays a pivotal role in energy savings. The proper control of the speed or torque of the drive and the utilization of regenerated energy aids in reducing the overall power requirement of the drive [3].

Since the 19th century, electric drives have been used in domestic, industrial, and transportation applications [4]. With the availability of fast-switching power electronic devices, it is convenient to satisfy the load characteristics (regarding the speed and torque demands) by controlling the voltage and frequency of the electric motor. Thus, with the variable speed drive application, it is possible to discard ineffective throttle devices and mechanical gears to improve transmission efficiency. Moreover, the effective machine design plays an important role in reducing the weight per unit power of the motor as well as getting higher efficiency [5] For several decades, direct current (DC) motors dominated the electric drive sector [6] and were later replaced by the AC motors like Induction motors, Synchronous motors, Permanent Magnet motors, and so on with the advent of power electronic converter technology [7]. The DC motors offer excellent dynamic performance and the feasibility of decoupled control of the stator flux and torque using field current and armature current, respectively. However, the higher cost and maintenance requirement due to commutator segments and brushes make it obsolete. On the other hand, AC motors have lower costs and are devoid of commutators and brushes, i.e., more maintainable. They can sustain heavy loads and possess a robust structure so

that it can be used in corrosive and harsh working environments. With the advancement in digital signal processing and semiconductor technology, AC motor drives are more economic and suitable for even multi-motor applications [8].

Induction motors are the work horses of industries and have a simple and rugged construction. However, they succumb to larger torque ripples, moderate efficiencies, higher starting currents, and vibrations. This confines the pertinence of Induction motors for several drive applications. The limitation of lower power factor and slip power can be addressed using the Synchronous motors. However, it requires an external exciter for supplying DC power to the field winding. Switched Reluctance Motors (SRM) have features like simple and rugged construction, lower maintenance, and the absence of rotor magnets. However, the steady-state performance exhibits large torque pulsations, and this results in increased vibrations and acoustic noises. Further, their suitability to penetrate the electric vehicle industry is narrow due to lower power factor and low dynamic performance.

Permanent magnet motors like brushless DC (BLDC) motors and permanent magnet synchronous motors (PMSM) are popular due to higher efficiency, wide speed range operation capability, higher torque to weight ratios, and compact size. BLDC motors have higher power density than PMSM but exhibit pulsating torque under loaded conditions. PMSM has a distributed winding and the rotor has permanent magnets embedded or mounted on it. Both BLDC motor as well as PMSM offers excellent dynamic performance and are highly efficient. With the availability of permanent magnets with higher field strength, PMSM is one of the fastest-growing motors in adjustable speed drives [9].

The main features of PMSM that have increased its popularity in drive applications are listed below.

- Compact and simple structure
- High torque/inertia ratio
- Low maintenance cost
- Higher reliability
- High power factor
- High power density
- Ease of control

PMSMs find wider applications in position control applications, robotics, machine

tools, pumping applications, ship propulsion, electric vehicles, and domestic appliances like washing machines, and vacuum cleaners as given in Figure 1.1.

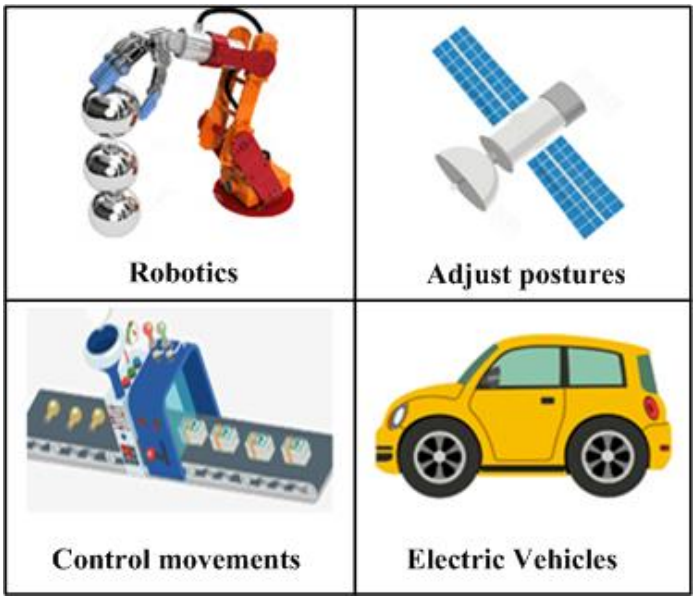

Figure 1.1 Applications of PMSM.[10]

Based on the magnet mounting on the rotor [11], the PMSM can be classified as:

i. Surface Mounted PMSM (SMPMSM)
ii. Interior PMSM (IPMSM)

The magnets are mounted on the peripheral of the rotor in SMPMSM while in the IPMSM, the magnets are embedded within the rotor. Figure 1.2 shows the cross-sectional view of the two types of PMSM.

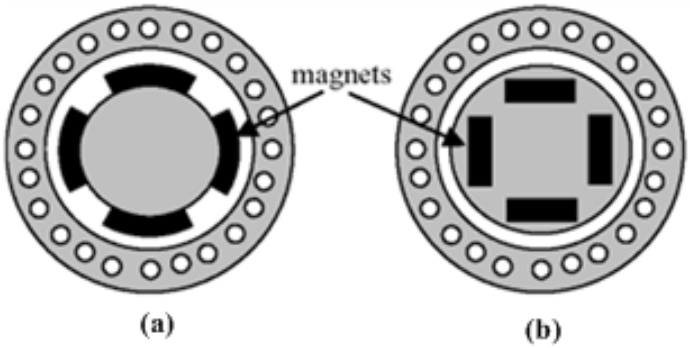

Figure 1.2 Types of PMSM (a) SMPMSM and (b) IPMSM.[12]

IPMSM exhibits saliency and can operate in a wider speed range. This implies that the direct and quadrature axis inductances of IPMSM are unequal and both reluctance, as well as magnetic torque, are generated. In SMPMSM, as the magnets are surface mounted, the air gap is uniform and thus, both direct and quadrature axis

inductances are equal. Moreover, the manufacturing cost of the SMPMSM is less than the IPMSM. The commonly used permanent rare-earth permanent magnets are alnico-5, samarium-cobalt, neodymium boron iron, and ferrites.

1.2 Speed control strategies for PMSM drive

The prominent speed control strategies for the PMSMs can be broadly classified into four major types [8], [9], [11], [13] (a) Scalar control, (b) Field oriented control (FOC), (c) Direct torque control (DTC), and (d) Model predictive control (MPC).

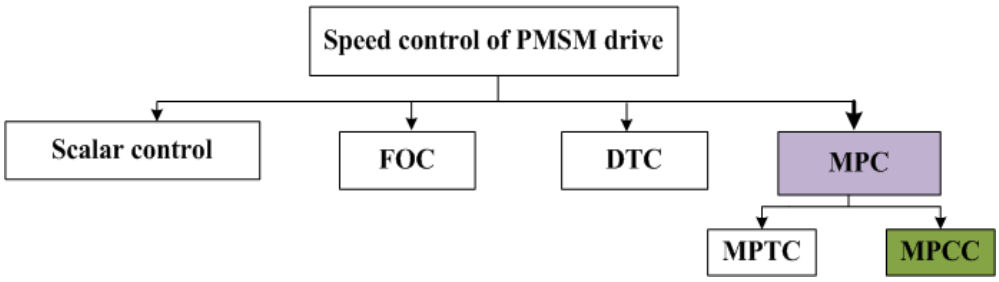

Figure 1.3 Speed control strategies for PMSM drive

1.2.1 Scalar control of PMSM drive

The scalar control scheme is also known as the v/f (voltage/frequency) control. Figure 1.4 shows the control diagram of the scalar v/f control.

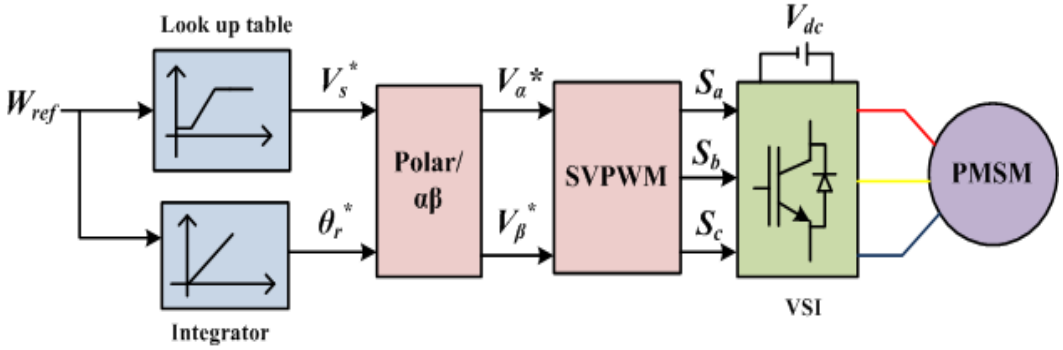

Figure 1.4 Scalar V/f control of PMSM

The v/f control aims to control the magnitude of the control variables, i.e., the supply voltage and frequency to maintain the stator flux constant. However, this scheme neglects the coupling effect in the motor. The flux can be controlled using the voltage magnitude and the speed as well as the torque can be controlled using the frequency. However, the torque and flux also depend on voltage magnitude and frequency, respectively. Thus, this method gives a poor performance even though it

is easy to implement.

The magnitude of the stator flux is retained as a constant in the v/f control. For the implementation of this control, the reference voltage vector (V_s^*) magnitude and its phase (θ_r^*) are determined from the reference speed. The switching pulses to be fed to the voltage source inverter (VSI) is obtained using the space vector pulse width modulation (SVPWM) technique. The limitations of the scalar control are listed below [14]–[17].

i. If there is a drift in the flux, the sensitivity of the torque with slip will tend to vary, which leads to improper control. Similarly, if there is a variation in the line voltage or incorrect v/f ratio, the flux may tend to become weak or saturated. Thus, for abrupt changes in speed and load, it is required to implement stabilizing loops.
ii. Sluggish transient performances as the large voltage is required to meet the higher torque demands.
iii. Slow dynamic response and not suitable for applications that demand precise control.

The scalar control concept is essentially developed from the steady-state model of AC machines. Thus, it offers a poor dynamic response. For instance, if the torque is increased by increasing the slip (i.e., the frequency), the flux will tend to decrease. In general, the flux variation is sluggish and to compensate for the drop in flux, the supply voltage is to be increased. However, the flux control loop is slow and takes some time to bring in the required changes in flux magnitude. The temporary dip in flux during sudden changes in torque or speed elongates the response time. This motivates to apply the vector control schemes for the precise speed control of the AC motors [18].

1.2.2 Field-oriented control of PMSM drive

The vector control schemes revitalized the high-performance ac drive sector and are also known as the decoupled or orthogonal control. The vector control schemes are developed to establish the fact that the AC motors can be controlled like the separately excited DC motors which offer a decoupled control of torque and flux using armature current control and field current control, respectively. The most popular and widely used vector control scheme is the Field-oriented control (FOC), which addresses the limitation of the scalar control scheme [19]. There are two

categories of FOC according to the orientation of the flux vector chosen for control, i.e., stator field-oriented as well as the rotor field-oriented control. As the stator field-oriented control requires the additional determination of compensating currents for decoupling, the rotor field-oriented control schemes are prominently used for PMSM drives. The rotor field-oriented control of the PMSM drive is shown in Figure 1.4. It can be noted that the stator and rotor control variables are interdependent. Thus, the control of stator control variables in PMSM requires the control of rotor variables. To overcome this coupling effect, the three-phase currents of the PMSM are transformed into the rotor frame of reference. Hence, the implementation of FOC requires accurate sensing of the rotor position. In order to replicate the control offered by the separately excited DC motor, the FOC scheme uses the transformed direct and quadrature-axis currents for stator flux and torque control, respectively. The stator current component along the direct axis is accountable for the flux generation. However, in PMSM, the permanent magnet flux along with the flux produced by the direct-axis current contributes to the total direct-axis flux [20]. In order to regulate the direct-axis and quadrature axis current errors, current proportional-integral (PI) controllers are required in FOC. The block diagram of the FOC scheme for the PMSM drive is shown in Figure 1.5.

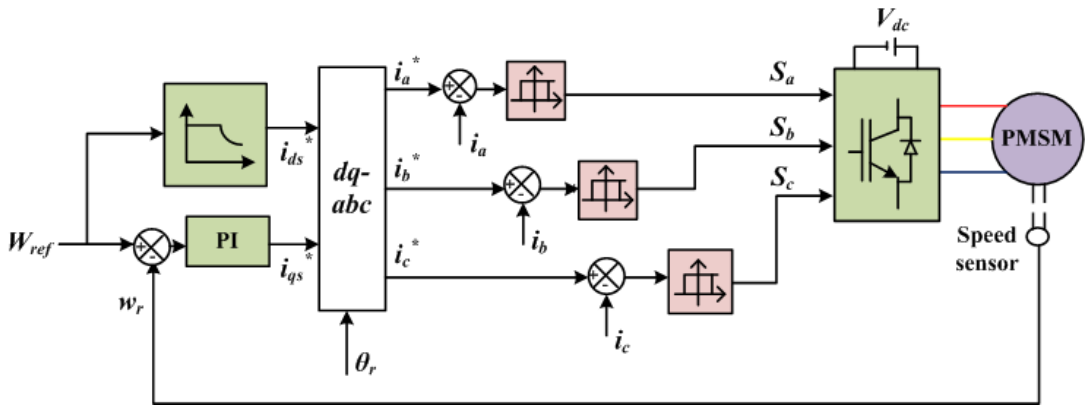

Figure 1.5 Rotor field-oriented control of PMSM drive.

The electromagnetic torque (T_e) generated by the PMSM in the rotor reference frame is given in (1.1).

$$T_e = \frac{3}{2} p \psi_f i_{qs} \tag{1.1}$$

where, p is the number of pole pairs, ψ_f is the permanent magnet flux and i_{qs} is the quadrature-axis current. In the FOC of PMSM drive, the stator field producing torque, i_{ds} is maintained constant and i_{qs} is changed for the torque variation. The

FOC scheme offers excellent steady-state torque and flux performance [21]. However, the following are the disadvantages of the scheme.

i. The torque and flux control are achieved using an indirect control of the currents. This offers a slower transient response.
ii. FOC requires the accurate determination of the rotor position which would otherwise degrade the steady-state and dynamic responses.
iii. The stator current transformations to the rotor reference frame make the control scheme more complex.
iv. The tuning of the PI controller is tedious and enlarges the control complexity.
v. The switching frequency, as well as losses, are comparatively higher in FOC due to the requirement of a dedicated Pulse Width Modulator (PWM) for the control implementation.

1.2.3 Direct Torque Control of PMSM drive

One of the most popular speed control schemes of recent times, Direct Torque Control (DTC), is a high-performance control technique for instantaneous torque and flux control [22]. The DTC concept was initially introduced for the Induction motors and further extended for the PMSM control [23]. As the name suggests, the direct control of torque and flux can be achieved in every sample time, based on the principle of error minimization. The voltage vector suitable for the control is chosen from a predefined look-up table and fed to the two-level VSI. Figure 1.6 shows the block diagram of the DTC of the PMSM drive.

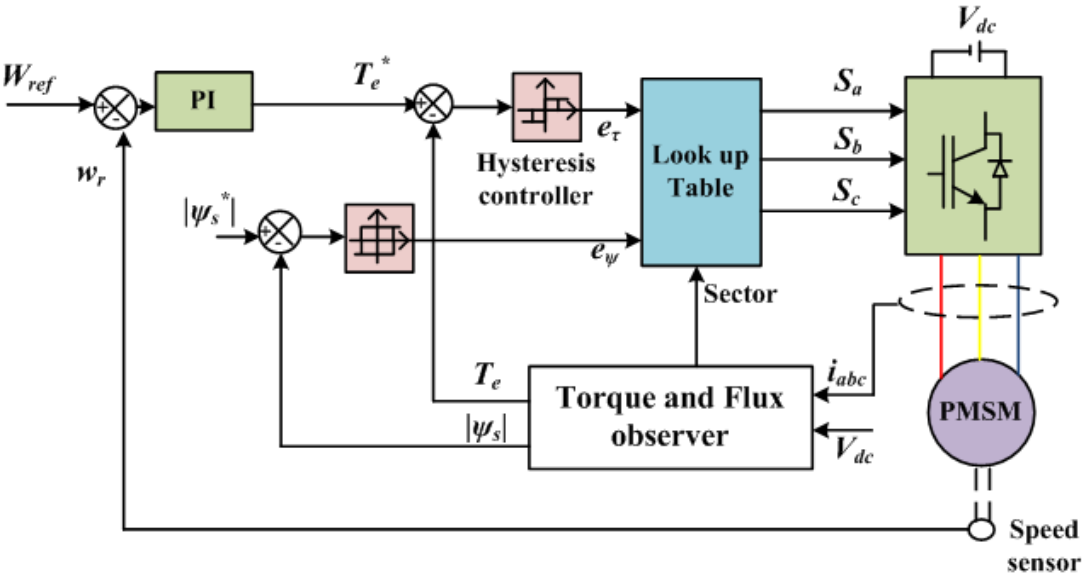

Figure 1.6 Block diagram of DTC of PMSM drive.

The electromagnetic torque in the stationary reference frame can be obtained as in (1.2).

$$T_e = \frac{3}{2} p\,(imag(\overline{\psi_s} \times i_s)) \tag{1.2}$$

where, ψ_s is the stator flux and i_s is the stator current. From (1.2), the change in the torque and flux can be obtained as shown below.

$$\Delta\psi_s = U_s T_s \tag{1.3}$$

$$T_e = \frac{3p}{2L_s}(|\psi_r||\psi_s| + \Delta\psi_s \sin\Delta\delta) \tag{1.4}$$

where, δ is the angle between the stator and rotor flux, also known as the load angle, L_s is the stator inductance, ψ_r is the rotor flux. It can be observed from (1.3) that the change in flux in a sample time can be achieved by varying the voltage vector applied to the three-phase VSI. Similarly, from (1.4) it can be noted that a change in torque can be brought about by a change in the load angle. To obtain the speed control, the stator flux reference and torque reference are compared with the estimated values of flux and torque, respectively. The hysteresis controllers process the errors and based on the intensity of errors as well as the sector location of flux, the voltage vectors are selected from a predefined look-up table.

The advantages of DTC are listed below [24]

i. Simple to implement and offers a fast dynamic response owing to the predetermined voltage selection scheme based on the torque and flux errors.

ii. DTC scheme does not require the precise determination of rotor position and complex transformations.

iii. The control scheme does not require current PI controllers, decoupling circuits, and modulators.

iv. There is no feedback control of currents, which makes the transient performance faster.

However, the limitations of DTC are:

i. Large undulations in torque, flux, and stator current.

ii. Hysteresis comparators cause the switching frequency to be variable.

iii. The effect of resistance variation is very dominant at low operating speed conditions.

1.2.4 Model predictive control of PMSM drive

In recent years, an effective and advanced control strategy, Model Predictive Control (MPC), has been introduced to negate the shortcomings offered by the FOC and DTC schemes for PMSM drives. With the progression in digital signal processing technology, computationally exhaustive MPC techniques have received wider attention [25]. In the late 1970s, the MPC scheme was introduced in the petrochemical industry for process control. MPC scheme explicitly predicts the future behaviour of the control variables using the system model and generates the optimal output that satisfies the objective [26]. This offers the feasibility of using multiple constraints, multiple objectives, and multiple variables while maintaining its simplicity and intuitiveness. The relevant features of MPC schemes are shown in Figure 1.7 [27].

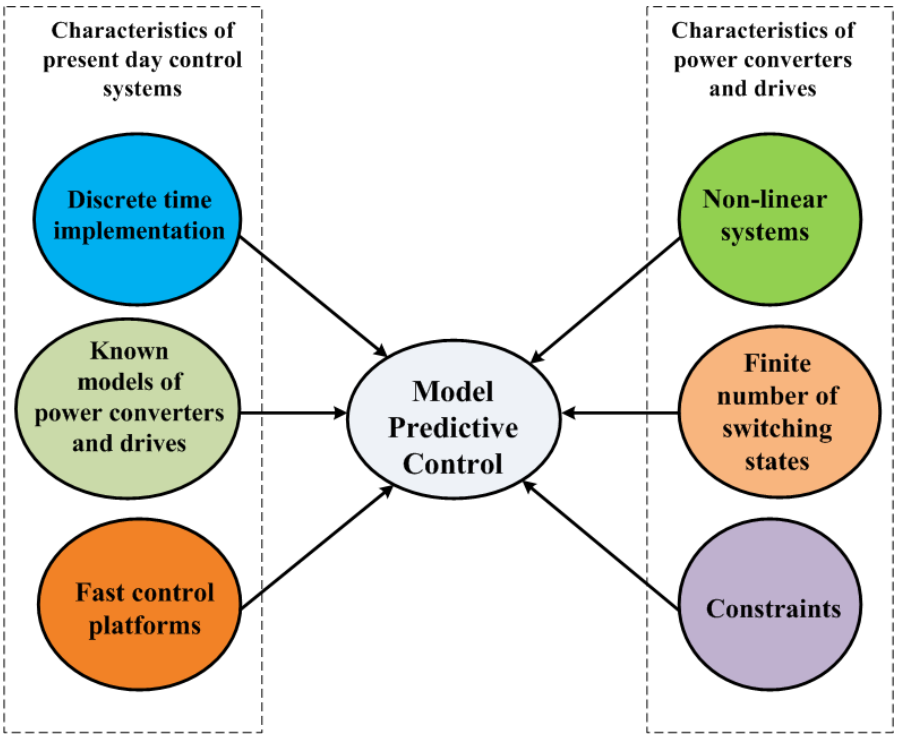

Figure 1.7 Features of Model predictive control.

The following are the steps involved in the implementation of the MPC scheme for electric drive applications.

i. Estimation of the control variables that are physically unmeasurable in drives.
ii. Predict the future behavior or state of the control variable using the system model.
iii. Optimize the output using an effective online optimization method. For drive

speed control, the optimum voltage vector or the corresponding switching state of VSI is chosen as the output variable.

The two prominent categories of the MPC scheme are Continuous Control Set-MPC (CCS-MPC) and Finite Control Set-MPC (FCS-MPC). The CCS-MPC scheme requires a modulator for the generation of switching states and thus, generates a fixed inverter switching frequency. On the other hand, the FCS-MPC scheme has a control set with a finite number of voltage vectors or switching states and the implementation is simple without any modulator requirement. However, this results in a variable switching frequency [28]. Model Predictive Torque Control (MPTC) and Model Predictive Current Control (MPCC) are the most widely employed FCS-MPC techniques, classified based on their control objectives. In the MPTC technique, accurate estimators and observers are used to obtain the actual torque and flux. The voltage vector that decreases the torque and flux fluctuations is chosen as the optimal state for the two-level inverter. The priority of the specific variable in a multi-objective cost function is included in terms of the weighting factor [29]. Thus, to obtain the actuating vector, a cost function carrying the constraints, variables, specific targets, and the associated weighting factors, is optimized. In every control interval, the prediction and actuation take a considerable amount of time, leading to the limitation of sample frequency and thereby, degradation in the flux and torque response. Another issue involved in this method is the tuning of the weighting factor. In MPCC, the current vector is considered the control variable in the cost function. This avoids the estimation of the stator flux and torque. Moreover, the weighting factor determination in MPTC can be evaded in the MPCC scheme. The control is also easy to implement and more feasible. Figure 1.8 shows the block diagram of the model predictive control scheme for the PMSM drive.

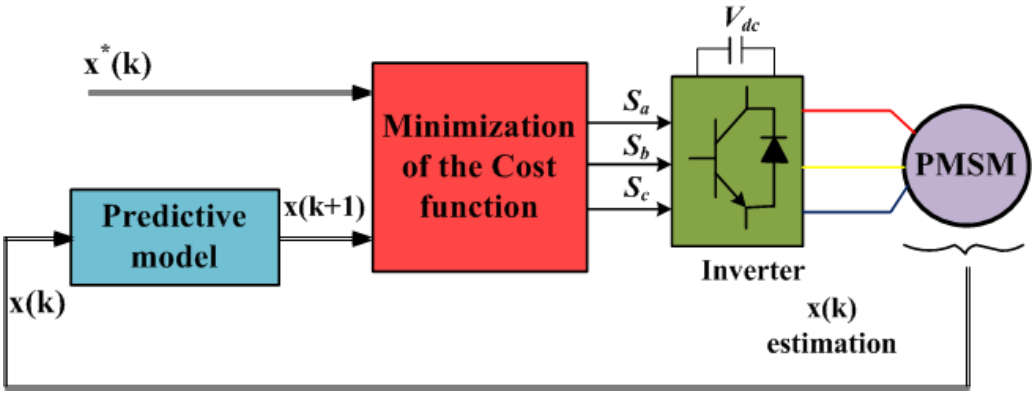

Figure 1.8 Model predictive control of PMSM drive.

Table 1.1 Comparison of different speed control techniques for PMSM drives

Parameter	FOC	DTC	MPTC	MPCC
No. of PI controllers	3	1	1	1
Flux angle requirement	Yes	Yes	No	No
System constraints inclusion	Difficult	Difficult	Easy	Easy
Conceptual Complexity	High	Medium	Less	Less
Steady-state ripples	Low	High	Medium	Medium
Stator current Harmonics	Low	High	Medium	Medium
Dynamics	Slow	Fast	Fast	Fast
Current THD	Better	Worse	Good	Good

Table 1.1 summarizes the characteristic features of the above-discussed speed control schemes [30]. FOC requires three current PI controllers for the speed control of the PMSM drive. It is difficult to include the system constraints in FOC and DTC. The provision to add multiple constraints and multiple objectives in the cost function makes the MPC scheme superior to other control strategies. The conceptual complexity is high in the FOC scheme compared to DTC and MPC schemes. It requires the rotor reference frame transformations and controls the torque and flux using the indirect approach using current control. Moreover, it requires an accurate rotor position. Similarly, the DTC scheme requires the flux angle for sector determination. FOC scheme offers the best steady-state performance out of all the schemes. However, MPC offers better steady-state performance than the DTC scheme due to the application of optimum voltage vector in every sample time. However, the ripples in torque and flux are still high due to the application of a single voltage vector in a sample time.

1.3 Motivation

MPCC scheme offers excellent dynamic performance but the steady-state torque and flux responses are affected by large ripples. The increase in torque ripples leads to an increase in vibrations and acoustic noises. Moreover, it enforces stress on the shaft as well as the bearings, leading to the eventual damage of the shaft and thereby, affecting the lifetime of the machine. The torque fluctuations will also contribute to slight oscillations in the speed. The stator current also exhibits higher total harmonic distortions. The state of art identifies the cause of enlarged ripples in

torque and flux to be the application of a single optimum voltage vector for the entire control duration without considering the error magnitude. For instance, if the error magnitude is quantitatively less, it is not required to apply the control voltage vector for the entire sample time. This may lead to overregulation and deteriorate the steady-state responses. Thus, in the state of the art, the application of two or three voltage vectors in each control period is identified as the solution to reduce the fluctuations in torque and flux. The potential method is to ensure the application of a null voltage vector along with the optimum voltage vector or using two optimum active voltage vectors or two active and a null voltage vector. This would eventually improve the stator current harmonic performance. It could also be observed from the existing MPCC schemes that the application of two or more voltage vectors augments the control complexity of the algorithm. MPC scheme in itself is computationally exhaustive owing to the large number of calculations involved in the prediction of current, cost function evaluation, and optimization. Moreover, the control algorithm gets updated during each sample time. Thus, with the addition of duty-calculation schemes for applying multiple voltage vectors, the computational complexity is further enlarged.

The voltage vector preselection schemes are employed to reduce the computational burden. However, the available schemes are either complex or involve additional parameter determination, which would not yield a substantial reduction in the computational time. Another cause identified for the increase in the torque and flux ripples is the selection of the sampling time. There is a minimum limit imposed while selecting the sample time based on the execution time of the control algorithm. The sampling time has a direct effect on the steady-state response. This can also be reduced when the computational time of the processor is less. The existing duty-ratio calculation schemes in the literature also motivate the research works in this thesis. Most of the duty ratio determination schemes are complex and the duty calculations involve the machine parameters. This would increase the parameter dependency of the control algorithm.

1.4 Thesis Aim and Objectives

The thesis aims to incorporate simple and effective MPCC-based speed control strategies for the PMSM drive to improve steady-state performance. The objectives of this thesis are enlisted as follows.

i. The collective benefits of FOC and DTC schemes can be obtained with the help of the MPCC scheme. However, the steady-state ripples generated in the conventional MPCC scheme are high. Thus, the objective is to improve the steady-state performance of the conventional MPCC-based PMSM drive using the dual voltage vector concept. An active and a null voltage vector can be applied during every sample time to improve the drive performance. The duty-ratio calculation should involve fewer machine parameters and thus, less sensitivity to variations in machine parameters.
ii. The dual voltage vector-based MPCC scheme improves the drive response at the expense of an increased computational burden. Moreover, an elevated computational time limits the sampling time of the algorithm. The combination of a reduced voltage vector-based MPCC scheme along with the application of a null and active voltage vector can bring about significant improvement in computational burden and drive performance.
iii. The multiple voltage vector-based MPCC scheme offers a significant reduction in the torque and flux ripples compared to dual voltage vector-based MPCC. The multiple vector application can be achieved using virtual vectors generated by extending the control set. However, this causes a catalyzed increase in the computational burden.
iv. Implementation of less parameter sensitive dual or multi-vector based computationally efficient MPCC scheme for the PMSM drive. The duty ratio calculation used for the application of multiple voltage vectors can be made less sensitive to machine parameter variations. Moreover, the dynamic performance offered by the conventional MPCC scheme must be retained while improving the steady-state performance and reducing the computational time.

1.5 Thesis Contribution

The contributions of this thesis are enlisted below.

i. A dual voltage vector-based MPCC is proposed to improve the steady-state performance of a two-level Voltage Source Inverter (VSI) based PMSM drive. To achieve this, two voltage vectors (one active and one null) are applied in every control interval. The proposed method retains the simplicity of the C-MPCC method while addressing the demerits of large torque and flux ripples caused due to single voltage vector application. In the proposed method, the calculations

involving current slopes are eliminated and the steady-state performance is improved due to the dual voltage vector application while maintaining the computational burden within its limit. Moreover, the dynamic performance is unaltered.

Publication:

Parvathy M.L., Kusuma Eshwar and T. Vinay Kumar, "A Modified Duty-Modulated Predictive Current Control for Permanent Magnet Synchronous Motor drive," ***IET Electric Power Applications***, vol.15, pp. 25-38, 2021.

ii. A low complex dual voltage vector-based MPCC scheme is proposed to address the limitation of increased computational time due to the duty ratio implementation. To achieve this, a voltage vector preselection scheme is proposed which chooses three voltage vectors in every sample time, thus considerably reducing the number of operations involved and the computational time. Moreover, an effective duty modulation based on the rms-current ripple minimization technique is proposed to attain a better steady-state response of the drive. The duty calculation neither requires any complex calculations nor alters the dynamic drive performance.

Publication:

Parvathy M.L. and T. Vinay Kumar, "An Effective Modulated Predictive Current Control of PMSM drive with Low Complexity,", ***IEEE Journal of Emerging and Selected Topics in Power Electronics***, vol. 10, no. 4, pp. 4565-4575, Aug. 2022.

iii. A multivector-based MPCC scheme is proposed to enhance the control precision and improve the steady-state response of the drive. The multi-vector operation is obtained using an effective virtual voltage vector synthesis, which yields an improvement in the control precision. The increase in the computational time is addressed with the help of a predefined look-up table-based voltage vector selection scheme. Further, the average error minimization technique is used to obtain the duration of application of the optimum extended control set-based voltage vector. The proposed method offers the feasibility to apply two or three voltage vectors in a sample time and the dynamic response of the drive is retained with the duty ratio calculation being less sensitive against parameter variations.

Publication:

Parvathy M.L. and T. Vinay Kumar, "A Multivector-based Model Predictive Current

Control of PMSM Drive with Enhanced Torque and Flux Response", ***IEEE Journal of Emerging and Selected Topics in Power Electronics***, vol. 10, no. 6, pp. 7527-7538, Dec. 2022.

iv. A low-complex multivector-based MPCC scheme is proposed for the PMSM drive. The voltage vector preselection scheme considers the magnitude of the error in the stator current and avoids the parameter-sensitive reference voltage vector determination. The novel voltage vector preselection scheme utilized in this work decreases the number of candidate voltage vectors used for computation from 8 to 1. Further, the torque performance of the drive is improved under steady-state conditions using a simple cost-function ratio-based duty modulation scheme. Further, the proposed scheme maintains the dynamic performance of the drive as offered by the C-MPCC scheme with improved steady-state performance and lower computational complexity.

Publication:

Parvathy M.L. and T. Vinay Kumar, "A Simplified Voltage Vector Preselection based Multivector Predictive Current Control for Improved Torque Performance of PMSM Drive," ***IEEE Transactions on Power Electronics***, vol. 38, no. 7, pp. 8775-8785, July 2023, doi: 10.1109/TPEL.2023.3267107.

1.6 Organization of thesis

The organization of this research work on the duty-based MPCC scheme for PMSM along with the brief overview of the chapter contents are given below.

Chapter 1 briefly presents an overview of the various speed control strategies employed for the PMSM drive. The motivations, as well as the objectives of the research work, are also highlighted in this chapter.

Chapter 2 presents a detailed literature review of the ongoing research works on MPCC-operated PMSM drives. The advantages and limitations of MPCC-based control for a two-level VSI-fed PMSM drive are analyzed in detail in this chapter.

Chapter 3 explains the operation of a dual voltage vector-based MPCC scheme for improved torque and flux performance of the PMSM drive. A null voltage vector is added to the optimum active voltage vector in this method to improve the drive performance. The duty ratio calculation is simple, does not necessitate additional parameter evaluation, and is less sensitive to parameter variations.

Chapter 4 addresses the limitation of the enlargement of computational burden due to the incorporation of duty ratio determination schemes in the MPCC scheme. A simple voltage vector preselection is introduced to reduce the number of voltage vectors used for the prediction, cost function evaluation, and optimization to three.

Chapter 5 describes a multi-vector-based MPCC scheme for the performance improvement of the PMSM drive. The multi-vector application can be achieved with the help of virtual voltage vectors generated using the extended control set. To address the limitation of increased computational burden, a voltage vector selection scheme is analyzed. An effective reduction in flux and torque ripples is achieved using the optimization of the amplitude of the optimum virtual voltage vector.

Chapter 6 presents a multivector-based MPCC scheme with direct determination of the optimum voltage vector. This helps to reduce computational complexity with improved steady-state performance. The duty ratios of the voltage vectors are obtained without the requirement of additional parameter evaluations and have good sensitivity towards machine parameter variations.

Chapter 7 summarizes the significant findings from the entire study and the future scope of the research works.

1.7 Summary

This chapter introduces the research work undertaken in this doctoral thesis. The motivation and objectives are established after the introduction of pertinent literature available on the speed control techniques of PMSM drive. Moreover, this chapter presents the organization of this thesis.

Chapter 2

Literature Review

2. Literature Review

2.1 Introduction

In the past decade, the research on MPC strategy has grown significantly due to the challenges involved in the FOC and DTC scheme for speed control applications of PMSM drive. Among the various MPC schemes, MPCC schemes are most commonly used due to their simplicity and ease of control. This chapter reviews the MPCC scheme for PMSM drives. Further, the various aspects of the MPCC scheme are discussed with respect to advantages, limitations, and significant ongoing research works in this area. In addition, the chapter will review the literature available on duty-based MPCC schemes for PMSM drives. The chapter ends with a discussion of the gaps identified from the extensive literature review.

2.2 Literature Review of MPCC for PMSM drive

Model predictive control (MPC) is an emerging non-linear control technique in the power electronics and drive area. The concept of MPC was initially introduced for process control in the petrochemical industry. Although the scheme has undergone several improvements and has a wider research interest globally [31], its product-level realization in the drive application is still under the radar. With the progression in semiconductor device technology and the availability of powerful digital processors, MPC schemes are expected to be extensively utilized for real-time drive applications in the near future [32]–[35].

The merits of the MPC scheme include the easy realization of the control concept, faster dynamics, easy inclusion of multiple variables as well as nonlinear constraints, etc. MPC scheme can be implemented in different control platforms based on the drive control requirements [36]. For instance, field programmable gate arrays (FPGA) [37], digital signal processors (DSP) [38] or even dSPACE controllers can be used to implement the control [39], [40]. However, the requirement for powerful processors is one of the challenges for the real-time application of the MPC scheme. The processor should possess exponentially increasing computational capability which can meet the control requirements like multi-step predictions and optimizations. Moreover, the MPC scheme is not drive-specific. It can be used to control any machine drive as long as the accurate mathematical model of the system

is available. The recent advancement in digital processing technology qualifies faster processors for the consideration of the MPC scheme. Thus, artificial intelligence-based controls like fuzzy logic, neural networks, and even speed sensorless approaches are combined with the MPC schemes for achieving powerful control strategies in electric drive applications.

MPC schemes can address the limitation of DTC and FOC schemes for speed control of electric drives. FOC offers excellent steady-state performance at the expense of a sluggish transient response [41]. Conversely, DTC offers excellent dynamic performance with larger undulations in torque response at low speeds. However, the MPC scheme has an excellent dynamic response and offers lesser steady-state ripples than DTC. MPC scheme utilizes the system model to predict the future state of the control variables such as torque and flux [42]. Thus, to obtain the actuating vector, a cost function carrying the constraints, variables, and specific targets is optimized. The voltage vector that minimizes the cost function is chosen as the optimal vector to be applied to the VSI feeding the PMSM [43]. Several constraints can be incorporated into the cost function like the maximum current limitation, common mode voltage [44], and switching frequency. For instance, to reduce the switching frequency [45], the number of switching transitions can be predicted for every candidate voltage vector. The cost function has the switching frequency term multiplied with an appropriate weighting factor and thus, the optimum voltage vector that minimizes the switching transitions can be selected.

The effectiveness of the MPC scheme is based on the cost function design to achieve the targeted control and the online optimization scheme improves the performance. In MPCC, the current vector is considered the control variable in the cost function [46]. This reduces the burden of estimation of the stator flux and torque. Moreover, the weighting factor tuning required in MPTC can be avoided in the MPCC scheme [47]. The control is also easy to implement and more feasible. Nevertheless, one important factor to be considered for the MPCC scheme is the time delay compensation, which is very crucial for digital real-time implementation.

In MPCC, the control vector is applied for an entire sample time and hence the torque and flux response are degraded as the error is not controlled accurately to a minimum value. In addition to this, in a two-level VSI, the control set contains only

eight voltage vectors with fixed amplitude and phase angle. With fewer voltage vectors in the control set, the freedom of control becomes limited, leading to increased ripples in torque and flux response. This is obvious especially when the control period is large. Thus, the major drawbacks of MPCC are the large ripples in flux and torque incurred due to the application of one active voltage vector in a control interval [48]. The available literature indicates that the application of two (or more) voltage vectors can enhance steady-state responses. However, the simplicity and robustness of the MPCC are negated in the available duty methods as it involves complex calculations and relies mainly on the accuracy of the parameters used [49]. The computational burden also increases with the number of voltage vectors utilized for prediction and optimization steps. It is specifically prominent while using multi-level or multi-phase inverters. Thus, longer sampling intervals are unavoidable, which inversely affects the performance of the target variables like current, flux, and torque. Nevertheless, the emerging research works in MPC schemes show that the boundary between CCS-MPC and FCS-MPC schemes is becoming very narrow. FCS-MPC can also be used to obtain a continuous reference voltage vector for modulated pulses for the inverter. In [50], a continuous FCS-MPC is proposed which realizes a similar performance to the deadbeat MPC scheme.

2.3 Literature Review of duty-based MPCC for PMSM drive

One of the factors that influence the steady-state response is the duration for which the optimal voltage vector is applied in every control period. The MPCC scheme lacks a modulator, and a single voltage vector is employed for the whole sample time regardless of the extent of error between the control variables. These yield large fluctuations in torque under steady-state conditions [51]

In [52]–[54] one active and one null vector is applied in a control interval, to enhance the steady-state performance in DTC and MPTC schemes, as the null vector causes only a small variation in current. The same principle is applied to MPCC to improve the steady-state response. However, this method is complex and requires a larger number of switching transitions. In [55], the torque ripple is dependent on the weighting factor, and the duration of voltage vectors is calculated with the optimized weighting factor. In this method, the priority is to calculate the weighting factor and then the prediction of torque and flux. The computations are thus increased in the

technique.

The dual vector-based method adopted in [56] enhances the steady-state drive performance. Nevertheless, the complexity involved in computations is not reduced. A model based on incremental prediction is utilized in [57] to enhance the MPCC scheme against parameter variations. The performance given by the method against inductance mismatch disturbance is analyzed and an inductance observer is used to reduce the parameter dependency. In [58] the duration of the active voltage vector is obtained from a current error projection method. The number of active voltage vectors for computation is reduced to three. The error is projected to the optimal voltage vector to obtain the duration of the active voltage vector. This method reduces the computational complexity but the drive performance can be affected due to erroneous motor parameters. In [59], a variable switching point technique is employed to obtain the duration of the active voltage vector. The calculation of quadrature-current slopes for each active voltage vector is required and the intersection points are obtained. The current errors are also calculated at these intersection points. The optimal vector which minimizes the error is chosen. This duty calculation method is complex and demands higher computational time.

When the duty calculation is cascaded with vector selection and optimization, the obtained machine performance is poor. Thus, the low-speed performance of the drive is improved by incorporating the duration of the active voltage vector in the cost function [60]. The stator flux slope and torque slope are used in [61] for duty determination. However, the control becomes infeasible if the calculation time exceeds the control period. The control performance also deteriorates with the parameter variation as the algorithm depends immensely on the machine parameters. The duty cycle is calculated based on the RMS torque ripple minimization principle and the duty obtained is insensitive to parameter variations [62]. The method is simple but requires additional tuning of two weighting factors.

In [63], a modulator based on fuzzy logic is utilized to obtain the duty cycles of active and null voltage vectors. A Luenberger observer is deployed to obtain the state variables. In [64], two similar duty control methods are proposed by the authors. In the first method, the duty is calculated based on the current slopes. The second method is based on the deadbeat principle where the reference voltage vector is first

obtained. The vector closer to the reference can be considered as the optimum vector. The current locus is predicted in [65] and a new reference frame is established. The null vector is chosen based on the error between the reference frame and the origin of the developed frame. The optimum voltage vector is also obtained based on the current locus, unlike conventional MPCC where the cost function is used. This aids in reducing the computational burden. The optimal voltage vector and duty are obtained using the Lagrange multipliers in [66], while in [67], vector modulation is used to make the voltage vector application more optimized and adaptive.

Several algorithms have been proposed for the improvement of control precision and steady-state response of the MPCC method. To enhance the control accuracy, the addition of virtual voltage vectors to the control set is widely researched. The virtual voltage vectors offer the advantage of variable amplitude and phase angle. Some of the prominent methods used can be categorized as an extended control set (ECS) with arbitrary amplitude and phase [68], a modified control set with variable amplitude and constant phase [69], and a modified control set depending on a table-based algorithm [70].

The first category involving ECS with variable magnitude and phase can be obtained using CCS-MPC employing space vector pulse width modulation [71], [72]. However, the burden on the processor is increased due to the additional predictions and optimizations required within a short time. Thus, offline optimization techniques such as generalized predictive control and explicit model predictive control are utilized [72]. In the second category, to realize a modified control set with adjustable amplitude and fixed phase, it is essential to vary the duration for which the optimum voltage vector is applied. This can be achieved either by adding a null voltage vector or extending the control set using virtual voltage vectors. The MPCC duty methods are applied for five-phase machines in [73]–[75], where, either virtual voltage vectors or sector determination is used to obtain good steady-state performance. However, all these methods have the limitation of the large computational burden. In [76], modulated MPCC is employed with virtual vectors to enhance performance. The duty can be determined by the optimization of the cost function and non-linearity compensation is used to reduce the error in tracking input current.

The above-mentioned methods have a fixed phase and the magnitude of the voltage vector is variable. However, if more control precision is required, multiple vectors should be applied in a sample time. This is explored in many research works [77], [78] and a considerable reduction in the steady-state ripples can be achieved as the subsequent vector offers better control than the null voltage vector. In [79], FCS-PTC based on flux vector cost function is employed and the control set is extended using six virtual voltage vectors. In this method, two voltage vectors are applied at every sample time. Moreover, the duty of the optimum voltage vector is calculated using the vector projection concept. A hybrid duty modulation scheme using multiple virtual voltage vectors is presented in [80] to improve the performance of the FCS-MPCC-based five-phase PMSM drive. The harmonic-free voltage vectors are used in the control set. In [81], the control set is augmented with 18 virtual voltage vectors synthesized using a new approach for the FSC-PTC scheme. The drive performance is improved by optimizing the magnitude of the ECS-voltage vector. Similarly, in [82], a computationally efficient MPCC scheme is used, where the steady-state response is improved with the shortcoming of the increased switching frequency. The virtual voltage vector concept is used in [83] for the DTC method, where the control set has 12 virtual voltage vectors along with the six active voltage vectors.

Three vectors are applied in one control period in [84], based on an integrated switching table. The purpose of the null vector employed at the end of each sample is to obtain a reduction in flux and torque ripple and this is realized by varying the duty ratios of the initial active vectors. A multi-vector approach obtained from space vector modulation based on deadbeat control is applied in [85] to calculate the optimal vector as well as the duty ratio of the active voltage vector. However, the complexity is increased due to the additional transformations. A modulated MPC scheme is utilized in [86] to minimize switching losses and improve drive performance. A switching table is introduced in [87] to reduce the computational burden while selecting the optimum active vector and duty optimization is performed to reduce the ripples in steady-state responses. A three-vector-based duty method is adopted in [88], where, an extended control set is developed to improve the torque and flux performance. An inverted triangular matrix is used for storing the duty information. Unlike conventional MPCC, this method uses voltage terms in the cost

function. In [89] a multivector-based approach is considered for a two-level inverter, where, the optimal vector, as well as duty, are obtained from the deadbeat control based on space vector modulation but the complexity is increased with more transformations. The MPCC method adopted in [90]–[92], employs three vectors in a control interval. A second-order super-twisting algorithm-based sliding mode observer, a Luenberger observer as well as a disturbance feedforward compensation based on a proportional-integral observer are employed to estimate the lump disturbance and to reduce the computational burden in the aforementioned methods. Although these methods ensure robustness against parameter mismatch, the overall complexity is enlarged.

2.4 Literature Review of low complex MPCC for PMSM drive

Most of the popular applications of digital processors are hard-time applications, where all the signal processing must occur within a specified amount of time. This constraint necessitates the programmers to determine the processing time required in each sample. Moreover, the worst-case scenario is mostly adopted for determining the processing time. This becomes obvious when high-performance digital processors are employed for real-time signal processing. Instead, for low-cost general-purpose processors, the execution time predictability is more flexible and easier. Thus, when choosing the processor, execution time predictability plays a vital role. The lack of execution time predictability leads to adverse performance as it affects the compiler's ability to effectively optimize the code [93]. This is one of the reasons why even with powerful processors available in the market, the application of MPC schemes for drive applications is still in the pipeline.

Even though MPC is an intuitive and simple scheme, the non-linearities and computations involved due to more predictions and optimizations increase its complexity. The optimization problem of FCS-MPC is essentially an integer programming problem, which is generally resolved by the exhaustive method. With the increase of the prediction horizon, the calculation burden will also increase exponentially [94]. Moreover, it is desirable to achieve faster control with reduced computations as many electric drive applications demand quick dynamic responses. Further, the analog-to-digital conversion and associated digitalization stages become a bottleneck even with powerful DSPs. Thus, to retain the intuitiveness and

simplicity of the MPCC scheme, it is essential to reduce the complexity and the computational burden.

Thus, the real-time implementation of MPCC is limited due to the shortcomings of the high computational cost associated with the predictive algorithm. The computational burden increases with the number of voltage vectors utilized for prediction and optimization steps [95]. It is specifically prominent while using multi-level or multi-phase inverters [96]. Thus, longer sampling intervals are unavoidable, which inversely affects the performance of the target variables like current, flux, and torque [97].

A total of seven voltage vectors must be used for the prediction and optimization steps in a two-level Voltage Source Inverter (VSI) fed PMSM drive. In the conventional MPCC scheme, the algorithm is updated during every sample period. Thus, the stator current prediction and sorting of the voltage vectors that minimize the cost function are carried out seven times in every control period. Hence, the iterative prediction and optimization stages occupy a substantial amount of time and increase the burden on the processor [98].

Considering the high computational time of the predictive algorithm, several kinds of literature propose the preselection of voltage vectors for reducing the operations associated with the shortlisting of the candidate voltage vectors. Furthermore, the torque and flux response can be improved by varying the length of the optimum voltage vector during steady-state operation. This can be achieved by adding a null voltage vector, another active voltage vector, or even multiple voltage vectors to the optimum voltage vector [99]. In [100], the redundant voltage vectors are neglected using the position of the reference stator current, and a null vector is used along with the optimum voltage vector to decrease the torque ripples. The proposed amplitude optimization depends on the stator inductance and causes higher machine parameter sensitivity. In [101], a deadbeat scheme is utilized to obtain the application time of the optimum voltage vector. The proposed scheme in [101] reduces the number of voltage vectors for computations from eight to two. Nevertheless, the tangent inverse calculation is essential to estimate the position of the reference voltage vector which contradicts the advantage acquired due to the reduced number of computations. Moreover, the parameter sensitivity of the scheme

is increased due to the need for reference voltage vector determination.

The addition of a null voltage vector to the optimum voltage vector does not yield an optimal steady-state performance under all operating conditions. Thus, it is required to apply multiple voltage vectors in a sample period to alleviate the reference current deviation from its predicted value. However, the main limitations of multivector schemes are increased computational burden and higher switching frequency. An enhanced predictive direct power control scheme is proposed in [102] that allows the selection of a null or active voltage vector as the second optimal voltage vector. However, the computational complexity is enlarged and the method does not eliminate the error. In [103], the magnitude and phase of the selected voltage vector are optimized for the precise tracking of the reference variable. However, this increases the complexity of the control algorithm. In [104], an extended control set is introduced to augment the control set of the VSI. This enlarges the control precision with three voltage vectors applied to improve the torque performance. The computational time is reduced using sector-based voltage vector preselection schemes. However, there is an inevitable surge in the switching frequency. To address the limitation of increased switching frequency, in [105], adjacent voltage vectors are applied based on the number of switching transitions required. The optimum solution with less switching transition is used for the control action. In [106], a duty-ratio correction scheme is proposed for a three-level converter, which offers reduced switching frequency using online tuning of the weighting factor. In [107], [108], the preselection of the voltage vector is based on 3D lookup table data, and the duration of application of voltage vectors is obtained using the space vector modulation scheme. This increases the complexity of the control scheme. Therefore, it can be concluded that there is a need for evaluating control schemes that can simultaneously reduce the complexity as well as improve the torque response.

2.5 Summary

This chapter comprehensively evaluates the relevant literature available on the Model Predictive control schemes. The advantages and drawbacks of the MPC schemes are identified and the gaps in the existing research field that motivate the research works in this thesis are highlighted.

The significant gaps identified are as follows.

i. Although the MPC scheme offers excellent dynamic performance, the steady-state response is affected by larger ripples in torque and flux. The large torque pulsations result in increased vibrations and eventually affect the lifetime of the electrical machine.

ii. There is a need to address the computational complexity of the MPC algorithm which limits its real-time applications in the electric drive sector.

iii. The existing duty control methods to improve the steady-state performance result in enlarged complexity and induce additional machine parameter dependency.

iv. The existing voltage vector preselection schemes are either complex or result in suboptimal voltage vector selection leading to the deterioration of dynamic performance of the MPC scheme.

Thus, it is essential to identify methods that can improve the steady-state performance without augmenting the control algorithm complexity. Moreover, careful consideration must be given to retain the dynamic performance of the drive and prevent the inclusion of parameter-sensitive terms into the algorithm.

Chapter 3

A Dual Voltage Vector-Based Model Predictive Current Control of Permanent Magnet Synchronous Motor Drive

3. A Dual Voltage Vector-Based Model Predictive Current Control of Permanent Magnet Synchronous Motor Drive

3.1 Introduction

MPCC is evolving as a powerful scheme for controlling the PMSM drives, due to its inherent simplicity, the capability to include non-linearities as well as quick dynamic response. In the MPCC method, the stator current for the next instant is predicted and the optimal switching state is obtained by minimizing a cost function. The performance of the method is based on the proper design of the cost function. The cost function, with a set of non-linear constraints, must be minimized to determine the optimal vector required to be applied in the next sampling period. The major drawback of MPCC is identified to be the large ripples in flux and torque incurred due to the application of one active voltage vector in every control interval. The available literature indicates that the application of two (or more) voltage vectors can enhance steady-state responses. However, the simplicity and robustness of the conventional MPCC (C-MPCC) are negated in the available duty methods as it involve complex calculations and relies mainly on the accuracy of the parameters used. This chapter proposes a dual voltage vector-based MPCC for a two-level VSI-based PMSM drive to improve the steady-state performance with two voltage vectors (one active and null) applied in every control interval. The chapter has the following organization: Section 3.1 describes the dynamic model of the SMPMSM, Section 3.3 presents the C-MPCC while, and Section 3.4 describes the proposed MPCC. Section 3.5 comprises the simulation and experimental results. Section 3.6 discusses the parameter sensitivity of the proposed scheme. The effectiveness of the proposed scheme is analyzed in Section 3.7 and the summary is presented in 3.8.

3.2 Dynamic Model of SMPMSM

An SMPMSM has symmetrically distributed three-phase stator windings. In SMPMSM, the direct and quadrature- axis stator inductances have the same magnitude. In order to avoid the intricate rotor coordinate transformations, SMPMSM in the stationary reference frame is considered. The mathematical model

can be obtained using the following equations.

$$u_s = i_s R_s + \frac{d\psi_s}{dt} \tag{3.1}$$

$$\psi_s = L_s i_s + \psi_r \tag{3.2}$$

Substituting (3.2) in (3.1) and re-arranging gives,

$$\frac{di_s}{dt} = \frac{1}{L_s}(u_s - R_s i_s - jw_r\psi_r) \tag{3.3}$$

where, $\psi_r = \psi_f e^{j\theta}$

The electromagnetic torque can be obtained as:

$$T_e = \frac{3}{2} p\,(imag(\overline{\psi_s} \times i_s)) \tag{3.4}$$

where,

The mechanical equation is given by (3.5).

$$J\frac{dw_m}{dt} = T_e - T_l - Bw_m \tag{3.5}$$

3.3 Model Predictive Current Control of PMSM drive

The block diagram of C-MPCC is given in Figure 3.1. In a two-level VSI-based MPCC, eight basic voltage vectors are used as shown in Figure.3.2. The developed electromagnetic torque in a PMSM is shown in (3.4). The torque is maximum when the angle between the stator current vector and rotor flux is 90°. In the rotor reference frame, this will make the direct axis current as zero. Moreover, the rotor flux linkages can be considered as time-invariant.

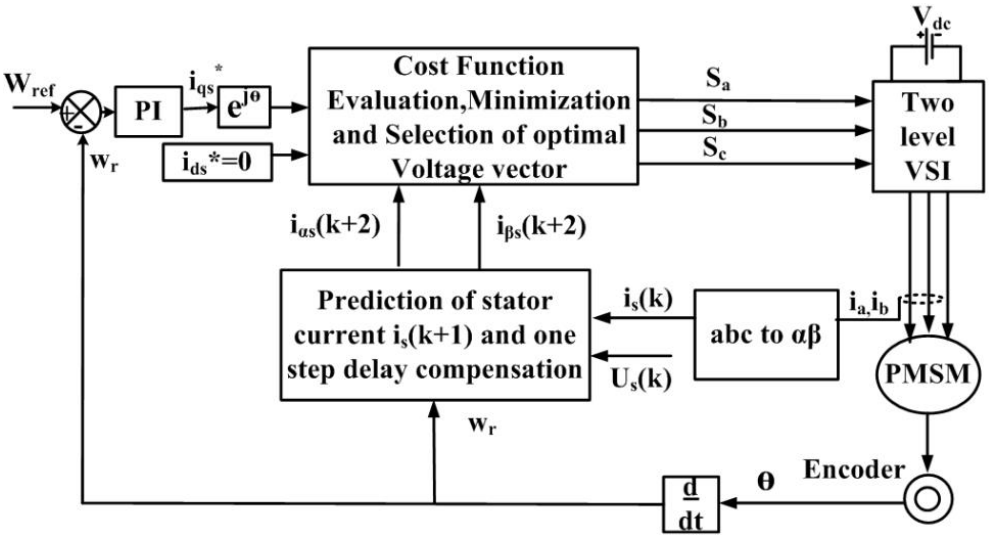

Figure 3.1 Block diagram of C-MPCC

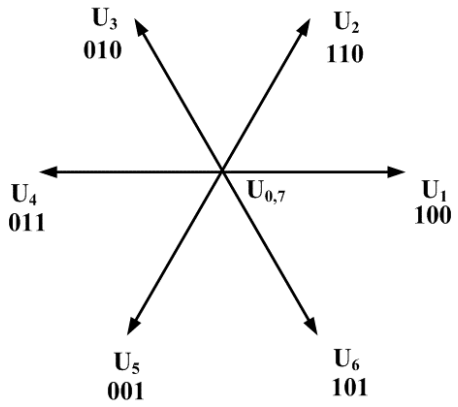

Figure 3.2 Voltage vectors of two-level VSI

The torque varies linearly with stator quadrature axis current, i_{qs}. Any deviations in i_{qs} will cause a similar change in the torque developed. Conversely, to reduce the ripples in torque, variations in i_{qs} must be reduced. Therefore, the control strategy is to give the direct-axis current reference, direct-axis current reference, i_{ds}^{*} as zero. The output of the speed PI controller is given as the quadrature axis current reference, i_{qs}* as the speed dynamics is proportional to the motor torque which further depends on the current i_{qs}.

The steps involved in C-MPCC are as follows:

(i) Prediction of current in the stator,

(ii) Cost Function estimation,

One-step delay compensation.

3.3.1 Prediction of the current in the stator

The stator currents, DC-link voltage, and speed of the PMSM at the k^{th} instant are fed to the analog-to-digital converter (ADC) to digitalize the signals. The predicted current is obtained from the following equations.

From equation (3.3),

$$\frac{di_s}{dt} = \frac{1}{L_s}(u_s - R_s i_s - jw_r\psi_r) \tag{3.6}$$

Applying the first-order Euler's discretization to (3.6),

$$i_s(k+1) = i_s(k) + \frac{T_s}{L_s}(U_s(k) - i_s(k)R_s - j\psi_r w_r e^{j\theta}) \tag{3.7}$$

The cost function (G), defines the deviation of the predicted current from the reference value of the current. This error should be minimized to get optimum actuating vectors.

MPCC cost function is given by,

$$G = | i_s^* - i_s(k+1) |^2 \tag{3.8}$$

3.3.2. One- step delay compensation

The real-time implementation of the control using a digital processor introduces a single-step delay between the voltage command and the actual voltage value. This deteriorates the performance of the MPCC. The delay can be compensated by predicting the control vectors at the $(k+2)^{th}$ instant instead of $(k+1)^{th}$ instant. The predicted current at the $(k+1)^{th}$ instant can be obtained from (3.7). The final values of the currents are obtained by replacing k by $(k+1)$ and $(k+1)$ by $(k+2)$ respectively. The stator current at the instant (k+2) is:

$$i_s(k+2) = i_s(k+1) + \frac{T_s}{L_s}(U_s(k+1) - i_s(k+1)R_s - j\psi_r w_r e^{j\theta}) \tag{3.9}$$

The cost function can be modified as:

$$G = | i_s^* - i_s(k+2) |^2 \tag{3.10}$$

The voltage vector which decreases the deviation in current error is opted as the optimum active voltage vector by the controller. The inverter switching pulses corresponding to the optimum voltage vector are generated by the controller. These pulses are fed to the two-level VSI after being passed to the driver circuit. The VSI is directly supplying the PMSM connected through the current sensors for feedback.

3.4 Proposed dual voltage vector-based MPCC for PMSM drive

In C-MPCC, the voltage vectors that reduce the error in the current according to the cost function will be chosen for one control interval. In a two-level VSI, only eight voltage vectors are offered and the best vector which minimizes the error is chosen for actuation. However, this results in unwanted ripples in the steady-state response. The necessity to apply two voltage vectors (one active and one null) is hence to improve the steady-state performance. This method utilizes two voltage vectors during the control interval. The block diagram of the proposed method is shown in Figure 3.3.

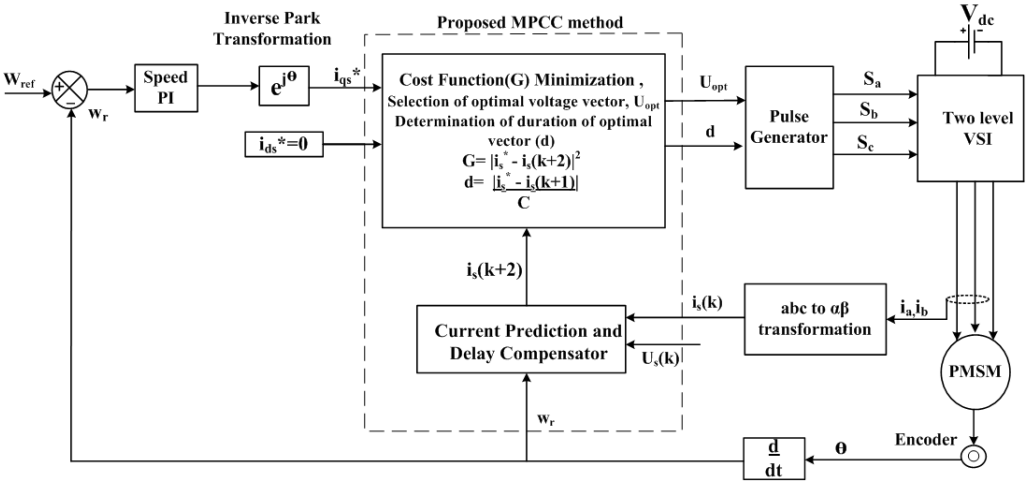

Figure 3.3 Block diagram of proposed MPCC.

In (3.7), substituting $U_s(k) = 0$,

$$i_{spo}(k+1) = i_s(k) + \frac{T_s}{L_s}(-i_s(k)R_s - j\psi_f w_r e^{j\theta}) \tag{3.11}$$

Thus, from (3.11),

$$i_s(k+1) = i_{spo}(k+1) + \frac{T_s}{L_s}U_s(k) \tag{3.12}$$

$$e(k+1) = i_s*(k+1) - i_s(k+1) \tag{3.13}$$

$$e_o(k+1) = i_s*(k+1) - i_{spo}(k+1) \tag{3.14}$$

where, $e(k+1)$ and $e_0(k+1)$ are the errors with respect to the reference current $i_s^*(k+1)$.

Substituting the value of $i_s^*(k+1)$ from equation (3.13) in (3.14) gives,

$$e_o(k+1) = e(k+1) + \frac{T_s}{L_s}(U_s(k)) \tag{3.15}$$

The entire sampling time is comprised of two intervals, one for active and the other for null vector application. The equation (3.15) (as shown in Figure 3.4) proves that error is reduced when the null voltage vector is applied.

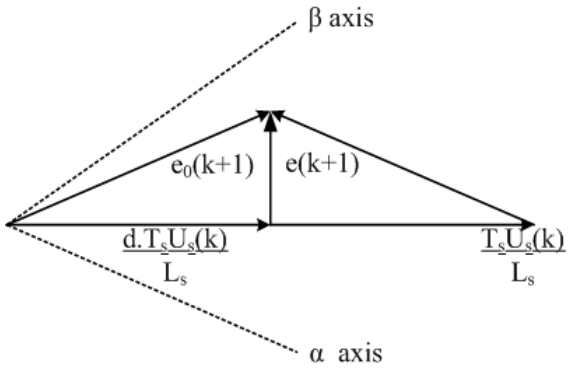

Figure 3.4 Effect of null vector addition in MPCC.

The proposed MPCC method uses a deadbeat control of current components under the stationary reference frame for calculating the vector duration. The steps involved in the method are shown in Figure 3.5.

The one-step delay compensation is considered to recompense the performance of the control during the digital implementation.

According to the principle of deadbeat control, the predicted current at the $(k+2)^{th}$ instant is assumed to reach the reference value at the end of the control period.

$$i_s(k+2) = i_s(k+1) + m_1 t_{op} + m_0 (T_s - t_{op}) \tag{3.16}$$

where, m_0 and m_1 are the current slopes as per Figure 3.6. and m_0 is the current slope due to the null vector. m_1 is the current slope due to the active vector, t_{op} is the active voltage vector duration and T_s is the sampling time.

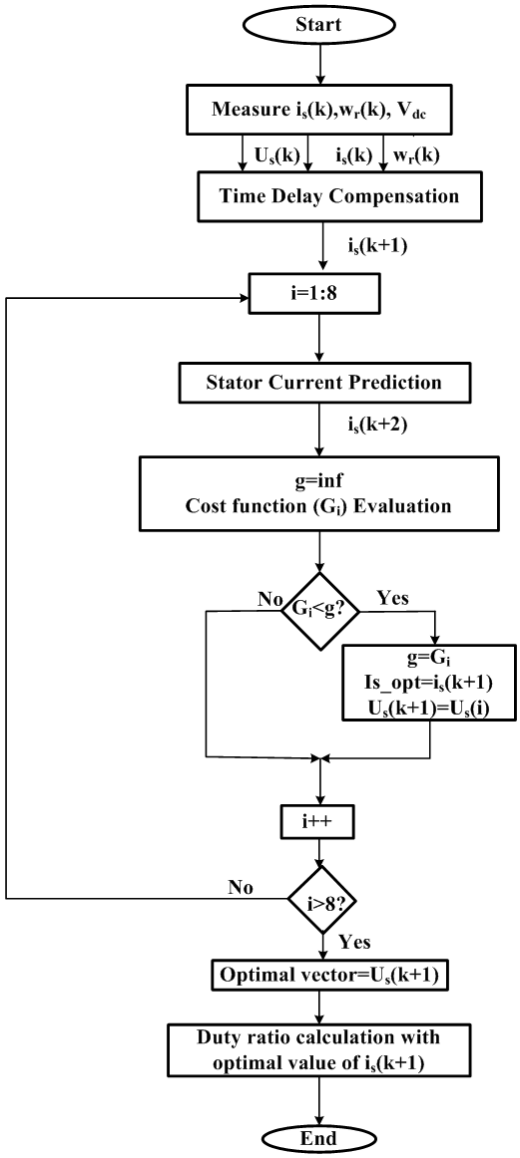

Figure 3.5 Flow chart of the proposed MPCC.

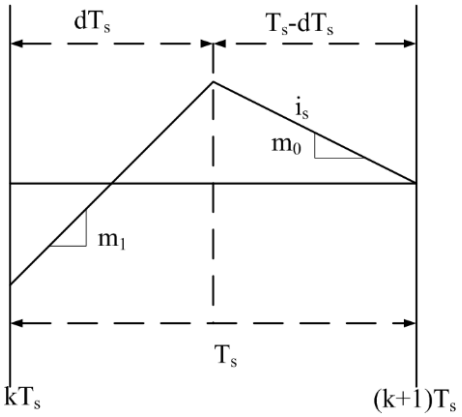

Figure 3.6 Stator current variation in a sample time (T_s)

The current slopes can be obtained from the equations given below:

$$m_1 = \frac{di_s}{dt}|_{active} = \frac{u_s - R_s i_s - jw_r\psi_r}{L_s} \tag{3.17}$$

$$m_o = \frac{di_s}{dt}|_{null} = \frac{-R_s i_s - jw_r\psi_r}{L_s} \tag{3.18}$$

In any sample time,

$$m_1 - m_o = \frac{|U_{opt}|}{L_s} \tag{3.19}$$

Substituting (3.16) in the cost function,

$$G = |\, i_s^* - i_s(k+1) - (m_1 - m_0)t_{op} - m_0 T_s \,|^2 \tag{3.20}$$

Applying the principle of minimization, $\frac{dG}{dt} = 0$ implies,

$$d = \frac{|\, i_s^* - i_s(k+1)\,|}{(m_1 - m_0)T_s} - \frac{m_0}{(m_1 - m_0)} \tag{3.21}$$

where, $d = \frac{t_{op}}{T_s}$, the duty ratio.

From (3.19), $(m_1 - m_0)T_s$ can be considered as a constant, C.

Substituting values from (3.17) and (3.18) we get,

$$\frac{m_0}{m_1 - m_0} = -\frac{R_s i_s(k+1) + e(k+1)}{T_s U_s(k+1)} \tag{3.22}$$

Discretizing (3.1) gives,

$$U_s(k+1) = R_s i_s(k+1) + \frac{L_s(i_s^* - i_s(k+1))}{T_s} + e(k+1) \tag{3.23}$$

where, the back emf, $e(k) = jw_r\psi_r$

From (3.23),

$$R_s i_s(k) + e(k) = U_s(k) - \frac{L_s(i_{sref} - i_s(k))}{T_s} \tag{3.24}$$

Substituting the numerator of (3.22) from (3.24),

$$\frac{m_o}{m_1 - m_o} = -\frac{L_s}{T_s}\frac{(U_s(k)T_s - L_s(i_{sref} - i_s(k)))}{U_s(k)}$$

$$= -(L_s - \frac{L_s^{\,2}(i_{sref} - i_s(k))}{U_s(k)T_s}) \tag{3.25}$$

As the squared term L_S multiplied with an error gives a negligible value, this term can be neglected in the duty calculation. Thus from (3.21), the duty ratio, *d*, can be obtained as,

$$d = \frac{|i_s^* - i_s(k+1)|}{C} \tag{3.26}$$

where, *C* is a constant.

$$C = \frac{|U_{opt}|}{L_s} T_s \tag{3.27}$$

Thus, from (3.27) it can be observed that the duty ratio can be obtained based on a simple current error. This eliminates the complex calculations involving the slopes and the consideration of both quadrature axis and direct axis currents will offer good control over the torque and flux response. Hence, the number of calculations is reduced and parameter dependency is eliminated in the proposed duty calculation method under the steady-state condition. As a result, there is a reduction in torque and flux ripples, while the simplicity of C-MPCC is retained.

3.5 Simulation and Experimental Results

3.5.1 Simulation Results

The proposed method is compared with the C-MPCC, MPCC [62], and MPCC[58] in MATLAB-Simulink. The parameters used for the simulation are given in Table 3.1. The parameters such as sampling time and load conditions are maintained the same for all the models for better comparison. For V_{dc}=415 V, T_S=100 μs, L_S=10.5 mH, from (3.27), the constant value, *C* is obtained as 2.65 in this method. Modern high-performance applications require quick speed and torque dynamics. To study the effect of the sudden change in speed and torque, all four methods are subjected to similar speed and torque dynamic changes. The dynamic conditions for step changes in speeds as well as load torque are shown in Figure 3.7, and Figure 3.8, respectively. The simulation results of obtained speed, torque, and flux are

shown for all the methods. The effect of the sudden change in speed from 300 rpm to 700 rpm to 1200 rpm under no-load conditions can be analyzed from Figure 3.7, where all the methods exhibit near-identical performance. However, the steady-state performance exhibited between each speed change shows that the proposed method has lower torque and flux ripples. Similarly, the effect of dynamic change in load torque is presented in Figure 3.8, where the load torque is suddenly increased from 0 to 50% of the rated torque.

Table 3.1 Machine Parameters

Parameters	Value
Stator Resistance (R_s)	1.12Ω
Stator inductance (L_s)	10.5mH
Rated Speed (N_r)	1500 rpm
Permanent magnet flux (ψ_f)	0.71
No. of pole pairs (p)	2
Rated Torque (T_e)	23.5 Nm
Moment of Inertia(J)	0.0055 kg-m^2

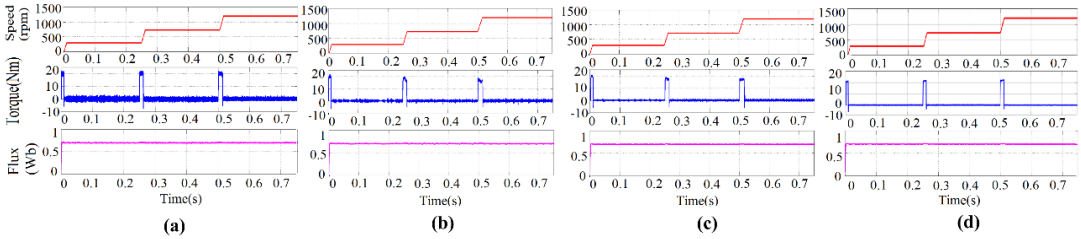

Figure 3.7 Step change in the speed from 300 rpm to 700 rpm to 1200 rpm (a). C-MPCC, (b). MPCC [64], (c). MPCC[56], (d). Proposed MPCC.

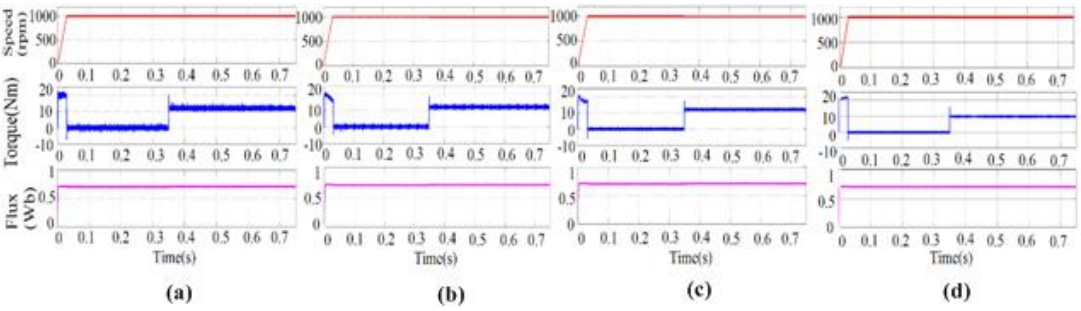

Figure 3.8 Step change in the load torque from 0- 50% of rated value (a). C-MPCC, (b). MPCC [64], (c). MPCC[56], (d). Proposed MPCC.

The simulation results show that the proposed method can quickly respond to sudden torque change. In addition, the ripples in flux and torque of the proposed MPCC under steady load conditions are lesser than the other three methods. Thus, it can be observed from the simulation results that the proposed MPCC has better performance under steady-state no-load and on-load operating conditions. The flux

and torque ripples in C-MPCC are higher than MPCC [64], MPCC [100], and proposed MPCC. Further, all the methods exhibit almost identical dynamic performance.

3.5.2 Experimental Results

A 5 HP, 1500 rpm, 415 V, 4 pole PMSM motor is used for the experimentation. All three methods are implemented in real-time for comparison. The PMSM is operated using a three-phase two-level VSI. The LEM sensors are used to sense the DC link voltage and stator currents. The 1024-point incremental shaft encoder gives the position and is fed back to sense the speed. The control is given through the dSPACE 1104 interface.

The PMSM motor shaft is coupled to a DC-generator. The electrical load is supplied to the machine using the DC-generator connected to a resistive bank. The one-step delay compensation is provided in all the methods and the sampling frequency is 10 kHz. For the proposed model, the calculated value of C=2.65 is used. The sampling time and load conditions are maintained the same for all the methods. The steady-state response at low (300 rpm), medium (700 rpm), and high speeds (1200 rpm) are observed as in Figure 3.9 to Figure 3.12.

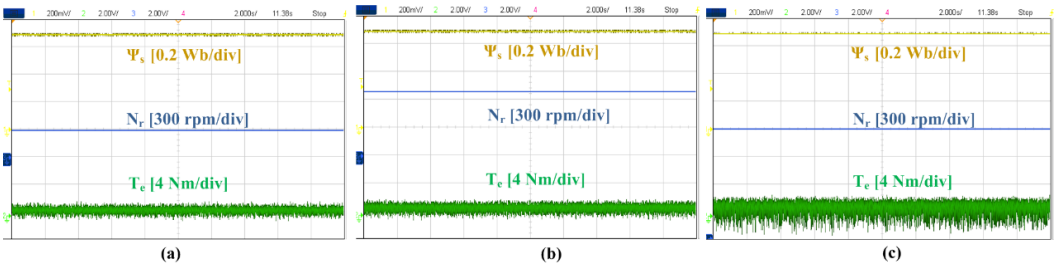

Figure 3.9 Steady-state torque and flux response of C-MPCC at (a) 300 rpm (b) 700 rpm (c) 1200 rpm

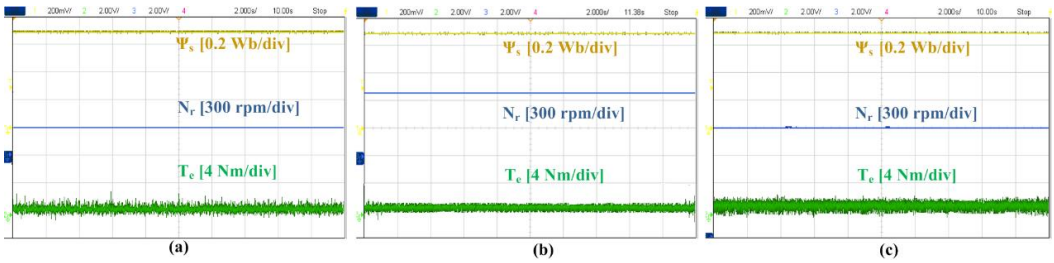

Figure 3.10 Steady-state torque and flux response of MPCC [64] at (a) 300 rpm (b) 700 rpm (c) 1200 rpm

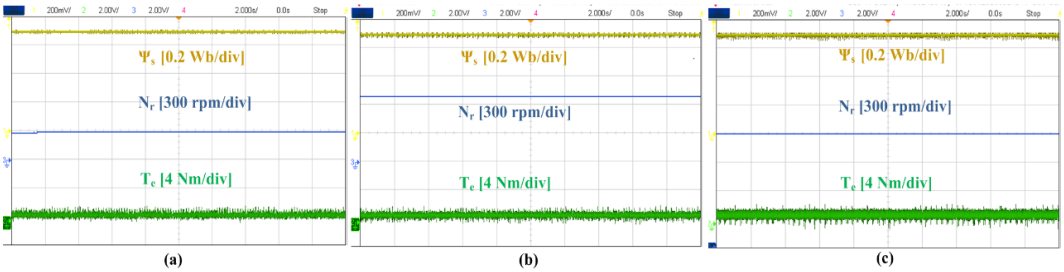

Figure 3.11 Steady-state torque and flux response of MPCC[56] at (a) 300 rpm (b) 700 rpm (c) 1200 rpm

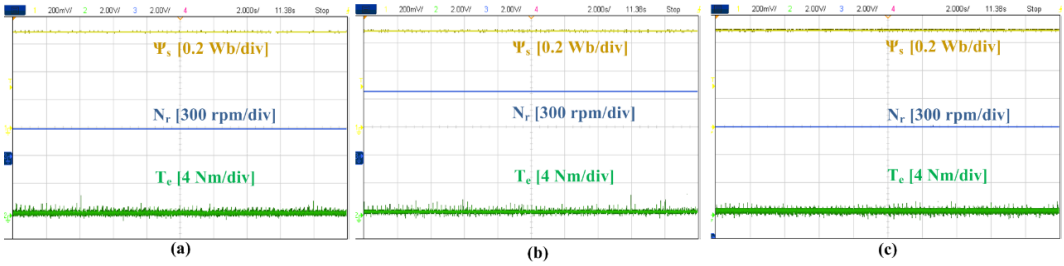

Figure 3.12 Steady-state torque and flux response of proposed MPCC at (a) 300 rpm (b) 700 rpm (c) 1200 rpm

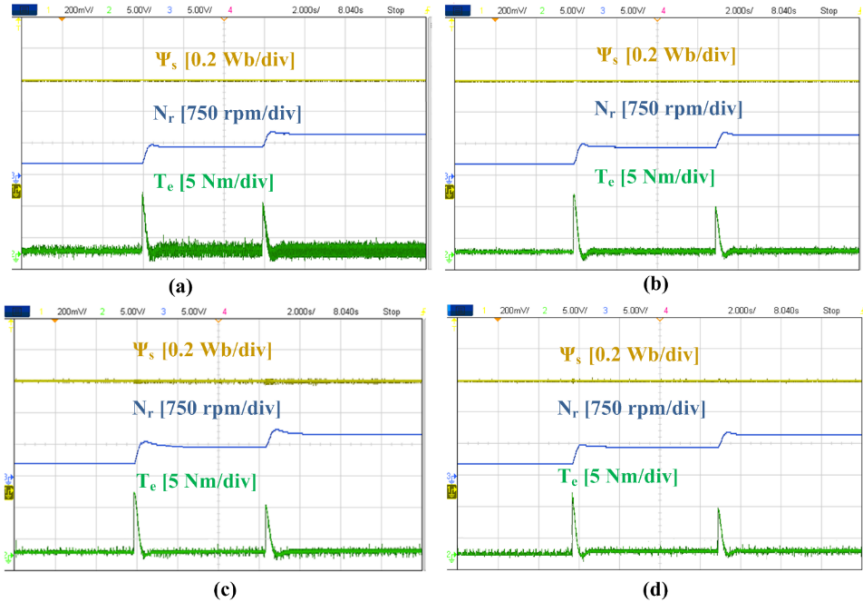

Figure 3.13 Step changes in speed from 300 rpm to 700 rpm to 1200 rpm (a). C- MPCC, (b). MPCC [62], (c). MPCC[56], (d). Proposed MPCC.

The dynamic speed performance is verified by providing the three-stage change in speed from 300 rpm to 700 rpm to 1200 rpm as in Figure 3.13. The sudden change in the load torque (0 to 50% of rated torque) at a speed of 1000 rpm is given in Figure 3.14. The harmonic distortions in the stator current are obtained in the steady-state. Figure 3.15. shows the steady-state response with a load of 12 Nm applied to the motor.

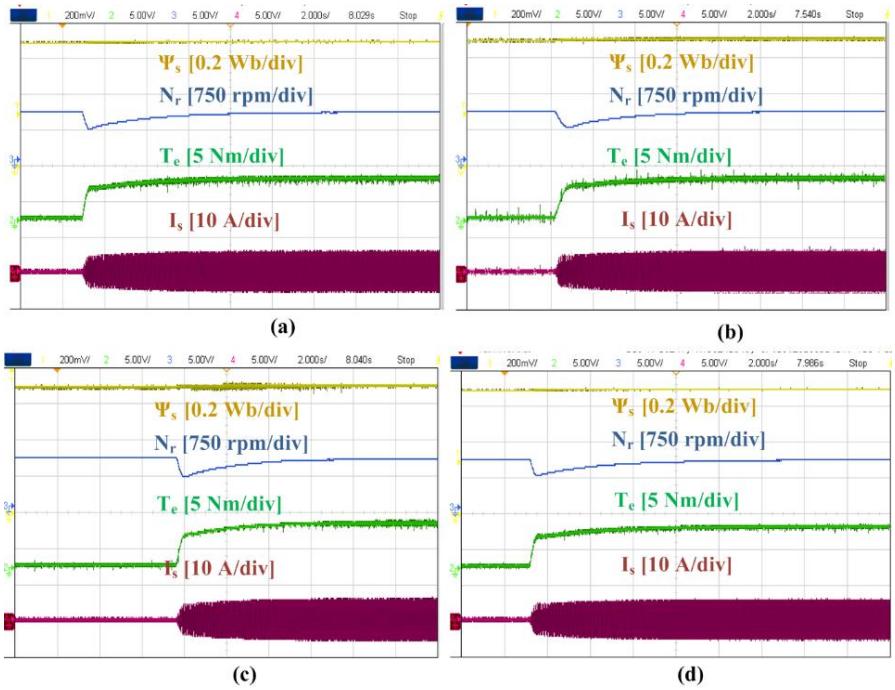

Figure 3.14 Step-variation in torque from 0 to 50% of rated load torque (a). C- MPCC, (b). MPCC [62], (c). MPCC[56], (d). Proposed MPCC.

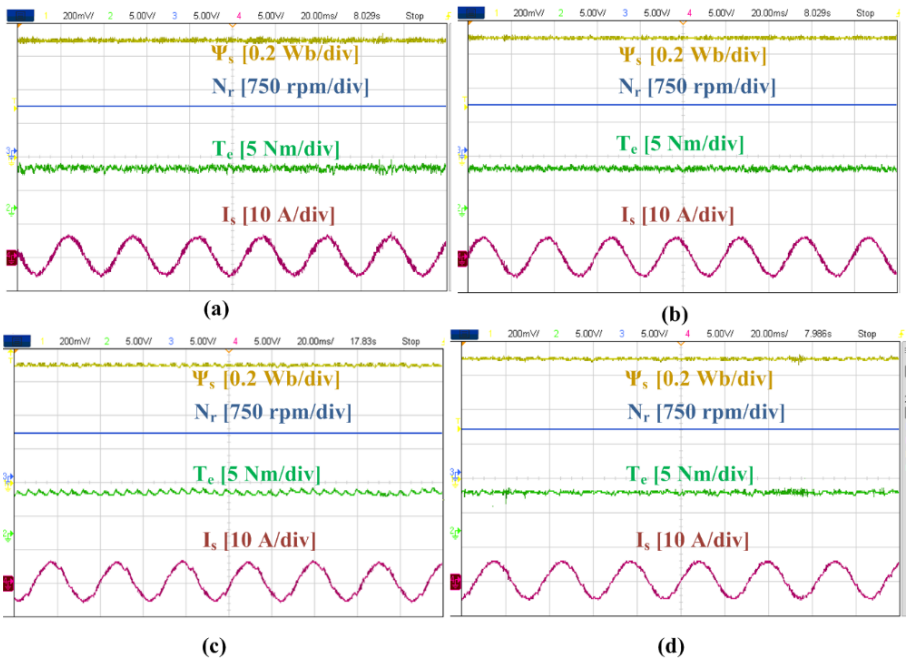

Figure 3.15 Steady-state performance with a load torque of 12 Nm (a). C- MPCC, (b). MPCC [62], (c). MPCC[56], (d). Proposed MPCC.

Further, the dynamics of the machine during the speed reversal from 1000 rpm to -1000 rpm is also confirmed in Figure 3.16. The waveforms of stator flux and torque for the corresponding speed are shown in all the above results.

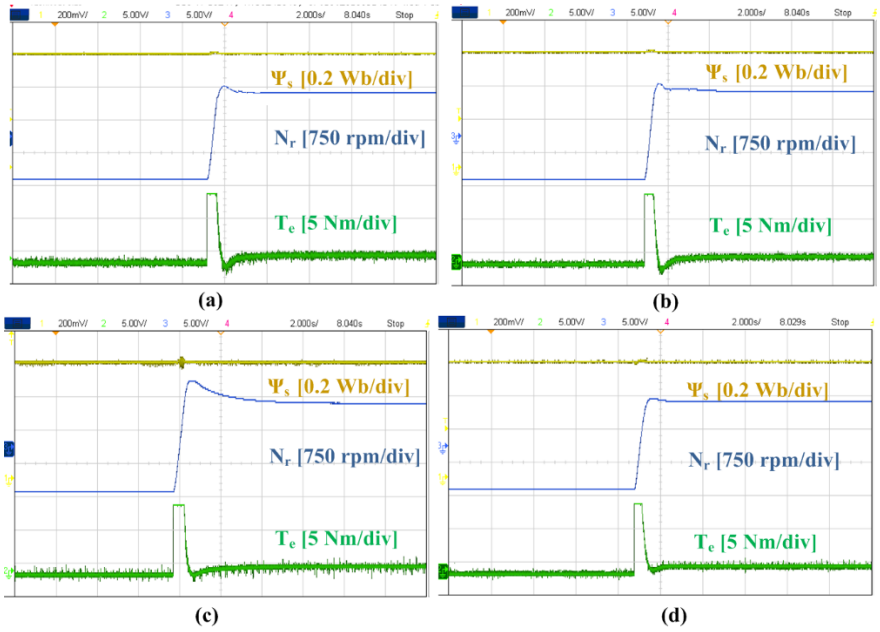

Figure 3.16 Speed reversal from -1000 rpm to 1000 rpm (a). C-MPCC, (b). MPCC [62], (c). MPCC[56], (d). Proposed MPCC.

In the C-MPCC method, the application of a single voltage vector for an entire sample time leads to over-regulation and hence it results in large torque and flux ripples in the steady-state response as shown in Figure 3.9. However, the duty-modulated methods help to reduce the torque and flux ripples with the application of two (or more) voltage vectors in a sample time, as evident from Figure 3.10-3.12. The waveforms of torque and flux for the particular speed are also included in Figure 3.9-3.12. The experimental results at different speeds also prove that the proposed method produces less flux and torque ripples compared to C-MPCC, MPCC [62], and MPCC[56].

The response of the machine subjected to dynamic changes in speed, shown in Figure 3.13, affirms that all four methods have similar dynamic performance. Moreover, the waveforms obtained for the dynamic step change in speed (Figure 3.13) and step change in torque (Figure 3.14) highlight the advantage of the MPCC method for modern speed control applications. Whenever a step-change in speed is applied, the control algorithm quickly responds to adjust the speed to the required reference value. The steady-state performance, with a load of 12 Nm in Figure 3.15, comprises of the obtained stator flux, torque, speed, and current waveforms.

The obtained results in Figure 3.15 show that the proposed method generates less torque and flux ripples under loaded conditions as compared to the other three methods.

The duty obtained in the proposed method is adjusted based on the error in quadrature axis current, $i_{qs,}$ and direct axis- current, i_{ds}. Any deviation in torque, as well as the flux, will be reflected as the error in currents and the duty will be simultaneously adjusted to reduce these errors. Thus, the proposed method yields better performance under no-load and on-load conditions based on experimental results. Moreover, Figure 3.17 presents stator current total harmonic distortion (THD) obtained based on the steady-state stator currents. Thus, it can be confirmed that the proposed method has less current harmonic distortion as compared to the C-MPCC, MPCC [62], and MPCC[56].

The torque and flux ripples are calculated as:

$$T_{e\_rip} = \sqrt{\frac{1}{n}\sum_{i=0}^{n}(T_e(i) - T_e^*)^2)} \tag{3.28}$$

$$\psi_{rip} = \sqrt{\frac{1}{n}\sum_{i=0}^{n}(\psi_s(i) - \psi_s^*)^2)} \tag{3.29}$$

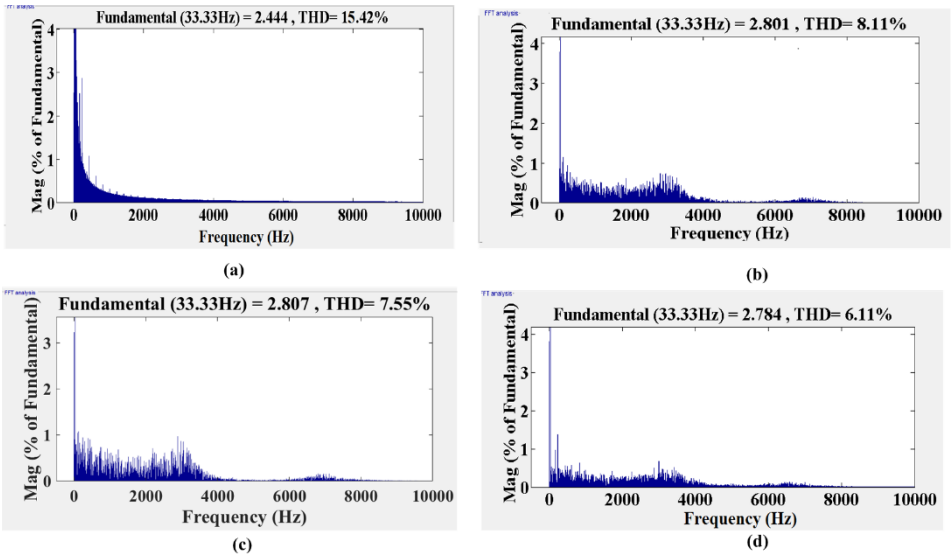

Figure 3.17 THD of stator current (a). C-MPCC, (b). MPCC [62], (c). MPCC[56], (d). Proposed MPCC.

The computational burden for the three methods is given in Table 3.2. From Table 3.2, it can be observed that the computational burden for the proposed method is less than the existing duty calculation method MPCC [62] as the slope calculation involved in MPCC [62] is eliminated in the proposed method. However, the computational burden of MPCC[56] is slightly less than the Proposed MPCC. In MPCC[56], the redundant voltage vectors are eliminated and only three active

voltage vectors are used for the selection of the optimal voltage vector. This reduces the computational time. The method still requires complex control and identification of the position of the voltage vector with respect to the reference vector.

Table 3.2 Computational time

C-MPCC	MPCC [62]	MPCC[56]	Proposed MPCC
36 µs	50µs	32 µs	39.5 µs

Table 3.3 Comparison of C-MPCC, MPCC [62], MPCC[56] and proposed MPCC.

Speed (rpm)	C-MPCC		MPCC[62]		MPCC[56]		Proposed MPCC	
	T_{e_rip} (Nm)	ψ_{rip} (mWb)	T_{e_rip} (Nm)	ψ_{rip} (mWb)	T_{e_rip} (Nm)	ψ_{rip} (mWb)	T_{e_rip} (Nm)	ψ_{rip} (mWb)
300	0.40	1.8	0.202	1.18	0.186	1.2	0.173	1.14
700	0.37	1.7	0.193	1.23	0.161	1.24	0.146	1.12
1200	0.6466	1.5	0.269	1.26	0.148	1.3	0.139	1.18

Table 3.4 Average switching frequency

C-MPCC	MPCC [62]	MPCC[56]	Proposed MPCC
2.1 kHz	3.6kHz	3.43kHz	3.5kHz

It can be observed from Table 3.3 that, compared to C-MPCC, MPCC [62], and MPCC[56], the ripples in the steady-state response of the proposed MPCC are considerably less. The flux ripples and torque ripples are calculated and are presented in Table 3.3. Although the switching frequency of the proposed method is slightly more than the C-MPCC as given in Table 3.4, the overall improvement in steady- state performance, as well as the reduction in computational burden, override this slight increase.

3.6 Parameter Sensitivity Test

The proposed method utilizes a parameter-independent duty calculation for improving steady-state performance. In order to verify the effectiveness of the proposed method against parameter variations, the parameter sensitivity test is conducted. This is achieved by increasing stator resistance as well as the inductance values by 20% in the MPCC algorithm.

The effect of stator resistance change can be observed in Figure 3.18. The machine is operated at 75 rpm (5% of the rated speed). The stator resistance is increased by 20% after 10s and the response shows that all the methods are insensitive to changes in the stator resistance. To analyze the effect of stator

inductance, change at high speed, the machine is operated at rated speed and the inductance is increased by 20% after 10s. The responses obtained are shown in Figure 3.19. The performance of MPCC [62] and MPCC[56] gets disturbed due to the change in inductance. After the change in inductance, the ripples are increased in both methods. However, in C-MPCC and the proposed method, the effect of inductance change is very small. The methods regain stability without much difference in the steady-state response after the inductance change.

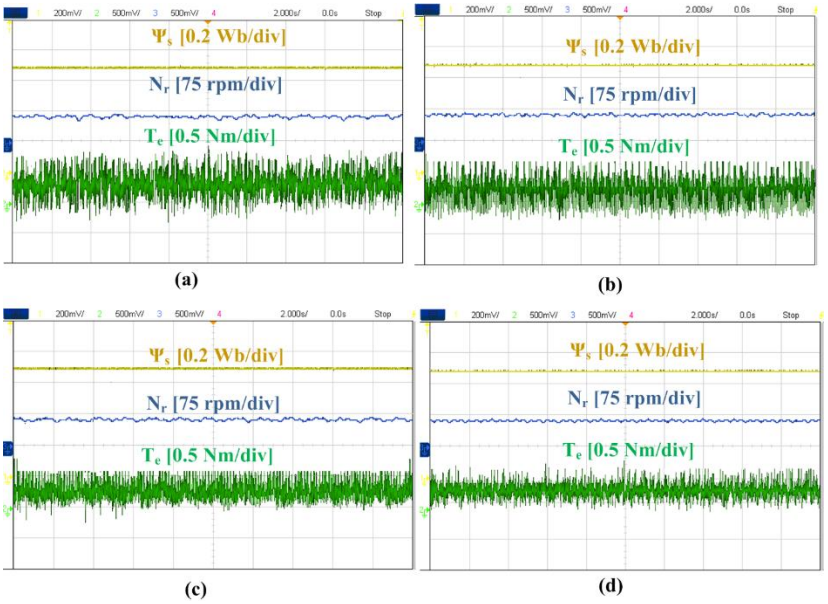

Figure 3.18 With 20% change in stator resistance at 75 rpm (a). C-MPCC, (b). MPCC [62], (c). MPCC[56], (d). Proposed MPCC.

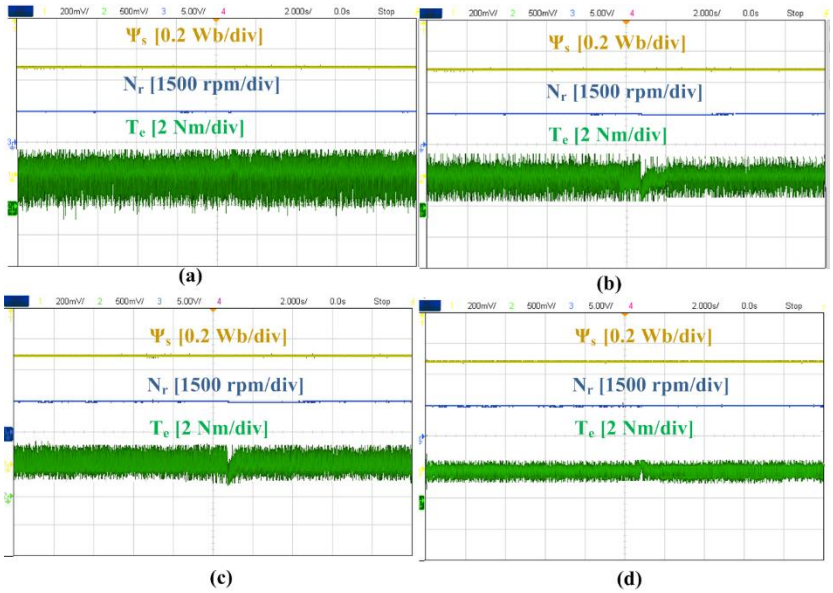

Figure 3.19 With 20% change in stator inductance at 1500 rpm (a). C-MPCC, (b). MPCC [62], (c). MPCC[56], (d). Proposed MPCC.

In MPCC [62] and MPCC [56], the duty calculation depends on the inductance value and hence the performance is affected by its variation. Thus, the proposed method offers a robust, parameter-independent duty operation with reduced torque and flux ripples.

3.7 Discussion of results

Table 3.3 presents the torque ripple, flux ripple, and switching frequency at different speeds under the steady-state condition for C-MPCC, MPCC [62], MPCC[56], and the proposed method. It can be observed from Table 3.3 that the proposed method removes at least 55% of the torque ripples existing in the C-MPCC under different speed conditions. Further, the torque ripple in the proposed method is 9.8% and 6.3% less than MPCC [62] and MPCC[56], respectively. The flux ripples at high speed are 36.6%, 4.8%, and 9.2% less than C-MPCC, MPCC [62], and MPCC[56], respectively in the proposed method. The switching frequency of the proposed method is comparable to the available duty methods, MPCC [62] and MPCC[56], but greater than the C-MPCC. However, this increase is trivial as there is a significant reduction in torque and flux ripples compared to the C-MPCC.

The reduction of torque and flux ripples in the proposed method is effective due to the application of one active and one null vector in a sample time. The duty calculation is proportional to the error between the reference and predicted current in the proposed method. The quadrature and direct axis currents are considered in the calculation, which results in the reduction of torque and flux ripples. The change in torque will be reflected as a change in the quadrature axis current and the change in flux will cause a change in the direct axis current. When the error is large, the duty is increased proportionally to reduce the deviation in predicted and reference current. Similarly, when the error is small, duty is also correspondingly reduced. Moreover, the constant value in the denominator ensures the duty calculation to be parameter-independent. However, in MPCC[56], the duty is proportional to the stator inductance, while in MPCC [62], the duty is proportional to current slopes. This affects the steady-state performance when the parameters are inaccurate.

3.8 Summary

This chapter presents a dual voltage vector-based MPCC method to mend the shortcomings of a C-MPCC scheme i.e., the ripples in the torque and flux responses. The C-MPCC scheme is simple and has excellent dynamic performance. However, it is confined to the use of only one active voltage vector for an entire control interval and this leads to poor steady-state performance. The method developed in this paper aims to control a PMSM with a two-level VSI based on a simple duty ratio calculation. Most of the available duty methods have tedious slope and angle calculations which are parameter dependent. The proposed method uses a simple error-based duty calculation to control the torque and flux through the stator current. This retains the simplicity of the MPCC scheme while improving performance. The comparison of the proposed method with the C-MPCC scheme, MPCC [62], and MPCC[56] is performed both through simulation and real-time experimentation. The obtained results confirm the effectiveness of the method. Although the switching frequency of the inverter obtained is slightly more than that of C-MPCC, owing to the advantages of torque and flux ripple reduction and reduced computational burden, this increase is trivial. Further, the proposed method is robust to parameter variations that are experimentally validated.

Chapter 4

A Dual Voltage Vector-Based Low-Complex Model Predictive Current Control of PMSM drive

4. A Dual Voltage Vector-Based Low Complex Model Predictive Current Control of Permanent Magnet Synchronous Motor Drive

4.1 Introduction

In the previous chapter, a dual voltage vector-based MPCC for the PMSM drive was discussed. A total of seven voltage vectors must be used for the prediction and optimization steps in a two-level VSI-fed PMSM drive. In the C-MPCC scheme, the algorithm is updated during every sample period. Thus, the stator current prediction and sorting of the voltage vectors that minimize the cost function are carried out seven times in every control period. Hence, the iterative prediction and optimization stages occupy a substantial amount of time and increase the burden on the processor.

With the inclusion of the duty-modulation scheme to the MPCC scheme as in the previous chapter, the computational burden is increased. Thus, there is still scope for improving the duty-based control scheme by reducing the computational complexity. The proposed work aims to reduce the computational burden caused due to the iterative prediction and optimization stages of the C-MPCC while enhancing the steady-state drive performance. In this work, an effective dual voltage vector-based MPCC scheme with low complexity is proposed for a two-level VSI-fed PMSM drive.

The first objective is to reduce the number of voltage vectors utilized in every control period from seven to three. The proposed scheme does not require any sector or angle determination to achieve this aim. In order to realize this, in every sample time, voltage vector groups are formulated based on the previous sample time voltage vector and reference speed command. This results in a reduced computational burden while retaining the performance offered by C-MPCC. The second objective is to achieve enhanced steady-state performance for the computationally effective proposed MPCC by applying an active and null voltage vector in each sample time. The duty determination is based on the rms-ripple minimization technique and effectively reduces the ripples in flux and

torque. Moreover, the proposed method offers a reduced parameter-sensitive operation. The chapter has the following organization: Section-4.2 describes the proposed MPCC. Section 4.3 comprises of experimental results. Section-4.4 presents the summary.

4.2 Proposed dual vector based- MPCC for PMSM drive

The main drawbacks identified in a two-level VSI-fed PMSM drive employing the MPCC scheme are: (i) increased processor burden with the increase in the number of voltage vectors to be predicted and optimized in every sample time, (ii) large ripples in the steady-state torque and flux. To rectify the above shortcomings of the C-MPCC scheme, a simplified MPCC scheme with the duty modulation based on the rms-ripple reduction method is proposed. Figure 4.1 describes the functional diagram of the MPCC scheme employed in the present work.

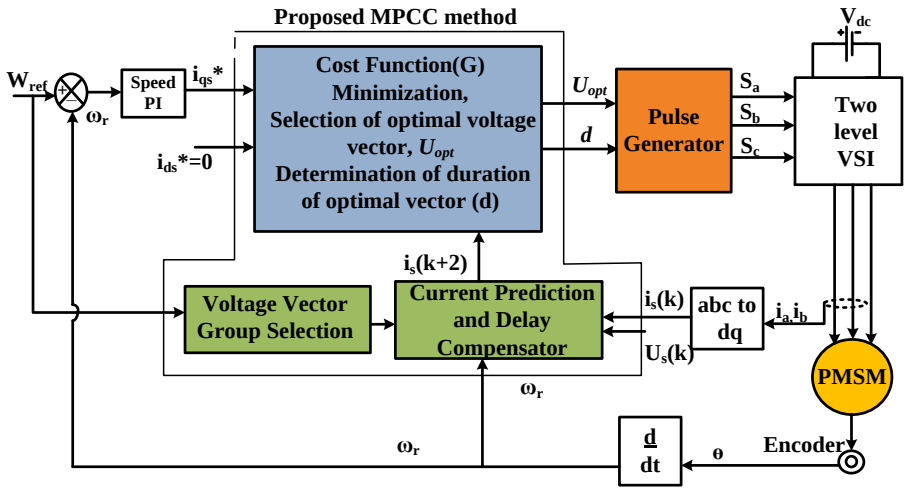

Figure 4.1 Functional diagram of the proposed MPCC.

4.2.1 Computational Burden Reduction:

In the C-MPCC method fed with two-level VSI, the cost function must be evaluated with seven different voltage vectors. The present method aims to employ only a group of three voltage vectors in every sample time based on the reference speed (W_{ref}) direction and the optimum voltage vector is selected from the obtained vector group (VG). This yields a substantial reduction in the computational burden pertaining to the steps involving prediction and optimization.

In the C-MPCC scheme, the voltage vectors tend to vary in a certain pattern in every cycle. The proposed method aims to replicate the C-MPCC scheme, where the voltage vectors vary in the sequence given in Figure 4. 2. When W_{ref} is in the counter-clockwise direction, the voltage vector tends to change in the forward direction. For example, v_1 is followed by v_2, further, v_2 by v_3, and so on as in Figure 4.2 (a). Similarly, when W_{ref} is in the clockwise direction, the voltage vectors tend to change in the reverse direction, i.e., v_7 is followed by v_6, v_6 by v_5 and so on as in Figure 4.2(c). This sequence is `observed to repeat in every cycle.

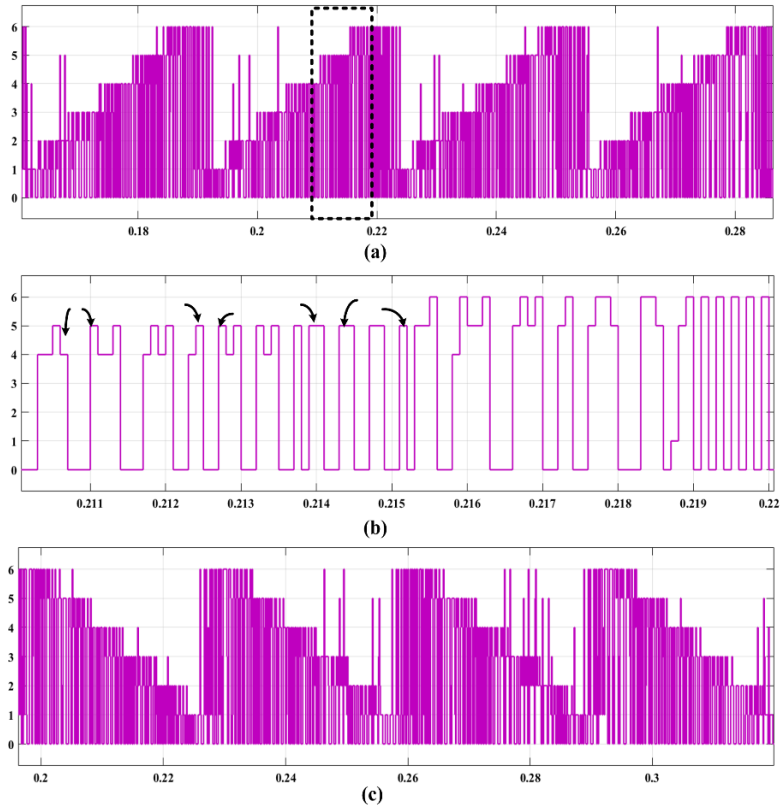

Figure 4.2 (a) voltage vector pattern in C-MPCC when W_{ref} is in counter-clockwise direction, (b) voltage vector variation when V_{prev} is null, (c) voltage vector pattern in C-MPCC when W_{ref} is in clockwise direction.

In the present scheme, the set of three voltage vectors is chosen in every sample time for computations based on the aforementioned sequence. The VGs are formulated based on the direction of rotation of the motor and the previous sample voltage vector (V_{prev}). If the previous sample voltage vector is a non-zero voltage vector, the VGs are framed based on V_{prev} as in Table 4.1.

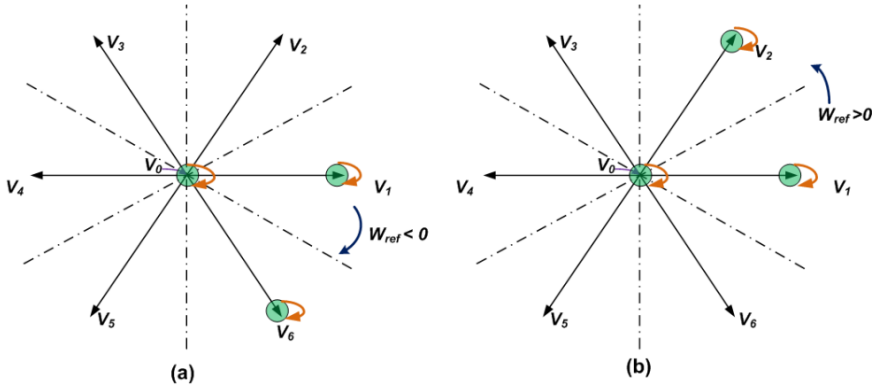

Figure 4.3 Vector group selection when: (a) W_{ref} is in counter- clockwise direction, (b) W_{ref} is in clockwise direction.

The VGs comprises of one null vector, $V_{prev,}$ and a voltage vector adjacent to it, based on the direction of rotation. However, in C-MPCC, if V_{prev} is a null voltage vector, the optimal voltage vector can typically be the last non-zero voltage vector (V_{n-z}) or the one adjacent to it. This is indicated in Figure 4.2 (b) with arrows. In this case, the VG will be selected from Table 4.1 based on V_{n-z}. The selection of voltage VG can be explained with the following example. Suppose, in the previous sample, the optimal voltage vector obtained is v_1, then the voltage vectors selected for computations are either v_0, $v_{1,}$ and v_2 or v_0, $v_{1,}$ and v_6, based on W_{ref} direction. This is represented in Figure 4.3.

Table 4.1 Proposed VG selection based on speed reference and previous voltage vector

ω_{ref} **counter-clockwise**		ω_{ref} **clockwise**	
V_{prev} **or** V_{n-z}	**VG**	V_{prev} **or** V_{n-z}	**VG**
v_1	[v_0,v_1,v_2]	v_1	[v_0,v_1,v_6]
v_2	[v_0,v_2,v_3]	v_2	[v_0,v_1,v_2]
v_3	[v_0,v_3,v_4]	v_3	[v_0,v_2,v_3]
v_4	[v_0,v_4,v_5]	v_4	[v_0,v_3,v_4]
v_5	[v_0,v_5,v_6]	v_5	[v_0,v_4,v_5]
v_6	[v_0,v_6,v_1]	v_6	[v_0,v_5,v_6]

During the dynamic speed changes, the voltage vectors are chosen based on the acceleration or deceleration condition. For example, if a sudden braking action is required, i.e., if both speed references are positive, the null voltage vector acts as the initial braking vector. Further, as the null-voltage vector is chosen to bring down the speed, VG based on the previous V_{n-z} is utilized for finding the optimum voltage vector in the next sample time. This selected VG contains a decelerating voltage vector, which can further aid the braking. A similar voltage vector selection also occurs during the speed reversal condition. As the voltage vector selection in the proposed method is inherited from the C-MPCC technique, an effective scheme

with low complexity can be achieved, while retaining the drive performance.

Table 4.2 Comparison of number of operations involved

Control Scheme	Task	No. of operations	Example
C-MPCC	Prediction	$(n)^h$	8
	Optimization	$(n)^h$	8
	Model	n	8
	Total	$\boldsymbol{(n)^h+(n)^h+n}$	**24**
Proposed method	Prediction	$(n')^h$	3
	Optimization	$(n')^h$	3
	Model	n'	3
	Total	$\boldsymbol{(n')^h+(n')^h+n'}$	**9**

The number of operations involved in the C-MPCC, as well as the proposed method, are compared in Table 4.2. While using a two-level three-phase inverter, the number of permissible voltage vectors, $n = 8$. For one prediction horizon (h=1), the total number of operations involved in prediction, optimization, and model evaluation becomes 24. However, in the proposed method, the number of voltage vectors used for prediction and optimization is n'=3. With the reduced number of voltage vectors, the total number of operations is reduced to 9. It can be observed from Table 4.2 that the proposed method eases the complexity with the reduced number of operations involved in prediction and optimization.

Hence, the present work offers an effective selection criterion based on the previous voltage vector applied and eliminates the need for sector or angle determination. VG is updated in every sample time based on the previously applied voltage vector, in the predetermined sequence. Moreover, simple comparisons are required to attain the VGs.

4.2.2 Improvement of the steady-state response of PMSM drive

When a single voltage vector is applied for the entire sample duration, flux and torque ripples will be more apparent, especially with the reduced number of voltage vectors. Thus, to enhance the performance of the proposed MPCC with the reduced number of voltage vectors, a simplified duty modulation scheme based on the rms-ripple reduction technique is evaluated in this section.

The square of the rms-current ripple, during the duration $T_{s,}$ is obtained as in (4.1).

$$I_{s\_ripple}^2 = \frac{1}{T_s}\int_0^{t_{opt}} (m_1 t + i_s(k+1) - i_s^*)^2\, dt$$

$$+ \frac{1}{T_s}\int_{t_{opt}}^{T_s} (m_0(t - T_s) + m_1 T_s + i_s(k+1) - i_s^*)^2\, dt \qquad (4.1)$$

where, t_{opt} is the active voltage vector duration for a control interval T_s. m_0 and m_1 are the slopes of stator current due to null and active voltage vectors as per Figure 4.4. i_s^* is the reference current and $i_s(k+1)$ is the predicted current at the $(k+1)$ instant. The optimum switching instant, t_{opt}, which minimizes the current ripple during the control period can be obtained by substituting the derivative of the square of rms-current to null, and this yields,

$$t_{opt} = \frac{2(i_s^* - i_s(k+1) - m_0 T_s}{2m_1 - m_0} \qquad (4.2)$$

The duty ratio can be obtained as,

$$d = \frac{t_{opt}}{T_s} \qquad (4.3)$$

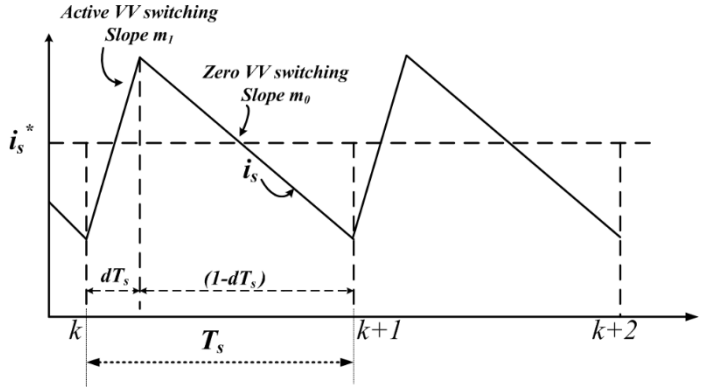

Figure 4.4 Stator current variation in a sample time.

From the mathematical model of SMPMSM, the stator current equation (4.4) can be obtained. The current slopes due to active and null voltage vectors can be obtained as in (4.5) - (4.7).

$$\frac{di_s}{dt} = \frac{1}{L_s}(u_s - R_s i_s - jw_r\psi_r) \qquad (4.4)$$

$$m_1 = \frac{di_s}{dt}|_{active} = \frac{u_s - R_s i_s - jw_r\psi_r}{L_s} \qquad (4.5)$$

$$m_o = \frac{di_s}{dt}|_{null} = \frac{-R_s i_s - jw_r\psi_r}{L_s} \qquad (4.6)$$

$$m_1 = m_0 + \frac{|u_s|}{L_s} \qquad (4.7)$$

To reduce the calculations involving current slopes, (4.2) is simplified.

Substituting (4.6) and (4.7) in (4.2) gives (4.8).

$$d = \frac{2|i_s^* - i_s(k+1)| + \frac{R_s i_s + e(k+1)}{L_s} T_s}{(m_0 + \frac{2|U_s|}{L_s})T_s} \tag{4.8}$$

Substituting equation (4.6) in (4.4) gives (4.9).

$$d = \frac{2|i_s^* - i_s(k+1)| + (\frac{U_s(k+1)}{L_s} - \frac{i_s^* - i_s(k+1)}{T_s})T_s}{(m_0 + \frac{2|U_s|}{L_s})T_s} \tag{4.9}$$

Assuming one step delay compensation and assuming $\varepsilon = |i_s^* - i_s(k+1)|$, (4.9) becomes,

$$d = \frac{2\varepsilon + (\frac{U_s(k+1)}{L_s})T_s - \varepsilon}{(m_0 + \frac{2|U_s|}{L_s})T_s} \tag{4.10}$$

$$d = \frac{\varepsilon + k}{m_0 T_s + 2k} \tag{4.11}$$

where, $k = |\frac{U_s(k+1)}{L_s}| T_s$, is a constant.

Thus, (4.11) shows the proposed duty calculation. As the duty ratio obtained in (4.2) involves the estimation of two current slopes in every sample time along with the current error, the computations increase. To reduce the computations, the proposed duty calculation eliminates the current slope involving the active voltage vector. The constant, *k,* in the duty ratio equation, can be pre-determined. Thus, the proposed method requires only the calculation of current error and the slope of current due to the null voltage vector in every sample time. The current slope due to the null voltage vector is significant as the null-voltage vector helps to reduce torque variations. Further, the elimination of one current slope helps to reduce the computations.

The proposed MPCC scheme is compared with the C-MPCC method and a low-complexity duty modulation [58] (LCDM [58]) method employing three voltage vectors, to confirm its effectiveness. In the LCDM [58] method, the error between the predicted and reference currents due to the null voltage vector is projected on the optimal voltage vector to decrease the number of voltage vectors. Further, the duty calculation is performed using the same projection technique. The method

exhibits a good response at low speed and has lower computational complexity. However, as the entire control is dependent on the projection of the current error on the optimal active voltage vector, the effect of machine parameters on the performance of the drive becomes prominent at high speed. The switching frequency is also increased in this method.

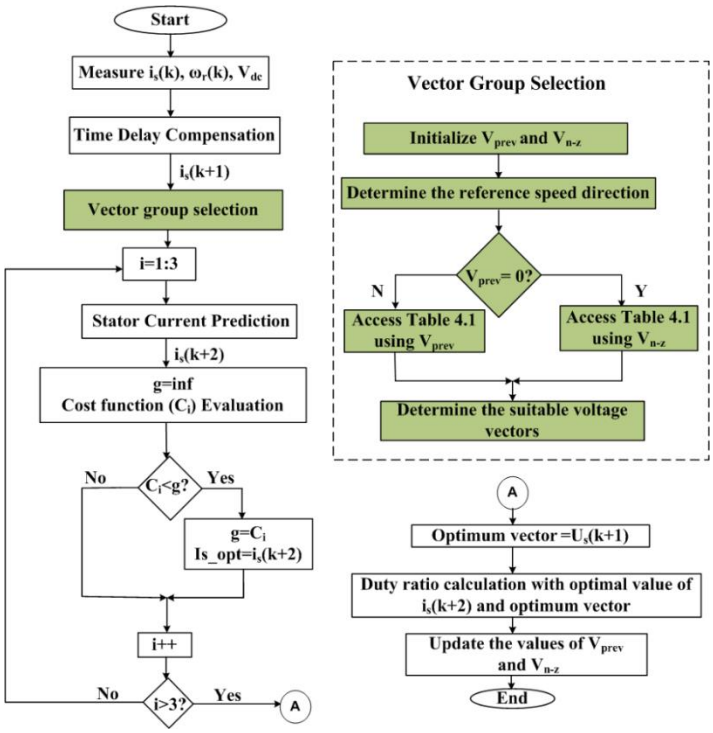

Figure 4.5 Flow chart of the proposed MPCC method.

The flow chart of the proposed scheme incorporating the two objectives is shown in Figure 4.5.

4.2.3 Advantages of the proposed method:

The merits of the present work on the MPCC scheme can be summarized as follows:

i. The number of voltage vectors to be predicted and optimized in every sample time is reduced from seven to three. The VGs are assigned in every sample, based on the previous sample optimum voltage vector and the speed reference direction. This achieves a considerable reduction in computational time.

ii. The switching transitions are minimized as the VGs utilize adjacent voltage vectors. These yields reduced switching frequency.

iii. The steady-state performance of the reduced voltage vector-based proposed MPCC is improved using a duty modulation scheme based on rms-ripple minimization.

iv. The proposed duty calculation requires the determination of only the current error and the current slope due to the null voltage vector. The constant involved in the calculation can be easily determined. The current slope due to the null voltage vector involved in the calculation is also significant in the reduction of torque ripples. Hence, the proposed scheme does not require any sector or angle determination, and the complex calculations are also eliminated.

v. The proposed duty calculation is directly proportional to the stator current error. The variations in torque and flux are thus implicated as variations in quadrature and direct-axis currents, respectively. This achieves good control over the torque and flux.

vi. The proposed method retains the drive performance offered by C-MPCC and is parameter insensitive.

4.3 Experimental Results

A 5 HP, 415 V, 1500 rpm, 4 pole PMSM drive fed with a three-phase, two-level VSI is used for the experimentation. LEM sensors are used to obtain the stator currents and DC link voltage. A 1024-point incremental encoder is utilized for the speed feedback. The dSPACE1104 interface is used to implement the predictive algorithm for the PMSM drive. The shaft of the PMSM is connected to a DC generator, which in turn is connected to a resistor bank for providing the electrical loading.

4.3.1 Steady-state Performance

The steady-state performance of the PMSM drive is investigated at very low (150 rpm) and high speeds (1400 rpm) as shown in Figure 4.6 and Figure 4.7, respectively. The torque, speed, and flux waveforms are included in all the steady-state results. The steady-state response of the drive with a load of 12 Nm, when operated at a speed of 1000 rpm is shown in Figure 4.8.

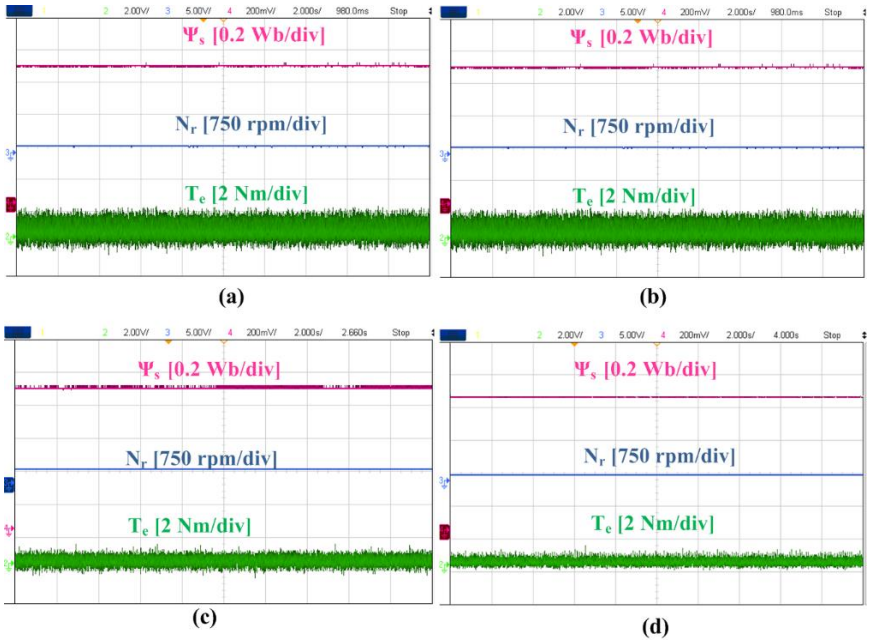

Figure 4.6 Steady-state response at 150 rpm speed. (a) C-MPCC, (b) PWDM, (c) LCDM [56] and (d) PEDM method.

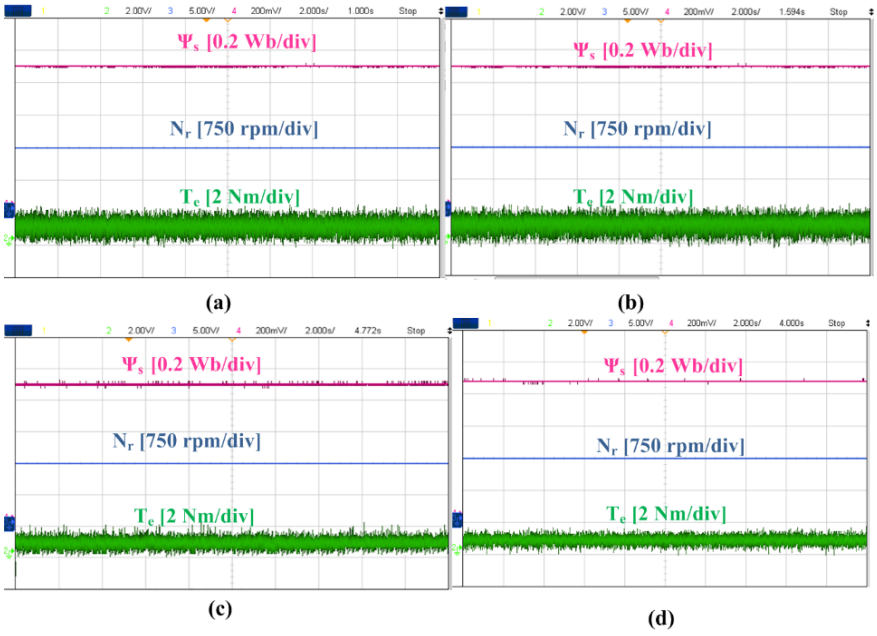

Figure 4.7 Steady-state response at 1400 rpm speed. (a) C-MPCC, (b) PWDM, (c) LCDM [56] and (d) PEDM method.

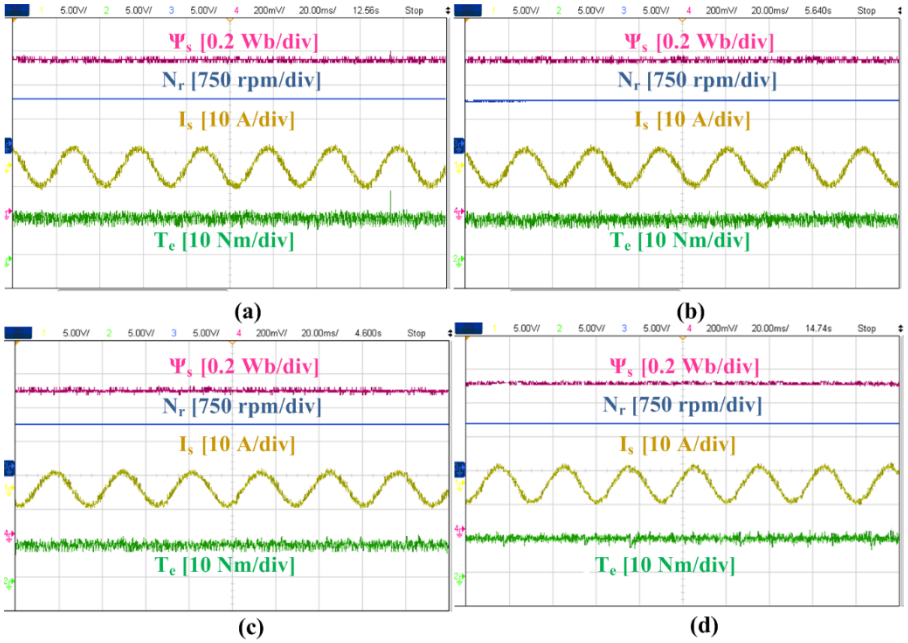

Figure 4.8 Steady-state drive performance with 50% load at a speed of 1000 rpm. (a) C-MPCC, (b) PWDM, (c) LCDM [56] and (d) PEDM method.

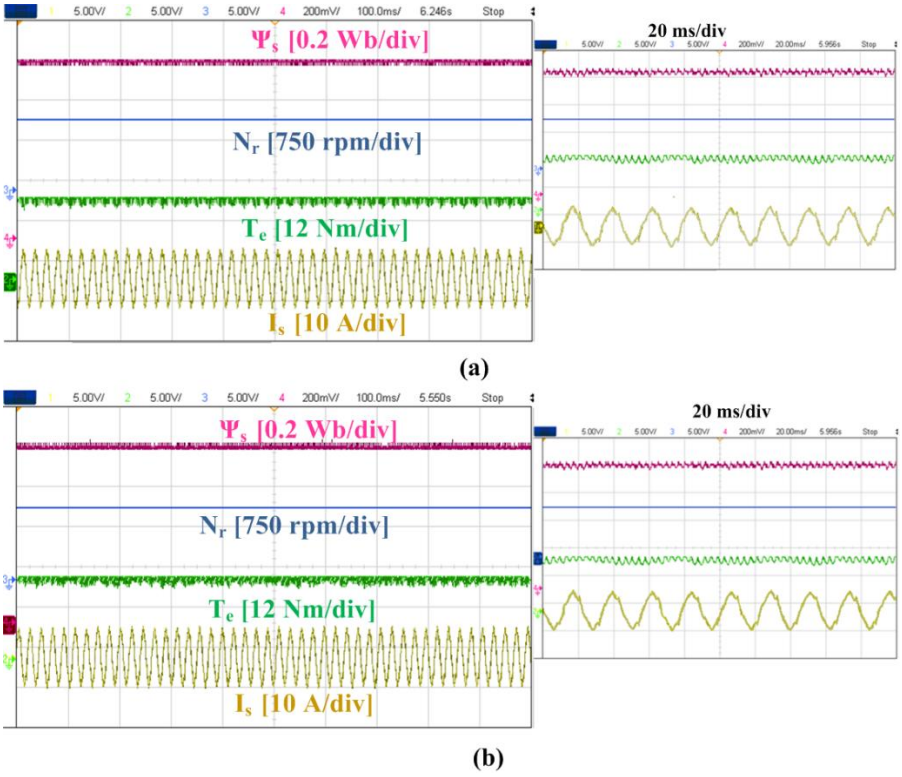

Figure 4.9 Steady-state drive performance with 100% load at rated speed. (a) C-MPCC, (b) PWDM.

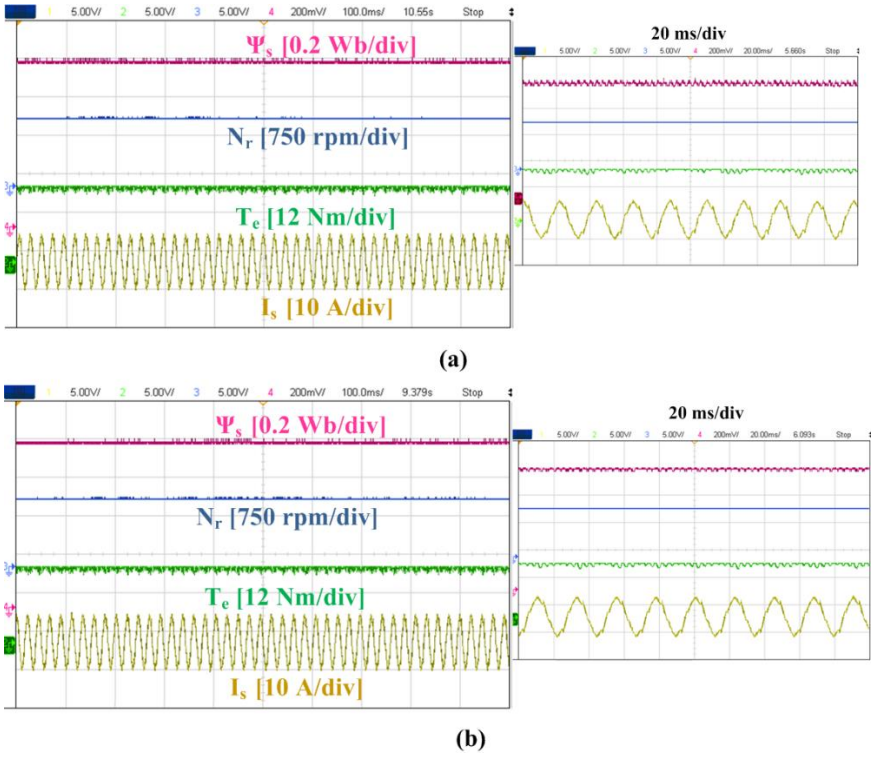

Figure 4.10 Steady-state drive performance with 100% load at rated speed. (c) LCDM [58], (d) PEDM method.

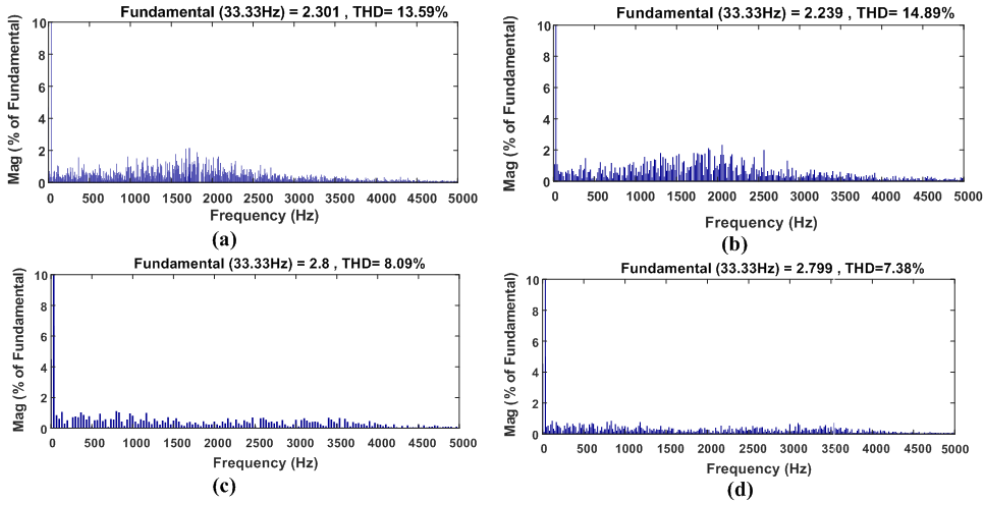

Figure 4.11 Stator current THD (a) C-MPCC, (b) PWDM, (c) LCDM [56], (d) PEDM methods.

It can be observed from all the results that the proposed method without duty modulation (PWDM) exhibits near identical performance to C-MPCC. Even though only three voltage vectors are selected in every control interval for the prediction and optimization stages, the performance of the drive is retained at all speeds. The proposed method employing the duty modulation (PEDM) method exhibits very less ripples in flux and torque compared to the C-MPCC, PWDM, and LCDM [56] method as it offers good control over both the direct-axis and the quadrature-axis stator currents.

Table 4.3 Comparison of steady-state performance of all methods

Method	**C-MPCC**		**PWDM**		**LCDM**[58]		**PEDM**	
Speed (rpm)	150	1400	150	1400	150	1400	150	1400
T_{e_rip} **(Nm)**	0.5257	0.4384	0.5291	0.4462	0.2871	0.2688	0.2643	0.2469
ψ_{rip} **(mWb)**	3.49	3.22	3.51	3.43	2.06	2.71	2.19	2.59
f_{sw} **(Hz)**	3985	2652	2438	1875	4215	3831	3766	3251

The ripples in torque and flux responses at different operating conditions during the steady-state operation are calculated based on the standard deviations and are presented in Table 4.3. To further ascertain the effectiveness of the proposed method, the machine is operated at rated speed with a full load. The steady-state performances for all the methods are obtained as in Figure 4.9 and Figure 4.10. The switching frequency obtained in LCDM [56] is greater than the PEDM method. In LCDM [56], the VV selection is based on a redundant VV elimination technique based on slopes. Thus, the LCDM [56] method requires more switching transitions than the PEDM method even though both methods utilize three VVs in every sample time. However, the PEDM method utilizes adjacent VVs during VG selection.

The stator current THDs for all the methods are shown in Figure 4.11. The PWDM technique has slightly more THD than C-MPCC due to the utilization of three voltage vectors. However, the PEDM shows a lower THD in stator current than C-MPCC, PWDM as well as LCDM [56] due to the application of dual voltage vectors in every sample time.

4.3.2 Dynamic Response

The C-MPCC, LCDM [56], PWDM, as well as PEDM, are subjected to forward speed change, reverse speed change, and load torque variations to verify the dynamic performance of the PMSM drive. In Figure 4.12, the dynamic response in the forward motoring condition is analyzed by altering the speed reference from 500 rpm to 1000 rpm. The speed reversal dynamics are also verified for all the methods. In order to achieve this, the speed is varied from 600 rpm to -600 rpm. The dynamic responses during speed reversal for all the methods are shown in Figure 4.13.

Further, the load dynamic performance during sudden load change from 0 to 50% of the rated torque value is verified. The performance of the drive during the load dynamics for all the methods is shown in Figure 4.14.

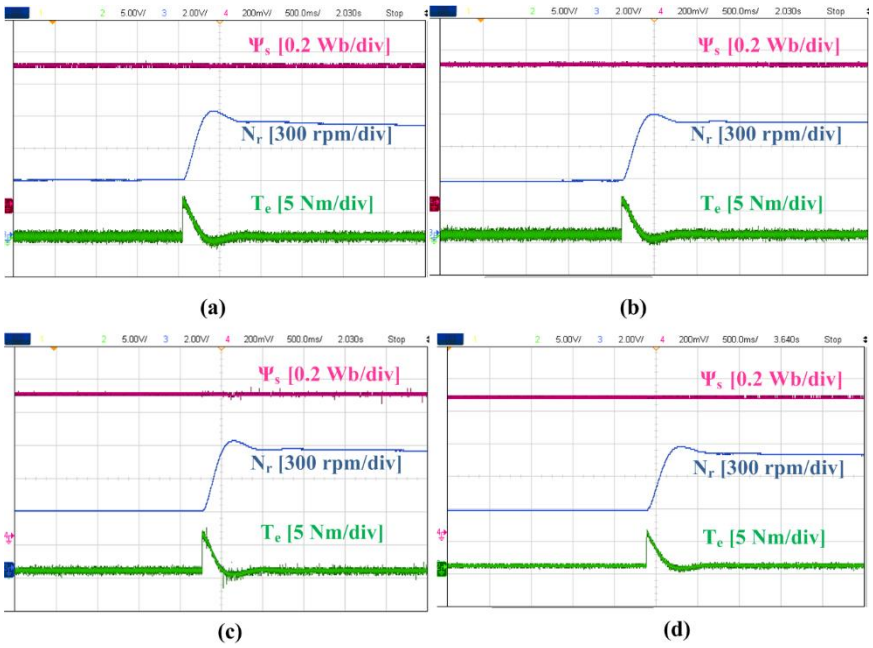

Figure 4.12 Dynamic drive performance corresponding to speed variation from 500 rpm to 1000 rpm. (a) C-MPCC, (b) PWDM, (c) LCDM [56] and (d) PEDM method.

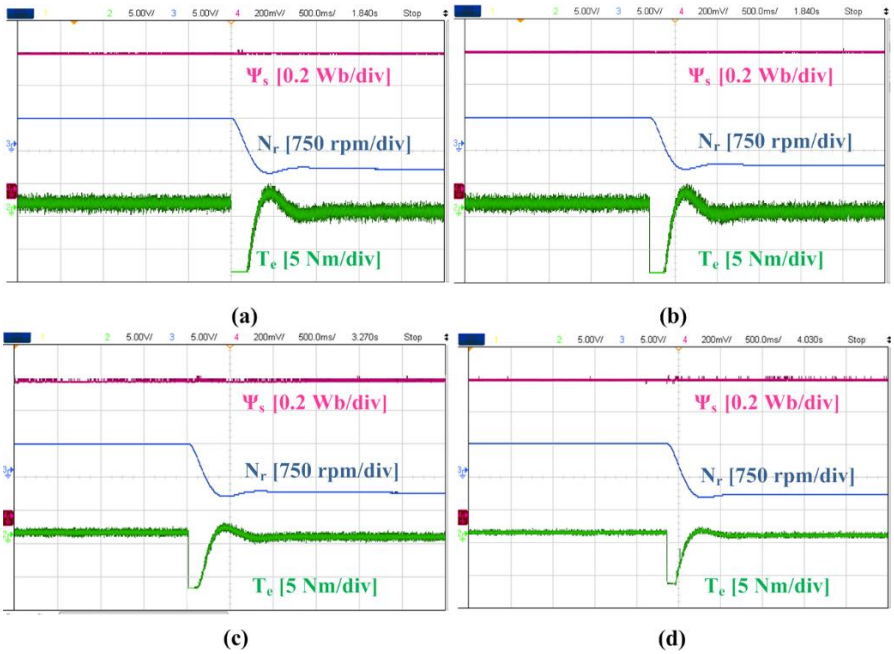

Figure 4.13 Dynamic drive performance corresponding to speed variation from 600 rpm to -600 rpm. (a) C-MPCC, (b) PWDM, (c) LCDM [56] and (d) PEDM method

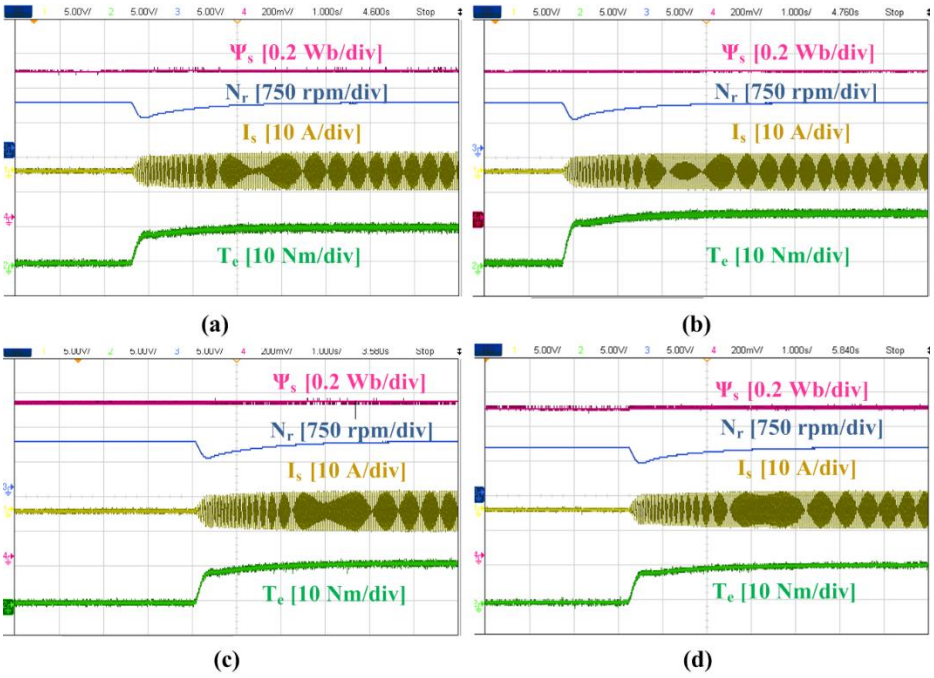

Figure 4.14 Dynamic response corresponding to step change in torque from 0 to 12 Nm. (a) C-MPCC, (b) PWDM, (c) LCDM [56] and (d) PEDM method.

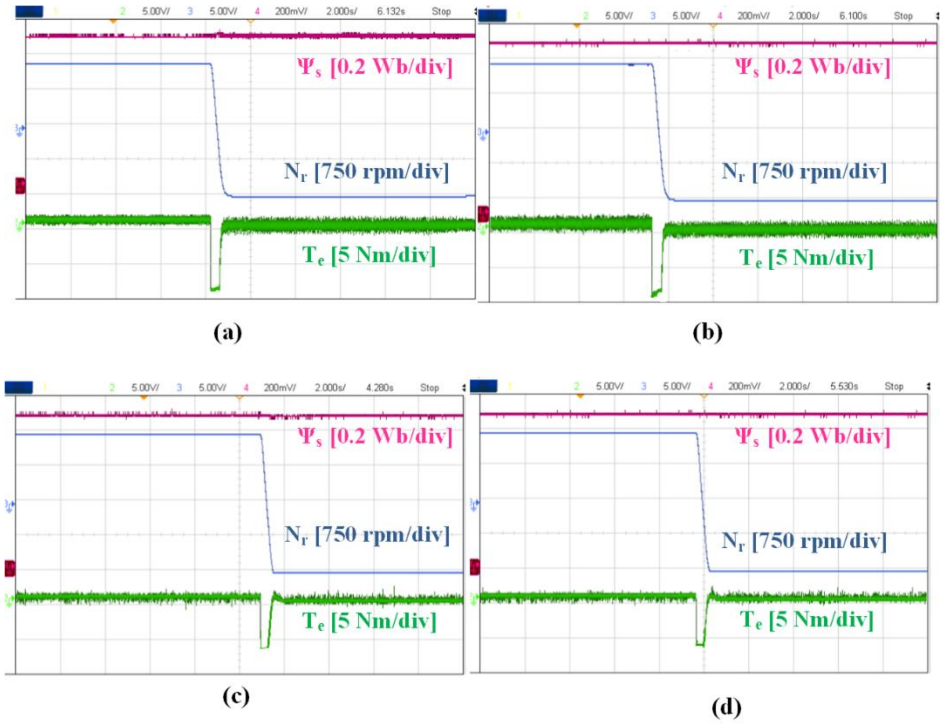

Figure 4.15 Rated speed reversal from 1500 rpm to -1500 rpm. (a) C-MPCC, (b) PWDM, (c) LCDM [56] and (d) PEDM method.

The rated speed reversal maneuver is shown in Figure 4.15. To analyze the dynamic response of the proposed method, a sudden change in speed from 1500

rpm to 750 rpm is applied. Figure 4.16 shows the performance of all methods during the decelerating mode.

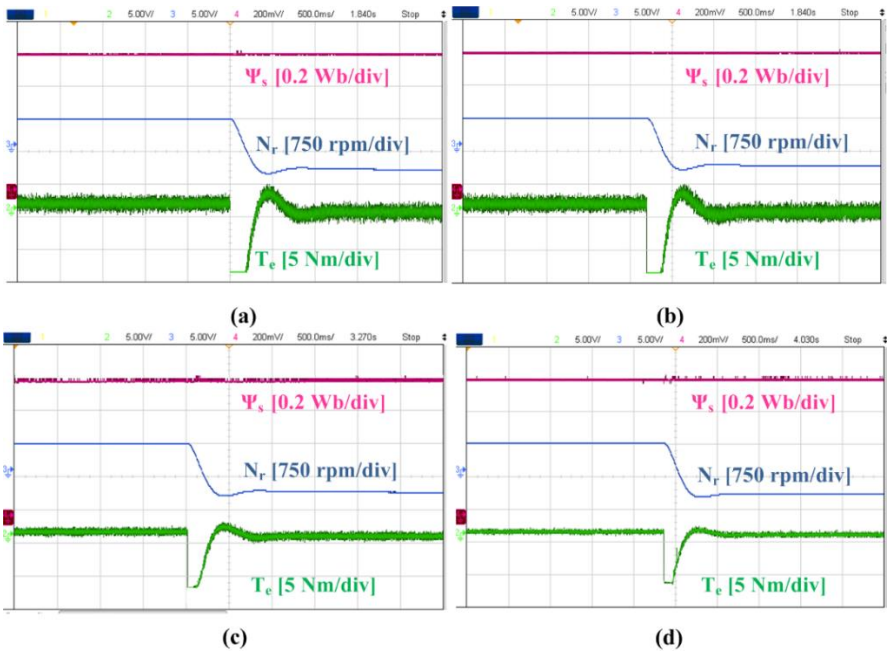

Figure 4.16 Speed reduction from 1500 rpm to 750 rpm (a) C-MPCC, (b) PWDM, (c) LCDM [56] and (d) PEDM method.

The voltage vectors chosen during the braking action are also shown in Figure 4.17(a). The sudden positive speed reduction can be explained with the following example. Suppose rapid braking is required, i.e., speed is reduced suddenly from 1500 to 750 rpm, the null-voltage vector is used for a larger duration to provide the braking torque as shown in Figure 4.17(b).

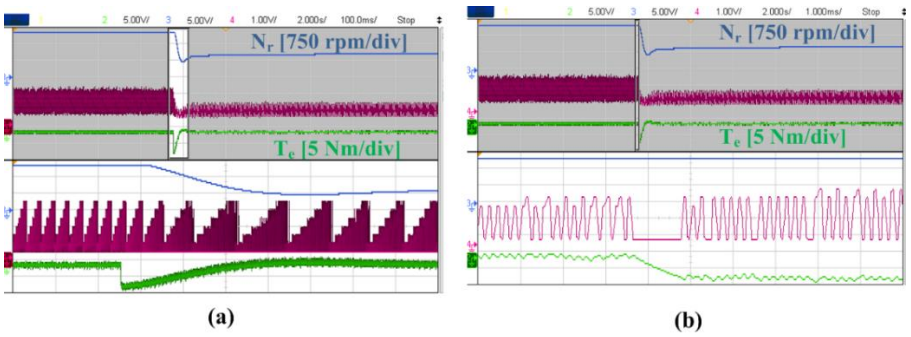

Figure 4.17 Speed reduction from 1500 rpm to 750 rpm for proposed method (a) voltage vectors during the speed change, (b) voltage vector used for braking action (magnified view).

As the null-voltage vector is used for the initial braking, the VG belonging to the previous non-zero voltage vector, $V_{n\text{-}z}$, is utilized for the next sample time. For instance, it can be observed from Figure 4.17(b) that due to null voltage vector

selection, $V_{n\text{-}z}$ vector used will be v_5 and the VG corresponding to v_5 selection is [v_0, v_4, v_5]. Now the proposed MPCC algorithm will apply voltage vectors v_4 and v_5 consequently with a null voltage vector to reduce the speed.

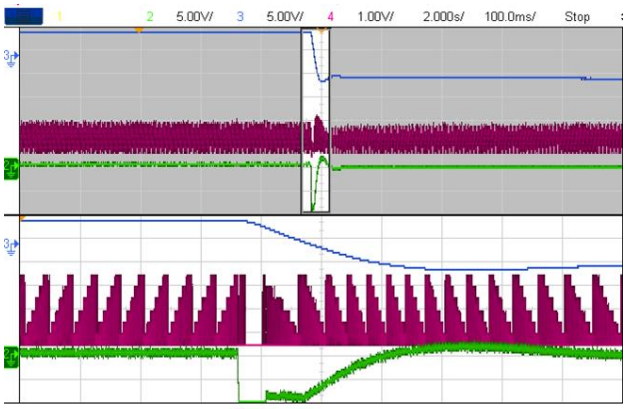

Figure 4.18 VVs during speed reversal from 750 rpm to -750 rpm for PEDM.

Similarly, the rated speed reversal dynamics can also be obtained as in Figure 4.18. Hence, it can be observed from the dynamic responses that all the methods exhibit similar performance.

4.3.3 Computational Time

The turnaround time is utilized as the criterion to calculate the computational burden, which can be directly obtained from the control desk. The turnaround time incorporates the time required for the communication between the processor and control desk, analog to digital and digital to analog conversion, code implementation, and data saving. The turnaround time required for each model part of the real-time program is tabulated in Table 4.4.

Table 4.4 Computational performance of C-MPCC and Proposed methods

Terms	Parameter	C-MPCC		PWDM		PEDM	
		No. of calculations	t_c (µs)	No. of calculations	t_c (µs)	No. of calculations	t_c (µs)
Measurement	$i_s(k)$, $u_s(k)$, ω_r , θ_r	-	4.76	-	4.76	-	4.76
Estimation	$i_s(k+1)$	1	1.21	1	1.21	1	1.21
Prediction and optimization	$i_s(k+2)$, C, g_{opt}	21	36.05	9	17.2	9	17.2
Vector group selection, duty calculation	$[v_o,v_i,v_j],d$	-	-	7	11.8	9	13.75
Total (µs)			**42**		**35**		**36.75**

Table 4.5 Computational time of MPCC methods.

Method	C-MPCC	LCDM[58]	PWDM	PEDM
Time (μs)	42	38	35	36.75

The computational time is represented as 't_c'. It can be observed that there is a considerable reduction in the computations involving prediction and optimization in PWDM. The C-MPCC evaluates the cost function for each discrete switching state. However, in PWDM, this is reduced to three times, which effectively reduces the computational complexity involved with C-MPCC. The C-MPCC method requires 42 μs, whereas the LCDM [56] method takes 38 μs. The PWDM technique requires 35 μs and PEDM takes up 36.75 μs. Thus, the proposed method requires less computational time (t_c) than the C-MPCC and LCDM [56] methods. The turn-around time obtained for all methods is shown in Table 4.5.

4.3.4 Parameter Variation Analysis

The PMSM drive performance under erroneous motor parameter assumption is analyzed in this section. Figure 4.19 shows the performance of the LCDM [56] and PEDM techniques with stator resistance and inductance increased by 30%. As the influence of stator-inductance is more pronounced at high speeds, the PMSM drive is operated at rated speed to analyze the parameter sensitivity of the methods. It is evident from Figure 4.19 that the effect of stator resistance and inductance change is much less in the proposed scheme. However, the LCDM [56] method has more sensitivity towards parameter variations at high speed, as the method exhibits an increased ripple in the torque response after the parameter change. The LCDM [56] method uses the stator inductance parameter in the duty calculation, which makes it parameter sensitive, especially at high speeds.

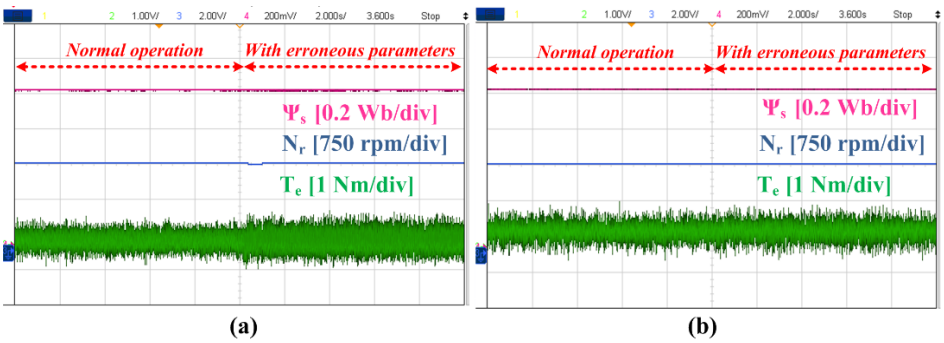

(a) (b)

Figure 4.19 Performances during parameter variations (a)LCDM [56] (b) PEDM.

On the other hand, the PEDM method calculates the active voltage vector duration based on the rms-current ripple minimization technique and exhibits lower sensitivity to the machine parameter changes. The proposed scheme retains the performance even with erroneous motor parameters. Thus, a robust, low-complex control can be obtained using the proposed MPCC scheme, in addition to the considerable reduction in the steady-state ripples.

4.3.5 Analysis of Experimental Results

Table 4.3 presents the ripples in torque and flux as well as switching frequency at low and high speeds for all the methods. The PWDM method has a lower switching frequency than C-MPCC as the algorithm is forced to follow the sequence involving fewer switching transitions. However, the reduced number of voltage vectors leads to a slight increase in ripples under steady-state operation. This can be negated by employing the PEDM method, which reduces up to 50% of the torque ripples existing in the C-MPCC and PWDM methods. Further, the torque ripples are 8% lower in the PEDM method when compared to the LCDM [56] method. The flux ripples are 30% and 7% less than C-MPCC and LCDM [56], respectively in the PEDM method. Due to the sequential voltage vector selection, the switching frequency of PEDM is also lesser than the LCDM [56] method. The torque and flux responses are effectively improved by applying an active and null voltage vector in each sample time. The duration of the optimal voltage vector is directly proportional to the current error in the PEDM method. The torque variations are redirected as the variation in quadrature-axis current, whereas the variation in flux will be replicated as a variation in direct-axis current. As the error between predicted and reference current increases, the duty correspondingly adjusts to reduce the ripples, realizing a better steady-state response.

4.4 Summary

In the present work, a simplified and effective duty-modulated MPCC scheme with low complexity is employed to address the limitations of the C-MPCC i.e., computational complexity with an increase in the number of voltage vectors and the large ripples in the flux and torque. C-MPCC scheme employs seven voltage vectors in every control period for the prediction and optimization stages, which leads to the deployment of a fast processor with a large data handling capacity. The algorithm gets updated every sample time and increases the processor burden.

Further, the C-MPCC method is confined to the use of only a single voltage vector during the entire control period, which inversely affects the steady-state drive performance. The proposed method achieves a less complex MPCC scheme with duty modulation for a two-level VSI-fed PMSM drive. The scheme utilizes only three voltage vectors for prediction and optimization. It should be noted that with a reduced number of voltage vectors, the control solution obtained is not always the optimal one, but it is sometimes sub-optimal. However, it is compensated by the additional benefit of a reduction in the computational burden. Moreover, an effective duty modulation based on the rms-current ripple minimization technique is proposed to attain a better steady-state response of the drive. The duty calculation does not require any complex calculations while retaining the dynamic drive performance. The effectiveness of the proposed scheme is validated through experiments and further ascertained through comprehensive comparisons with C-MPCC and LCDM [56] methods. The proposed method offers a parameter-insensitive duty calculation.

Chapter 5

A Multivector Based Model Predictive Current Control of PMSM drive for Improved Torque and Flux Performance

5. A Multivector Based Model Predictive Current Control of PMSM drive for Improved Torque and Flux Performance

5.1 Introduction

In the previous chapter, a low complex dual voltage vector-based MPCC for PMSM drive was presented. The computational time was effectively reduced and the steady-state response was improved using the dual voltage vector application. However, it can be observed that with a reduced number of voltage vectors, the control solution obtained is not always the optimal one, for it is sometimes sub-optimal. Hence, if enhanced control precision is required, multiple vectors should be applied in a sample time.

In the present work, a multi-vector-based MPCC is proposed for the speed control of a two-level voltage source inverter-fed PMSM drive, to improve steady-state torque and flux response. The multi-vector operation is obtained using an extended control set (ECS) that utilizes two adjacent-active voltage vectors with an appropriate distribution coefficient. However, the augmentation of the control set catalyzes an undesirable increase in the computational burden. To address this limitation, a look-up table-based voltage vector pre-selection scheme using the stator current error is employed. Further, the present work aids in improving the steady-state torque and flux response of PMSM through optimization of the amplitude of the candidate voltage vector based on the average current error minimization principle. Moreover, the proposed scheme does not require SVPWM to determine the duration of the candidate voltage vector. Thus, the algorithm is less complex, offers a better steady-state response than conventional MPCC, and preserves dynamic performance.

The chapter has the following organization: Section-5.2 describes the proposed MPCC. Section 5.3 comprises experimental results. Section-5.4 presents the summary.

5.2 Proposed Multivector based-MPCC of PMSM

In C-MPCC, irrespective of the magnitude of error between the reference and predicted stator current, the application of the optimum voltage vector for an entire control period results in large pulsations in torque and flux. It is clear from Figure 5.1. that the application of multiple optimum voltage vectors in a sample time yields fewer ripples in the steady-state output response.

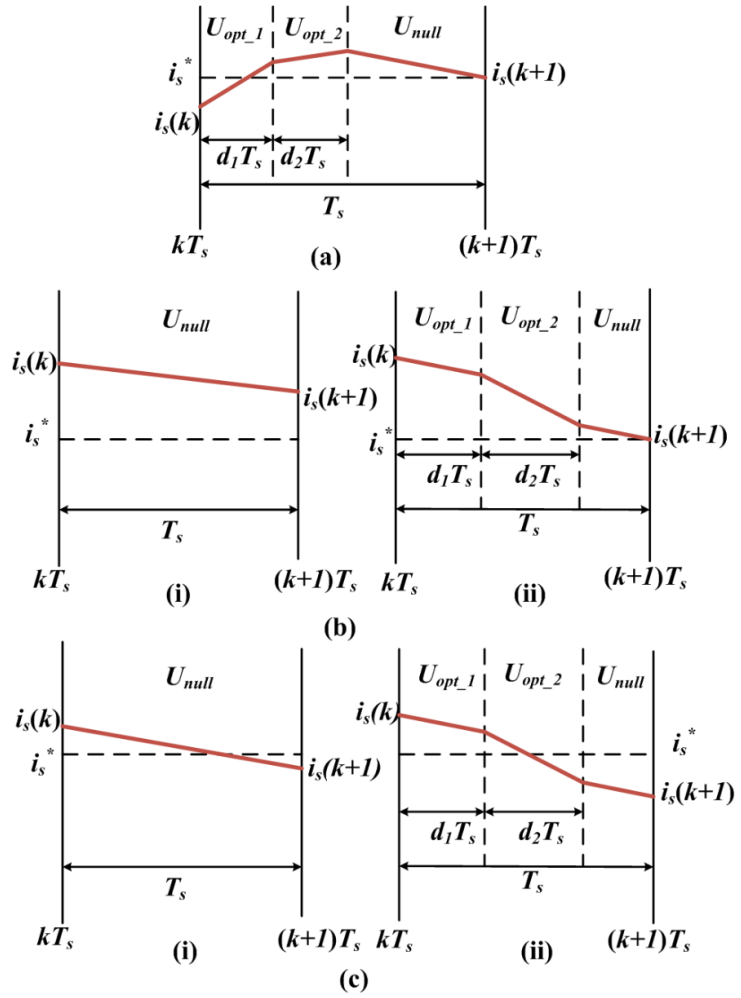

Figure 5.1 Stator current response: (a) when estimated current is lower than the reference current, (b) when estimated current is higher than the reference current with large initial error (i) with null voltage vector (ii) with two active and a null voltage vector

For instance, if the estimated current is lower than the reference stator current (Figure 5.1 (a)), two adjacent voltage vectors with increasing stator current slope followed by the null voltage vector can result in a minimum error. Similarly, if the estimated current is higher than the reference stator current with a large initial current error as in Figure 5.1 (b), the application of two adjacent voltage vectors with

decreasing current slope followed by a null voltage vector can be utilized. However, if the estimated current is higher than the reference stator current with a small initial current error as in Figure 5.1 (c), the null voltage vector itself is sufficient to bring down the error as the application of two active voltage vectors can bring the current response further below the reference. Based on this concept, the proposed method is framed to apply multiple voltage vectors using the stator current error.

The functional block diagram of the proposed MPCC scheme is given in Figure 5.2. The stages involved in the proposed scheme are broadly presented in the following description.

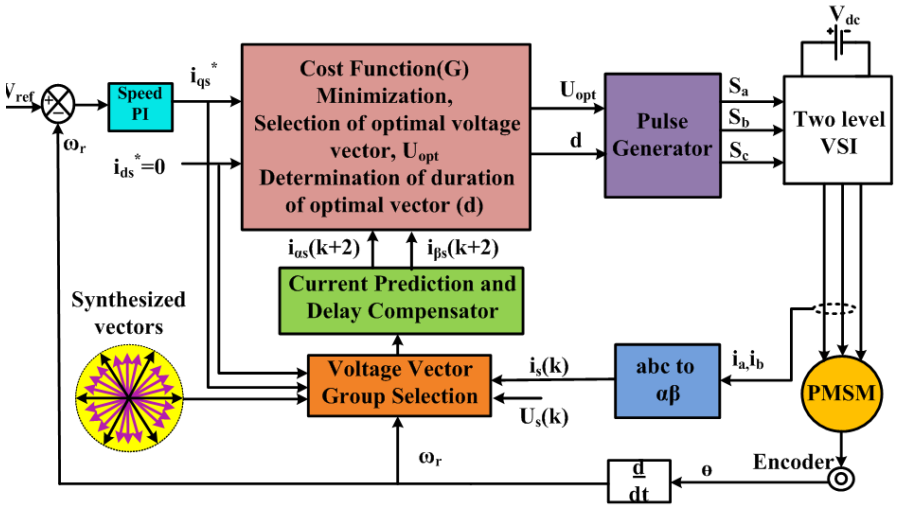

Figure 5.2 Functional block diagram of the proposed MPCC

5.2.1 Synthesis of virtual voltage vectors

In the MPCC algorithm of the PMSM drive operated with a two-level VSI, the control set (CS) contains eight switching states. The switching states can be transformed into eight voltage vectors, where, two voltage vectors are null vectors and the six active voltage vectors possess both amplitude as well as fixed phase as shown in (8).

$$V_i = \frac{2}{3} V_{dc} e^{j(i\frac{\pi}{3} - \frac{\pi}{3})} \qquad i = 1,2\ldots6 \tag{5.1}$$

In the MPCC scheme, with the inclusion of additional voltage vectors in CS, it is possible to achieve precise control of output torque and flux using multi-vectors. For instance, by synthesizing '*n*' virtual voltage vectors between every two active voltage space vectors (VV), the CS can be augmented by $6\times n$ additional voltage vectors. In a continuous control set-based MPCC scheme, the three-phase duty ratio

is obtained using the SVPWM technique. However, the proposed method utilizes a simple voltage vector synthesis scheme and the duty ratio of ECS-voltage space vectors (ECS-VV) is determined after the optimization process.

In the present work, the stationary α-β plane is distributed into six sectors with one principal active VV (V_{prin}) in every sector, similar to the C-MPCC scheme. The ECS-VVs are synthesized using two adjacent active VVs. The synthesis equation is given in (5.2).

$$V_{syn} = (1 - d_n)V_m + d_n V_n \tag{5.2}$$

where, d_n is the distribution coefficient of the active VVs, $d_n \in [0,1]$. As the virtual VVs are distributed at equal phase angles in every sector, for '*n*' VVs between two adjacent active VVs, d_n assumes values $0, \frac{1}{n+1}, \frac{2}{n+1} \ldots \frac{n}{n+1}, 1$ in the counter-clockwise direction. If *n*=1, there will be six additional VVs with two VVs in the boundary of every sector. However, there will be only two additional virtual VVs in every sector. Similarly, if *n*=2, two virtual VVs are available in every sector, even though boundary VVs are absent. Consequently, in the proposed scheme, *n* is chosen as three. This would ensure two VVs at the boundary and a total of four additional VVs in every sector.

In the present work, *n* is limited to 3 so that the implementation complexity and computations are not further elevated while improving the performance of the drive. Therefore, in the proposed scheme, CS is composed of six active VVs, two null VVs, and 18 virtual VVs, i.e., 26 VVs in its ECS. Figure 5.3 shows the VV diagram after including the virtual VVs in CS.

Table 5.1 shows the synthesized VVs and the corresponding distribution coefficients when three virtual VVs exist between two adjacent-active VVs. For instance, to synthesize the second virtual VV that exists in the counter-clockwise direction between adjacent active VVs V_1 (V_m) and V_2 (V_n), choose d_2=0.5. The resulting vector is obtained according to (5.2) as, $V_9 = 0.5V_1 + 0.5V_2$ Substituting the values of V_1 and V_2 from (5.1), it can be observed that the amplitude of V_9 is $0.577V_{dc}$, which is 0.866 times that of the active VVs and displaced by an angle of 30° from the stationary α-axis.

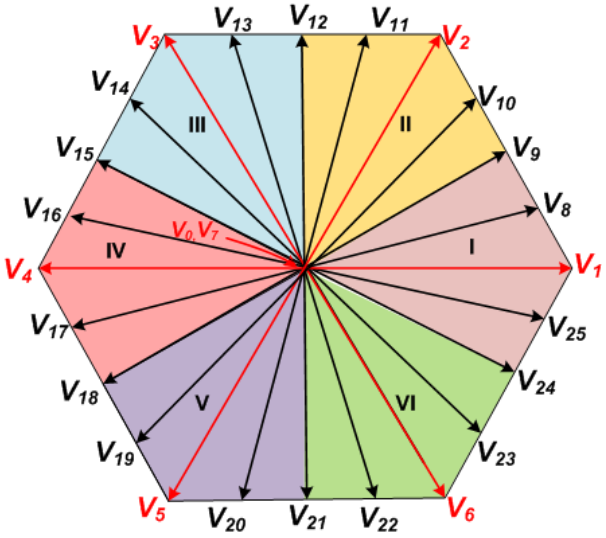

Figure 5.3 VVs obtained after including the virtual VVs to CS.

Table 5.1 Proposed Virtual VV synthesis

Active VVs		**Virtual VV Synthesized**		
Vm	***Vn***	***d1=0.25***	***d2=0.5***	***d3=0.75***
V_1	V_2	V_8	V_9	V_{10}
V_2	V_3	V_{11}	V_{12}	V_{13}
V_3	V_4	V_{14}	V_{15}	V_{16}
V_4	V_5	V_{17}	V_{18}	V_{19}
V_5	V_6	V_{20}	V_{21}	V_{22}
V_6	V_1	V_{23}	V_{24}	V_{25}

In the proposed scheme, the number of prediction and optimization operations required in every sample period is more than thrice that of the C-MPCC scheme due to the augmented CS. Consequently, it leads to the requirement of a higher sampling time. In order to reduce the burden on the processor, a low-complex VV selection scheme is adopted in the present work. From the Direct Torque Control (DTC) concept, the stator flux error ($\Delta\psi_s$) for a control period T_s can be obtained as,

$$\Delta\psi_s = \psi_s^* - \psi_s(k) = U_s^* T_s \tag{5.3}$$

where, U_s^* is the reference VV. However, it can be observed that stator current is directly proportional to stator flux. Neglecting the influence of stator resistance, (5.3) can be modified based on (2) and (6) as,

$$\Delta i_s = i_s^* - i_s(k) = (U_s^* - e(k))\frac{T_s}{L_s} \tag{5.4}$$

where, $\Delta i_s = \Delta i_{\alpha s} + j\Delta i_{\beta s}$ and $e(k) = jw_r\psi_r$. Thus, similar to stator flux error, the stator current error (Δi_s) is directly proportional to U_s^*. Hence, the estimation of the

position of the stator current error can be inferred as the estimation of the U_s^* position. This reduces the hassles involved with parameter-sensitive reference VV determination while replicating the control action achievable using U_s^*.

The present work thus employs a VV preselection scheme based on the error between the reference and predicted stator current, (Δi_s). To filter out the dispensable VVs involved in the proposed scheme with 26 VVs, a VV pre-selective scheme with a reduced number of candidate VVs for the prediction and optimization stage is utilized, which is hereafter referred to as PMPCC.

Subsequent to the conventional sector distribution, one active VV (V_{prin}) with a fixed magnitude and fixed phase exists in every sector. Although the proposed scheme generates 4 virtual voltage vectors in every sector, it is unessential to evaluate the cost function using all the vectors included in a sector as some of the vectors may not realize the optimum current error. For instance, if Δi_s lies ahead of the V_{prin}, while grouping it is unnecessary to include the VVs that lie behind V_{prin}, i.e., the ECS-VVs in the clockwise direction of V_{prin}.

Similarly, when Δi_s is positioned in the clockwise direction of V_{prin}, the VVs in the anticlockwise direction of V_{prin} are not included in the VV group during preselection. To identify the position of Δi_s with respect to V_{prin}, a simple gradient-based calculation is utilized. The VV preselection forms a group of VVs in the counter-clockwise direction of $V_{prin,}$ if the gradient of Δi_s is greater than V_{prin}. Similarly, VVs in the clockwise direction of the V_{prin} are selected when the gradient of Δi_s is less than V_{prin} as given in Table 5.2. This evades the chances of selecting sub-optimal VVs, even though a restricted number of VVs are used in the prediction and optimization stage. Thus, the proposed VV selection aids in replicating the dynamic performance of the C-MPCC scheme, with improved control accuracy.

The following steps are involved in the VV selection in the PMPCC scheme.

vii. Determine the stator current error, Δi_s and find the sector in which it lies.

viii. To select the appropriate VVs, the following criterion is utilized. Group of VVs in the counter-clockwise direction of V_{prin} (including V_{prin}) are selected when:

$$(\Delta i_{\beta s} \times V_{prin\_\alpha}) > (\Delta i_{\alpha s} \times V_{prin\_\beta}) \tag{5.5}$$

ix. Similarly, the group of VVs in the clockwise direction of V_{prin} (including V_{prin}) is selected if:

$$(\Delta i_{\beta s} \times V_{prin\_\alpha}) < (\Delta i_{\alpha s} \times V_{prin\_\beta}) \tag{5.6}$$

For instance, if Δi_s lies in the second sector of the α-β plane, the VV groups selected can be either [V_2, V_{11}, V_{12}] or [V_2, V_9, V_{10}] based on (12) and (13), respectively. VV selection based on (5.5) is shown in Figure 5.4.

The look-up table shows the VV groups developed for the proposed VV selection.

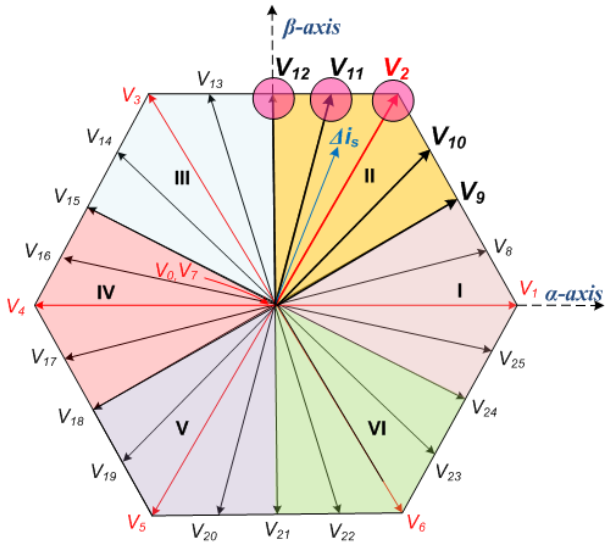

Figure 5.4 VV selection based on (5.5).

Table 5.2 PMPCC voltage space vector selection

Sector	**Voltage vector selection**		
	V_{prin}	**(5.5) is true**	**(5.6) is true**
I	V_1	[V_1, V_8, V_9]	[V_1, V_{24}, V_{25}]
II	V_2	[V_2, V_{11}, V_{12}]	[V_2, V_9, V_{10}]
III	V_3	[V_3, V_{14}, V_{15}]	[V_3, V_{12}, V_{13}]
IV	V_4	[V_4, V_{17}, V_{18}]	[V_4, V_{15}, V_{16}]
V	V_5	[V_5, V_{20}, V_{21}]	[V_5, V_{18}, V_{19}]
VI	V_6	[V_6, V_{23}, V_{24}]	[V_6, V_{21}, V_{22}]

In a two-level three-phase VSI, the number of VVs involved is m=8. Considering a short-prediction horizon, h=1, the number of tasks required in model evaluation, prediction, and optimization sum up to 24. However, the number of operations involved in the proposed method with 26 VVs with m'=26 becomes 78. Thus, the number of operations in the proposed method with all ECS-VVs is increased by more than three times the C-MPCC scheme. However, by employing the PMPCC scheme (m''=3), a reduced number of operations is required, i.e., the total number of tasks is curtailed to 9. Table III shows the number of tasks involved in each scheme. PMPCC uses a VV grouping that sorts out the essential VVs using the conventional two-level sector scheme. Even though a restricted number of VVs are utilized for

prediction and optimization steps, the selected group is sufficient to meet the control requirements, while easing the complexity of the algorithm.

Table 5.3 Operations involved in control schemes

Technique	Task	No. of Operations	Example
C-MPCC	Predictions	$(m)^h$	8
	Optimizations	$(m)^h$	8
	Model	m	8
	Total	$\boldsymbol{(m)^h+(m)^h+m}$	**24**
Proposed method with 26 VV	Predictions	$(m')^h$	26
	Optimizations	$(m')^h$	26
	Model	m'	26
	Total	$\boldsymbol{(m')^h+(m')^h+m'}$	**78**
Proposed method with 3 VV (PMPCC)	Predictions	$(m'')^h$	3
	Optimizations	$(m'')^h$	3
	Model	m''	3
	Total	$\boldsymbol{(m'')^h+(m'')^h+m''}$	**9**

As three adjacent ECS-VVs are grouped in every sample time for obtaining optimum VV, the control freedom to achieve faster dynamics during transients is guaranteed, although, under steady-state operation, error minimization is given priority. Further, with more VVs available in proximity, more accuracy in control can be achieved. Thus, the PMPCC scheme effectively replicates the proposed scheme with 26 VVs.

5.2.2 Optimization of candidate ECS vector amplitude

Among all the VVs based on ECS, the optimal vector has the best control over output torque and flux. However, if a null VV is added to the optimal ECS-VV, the amplitude of the shortlisted VV can be adjusted and further improvement can be achieved in the steady-state performance. Succinctly, to enhance the performance of the drive, it is essential to determine the duration for which optimal ECS-VV must be applied. The effect of active VV and ECS-VV on the current error can be analyzed using Figure 5.5 and Figure 5.6, respectively. Consider that Δi_s lies in the second sector of the stationary α-β plane. In the C-MPCC scheme, VV V_2 will be selected as the optimal VV, which minimizes the cost function as shown in Figure 5.5. However, with the deployment of an augmented CS, the virtual VV V_{10} will be chosen as the optimum ECS-VV as shown in Figure 5.7. The placement of null VV employed in the C-MPCC and PMPCC scheme for amplitude optimization is shown in Figure 5.5 and Figure 5.6, respectively. This ensures the application of optimum

ECS-VV for the optimum duration and the rest of the period is allotted to the null VV to bring down the ripple. With the amplitude of V_{10} modified according to the optimum duration, effective and precise control can be obtained by applying three VVs (say, V_1, V_2, and V_0). Further, tighter control can be obtained with the proposed scheme as compared to the C-MPCC scheme since voltage vectors are available in closer proximity to the reference current vector. This results in a reduced steady-state current error and hence enhances the steady-state performance of the drive.

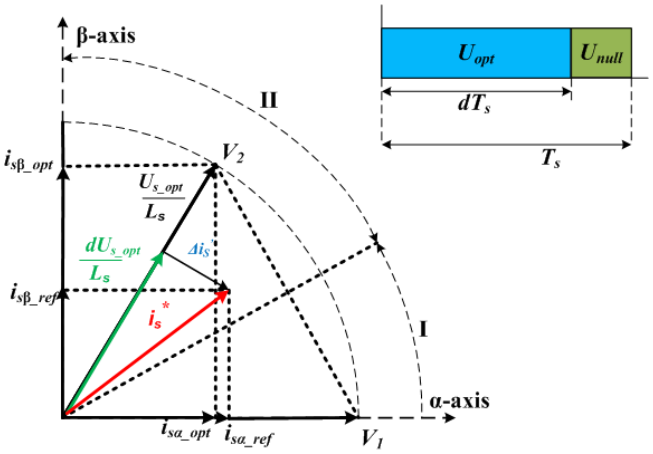

Figure 5.5 Effect of adding a null vector to active VVs in C-MPCC scheme.

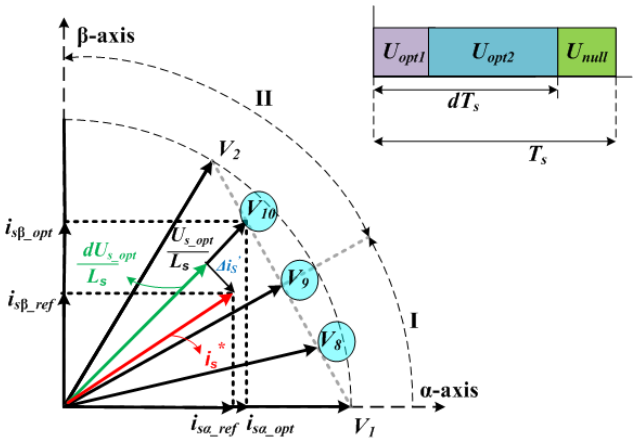

Figure 5.6 Effect of adding a null vector to proposed ECS-VV.

The duration of application of ECS-VV to minimize the control variable error is determined using the average current error minimization technique. Considering the average current at the $(k+1)^{th}$ instant to be equal to the reference value of stator current over the entire cycle (Figure 5.7), (5.8) is obtained.

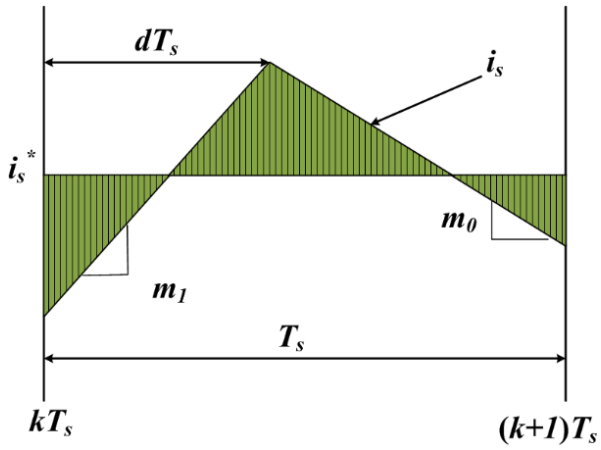

Figure 5.7 Variation of stator current in a control period.

$$\frac{1}{T_s}\int_{kT_s}^{(k+1)T_s} i_s dt = \frac{1}{T_s}\int_{kT_s}^{(k+1)T_s} i_s^* dt \tag{5.8}$$

The rate of change of stator current can be obtained as in (5.9), where, back emf, $e = jw_r\psi_r$

$$\frac{di_s}{dt} = \frac{1}{L_s}(u_s - R_s i_s - e) \tag{5.9}$$

$$m_1 = \frac{di_s}{dt}|_{active} = \frac{u_s - R_s i_s - e}{L_s} \tag{5.10}$$

$$m_0 = \frac{di_s}{dt}|_{null} = \frac{-R_s i_s - e}{L_s} \tag{5.11}$$

$$m_1 = m_0 + \frac{|u_s|}{L_s} \tag{5.12}$$

From (14), the optimum ECS-VV duration can be obtained as,

$$dT_s = T_s - \sqrt{\frac{T_s}{m_1 - m_0}(2(I_s^* - I_s(k)) + m_1 T_s)} \tag{5.13}$$

Applying one-step delay compensation,

$$d = 1 - \sqrt{\frac{1}{(m_1 - m_0)T_s}(2(I_s^* - I_s(k+1)) + m_1 T_s)} \tag{5.14}$$

Replacing $(I_s^* - I_s(k+1)) = \Delta i_s$,

$$d = 1 - \sqrt{\frac{1}{(m_1 - m_0)T_s}(2\Delta i_s + m_1 T_s)} \tag{5.15}$$

where, $\Delta i_s = \Delta i_{\alpha s}(k+1) + j\Delta i_{\beta s}(k+1)$

(5.16) can be obtained from (5.12).

$$(m_1 - m_o)T_s = \frac{|U_{opt}|T_s}{L_s} = k \tag{5.16}$$

Substituting (5.16) in (5.15) and replacing m_1, (5.17) can be obtained.

$$d = |1 - \sqrt{\frac{2\Delta i_s + m_0 T_s}{k} + 1}| \tag{5.17}$$

The value of constant 'k' can be predetermined to alleviate the parameter sensitivity. It can be observed from (5.17) that optimum ECS-VV is applied for a duration that relies upon the difference between the control variables.

The advantage offered by multi-vector application as shown in Figure 5.1. can be analyzed with the help of the VV diagram for the proposed scheme. The vector diagrams are drawn based on the stator current equation, neglecting the effect of resistance. Figure 5.8. shows the VV diagram when the estimated current is less than the current reference.

For instance, let the optimal VV that can reduce the error between the reference and predicted current be V_8, which is composed of V_1 and V_2 with increasing current slopes. By applying the optimal ECS-VV for the optimum duration, the steady-state error can be reduced, as shown in Figure 5.8. (b). Figure 5.9. shows the VV diagram when the estimated current is higher than the reference current with a large initial error.

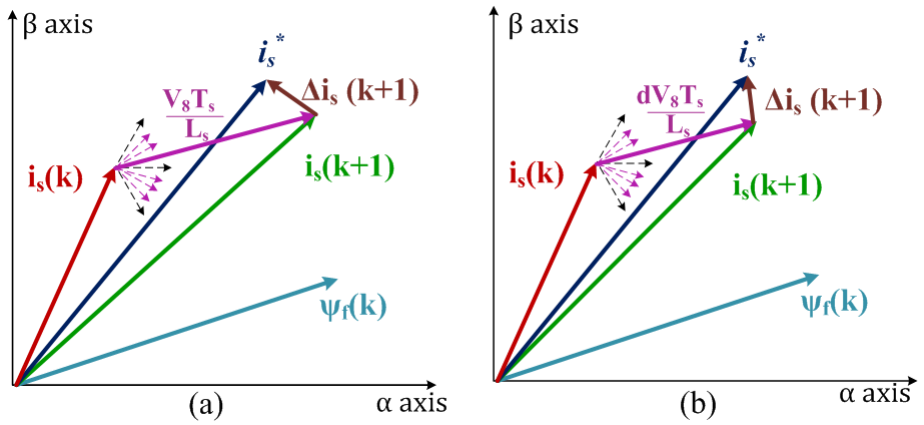

Figure 5.8 VV diagram when estimated current is lower than the reference current (a) with only ECS-VV (b) with optimized amplitude of ECS-VV.

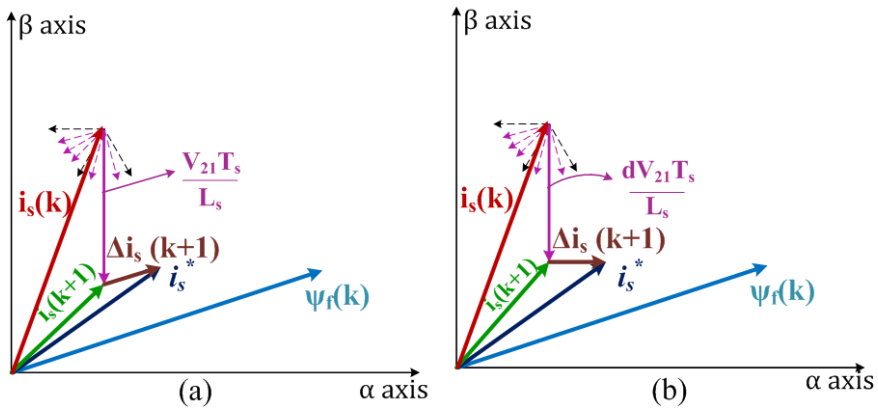

Figure 5.9 VV diagram when estimated current is higher than the reference current with large initial error (a) with only ECS-VV (b) with optimized amplitude of ECS-VV.

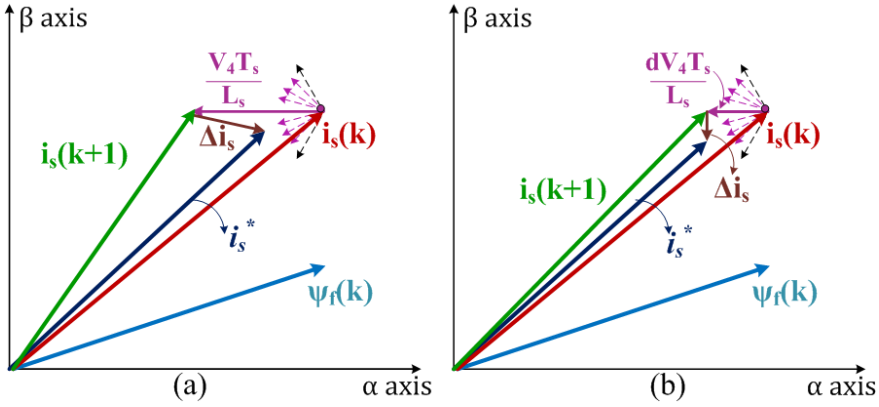

Figure 5.10 VV diagram when estimated current is higher than the reference current with small initial error(a) with only active VV (b) with optimized amplitude of VV.

Let V_{21} composed of V_5 and V_6 with a negative current slope be the optimum ECS-VV. The error between the reference and predicted current is effectively reduced with the addition of null VV to V_{21}. Similarly, Figure 5.10 shows the VV diagram when the estimated current is more than the reference current by a small margin. In this case, the PMPCC scheme will apply the active VV, say, V_4 for the optimum duration, and the rest of the period is allotted for the null VV. Thus, based on the error, it is possible to apply at least two VVs (V_{prin} and null VV) or at most three VVs (synthesized ECS-VV and null VV) in a sample time to reduce the steady-state ripples.

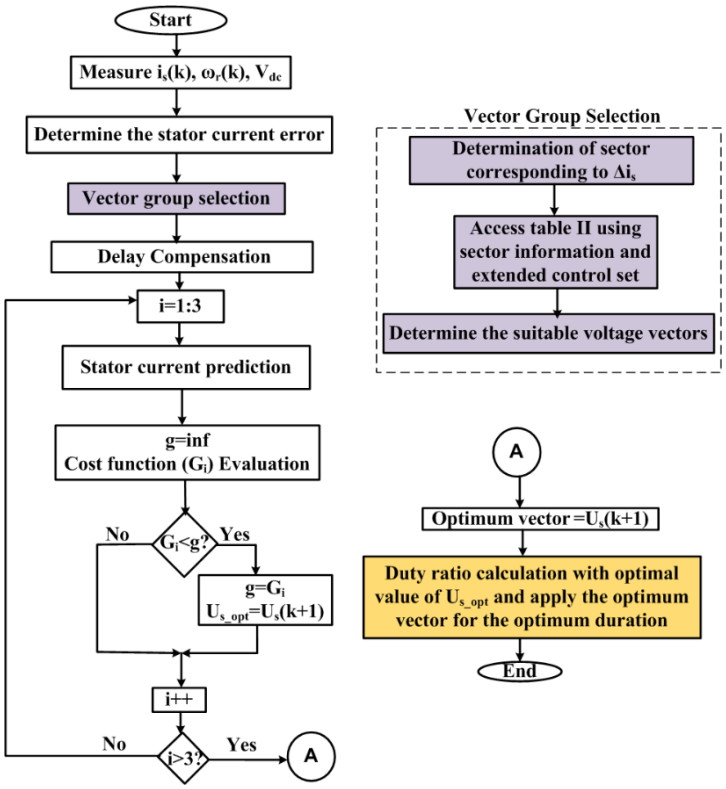

Figure 5.11 PMPCC method flow chart.

Figure 5.11. shows the flow chart of the PMPCC method. The VV grouping in PMPCC requires the estimation of the sector of Δi_s, which improves the precision of VV preselection.

5.3 Experimental Results

A 5 HP, 4 pole, 415 V, 1500 rpm PMSM operated with a two-level VSI is utilized for analyzing the feasibility of the PMPCC using a dS1104 processor. The DC link voltage and stator currents are sensed using LEM sensors and speed feedback is externally obtained using a 1024 points incremental encoder. The load is fed from a DC generator connected to the resistor bank, attached to the shaft of the PMSM. The sampling frequency of 10 kHz is utilized for all the methods. To analyze the performance of the PMPCC method, the steady-state and dynamic responses obtained in the present work are compared with a Duty-modulated MPCC scheme and the ECS-MPCC [79] scheme at different speeds and load conditions. In DMPCC [58] the duty ratio is calculated by projecting the deviation between the reference and predicted current due to null VV onto the optimal VV, which minimizes the cost function. In ECS-MPCC [77], the control set is expanded by including six additional

VVs, and two generalized base VVs are applied in every sample time.

The steady-state performance of the PMSM drive is evaluated under different speed and load conditions. The drive response is analyzed at different speeds and load conditions to affirm the effectiveness of the PMPCC scheme. The motor is loaded by 20%, 50%, 75%, and 100% of the rated load at different speeds. Figure 5.12 shows the steady-state response of the motor-operated at 250 rpm and 20% load. The drive response at 500 rpm- 5 Nm load and 500 rpm -10 Nm load are shown in Figure 5.13 and Figure 5.14, respectively.

Further, Figure 5.15 shows the performance at 1000 rpm-12 Nm load. The performance at 750 rpm-18 Nm load is shown in Figure 5.16. The performance at 20% of the rated load and full load at the rated speed of 1500 rpm is shown in Figure 5.17 and Figure 5.18, respectively. The flux, speed, torque, and current waveforms are shown in Figure 5.12 to Figure 5.18.

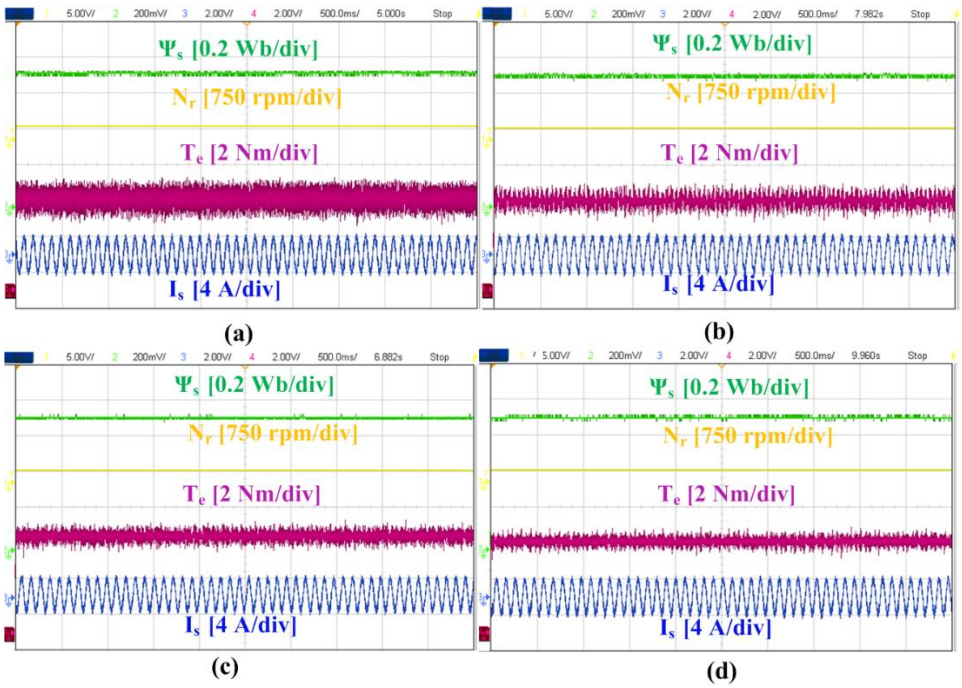

Figure 5.12 Response under steady-state condition with 20% load at 250 rpm speed (a) C-MPCC, (b) DMPCC [58], (c) ECS-MPCC [77], (d) PMPCC.

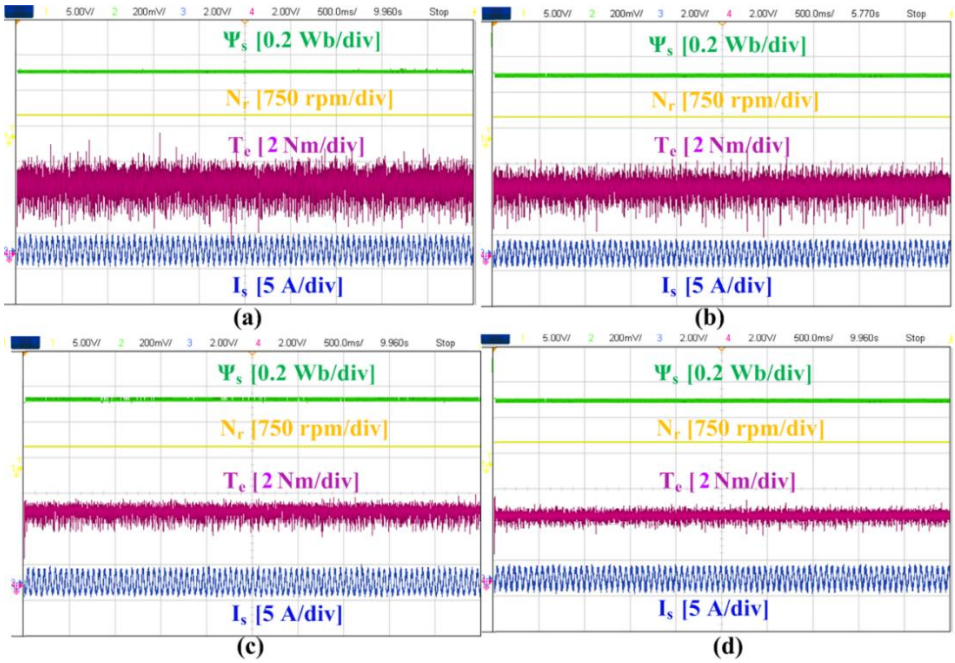

Figure 5.13 Response under steady-state condition with 20% load at 500 rpm speed (a) C-MPCC, (b) DMPCC [56], (c) ECS-MPCC [77], (d) PMPCC.

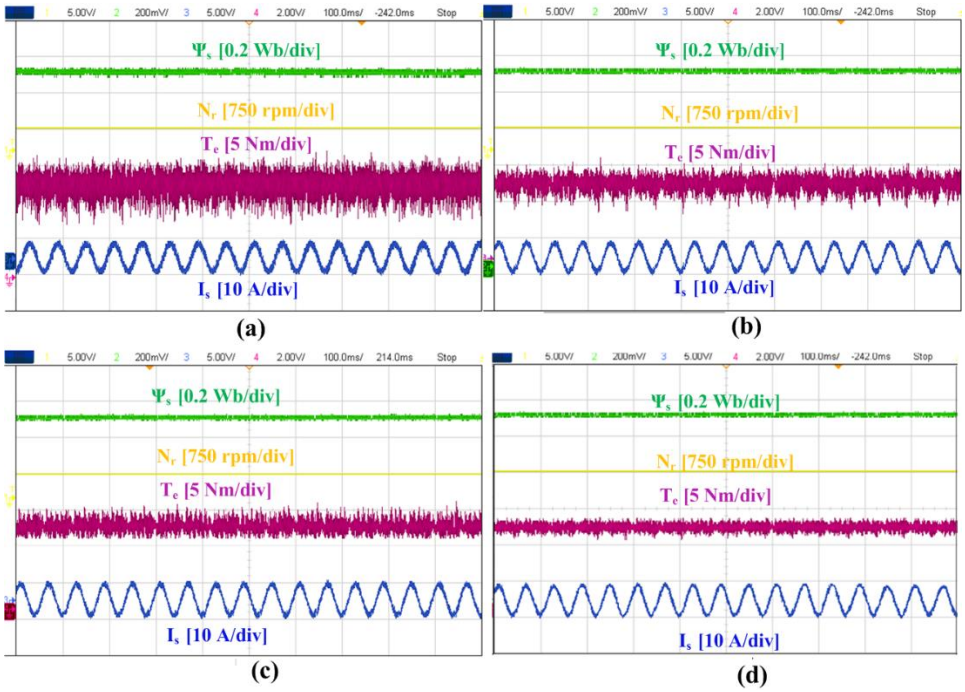

Figure 5.14 Response under steady-state condition with 10 Nm load at 500 rpm speed (a) C-MPCC, (b) DMPCC [56], (c) ECS-MPCC [77], (d) PMPCC.

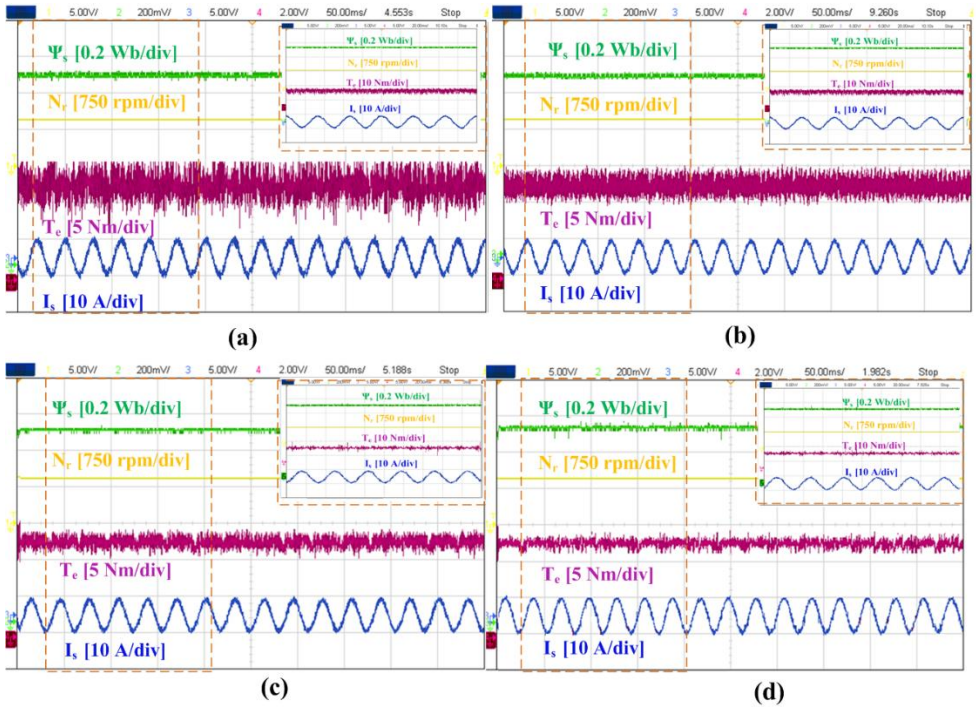

Figure 5.15 Response under steady-state condition with 12 Nm load at 1000 rpm speed (a) C-MPCC, (b) DMPCC [56], (c) ECS-MPCC [77], (d) PMPCC.

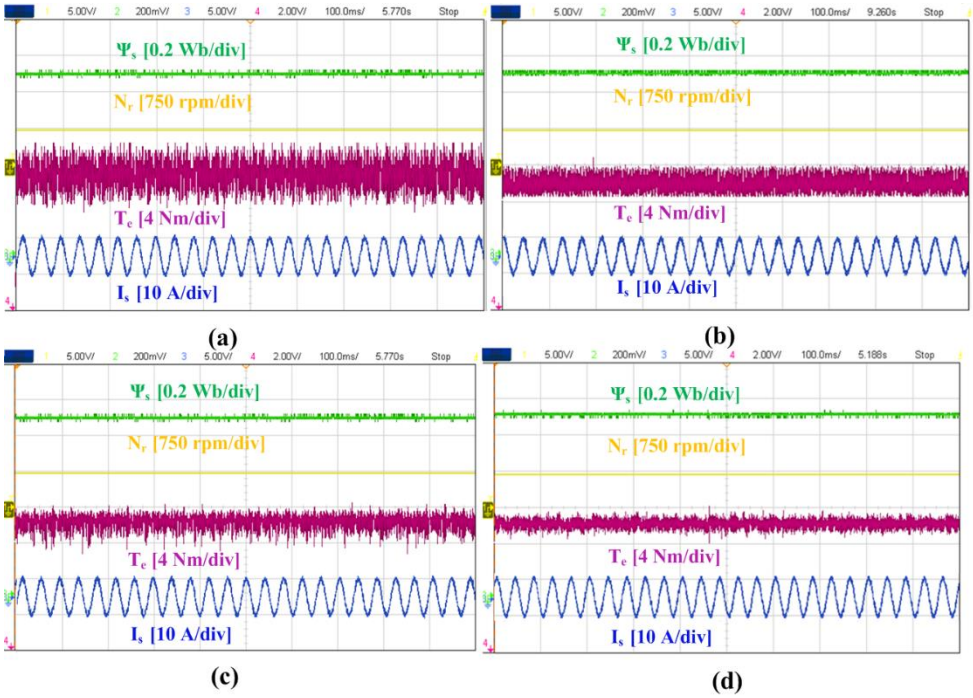

Figure 5.16 Response under steady-state condition with 75% of rated load at 750 rpm speed (a) C-MPCC, (b) DMPCC [56], (c) ECS-MPCC [77], (d) PMPCC.

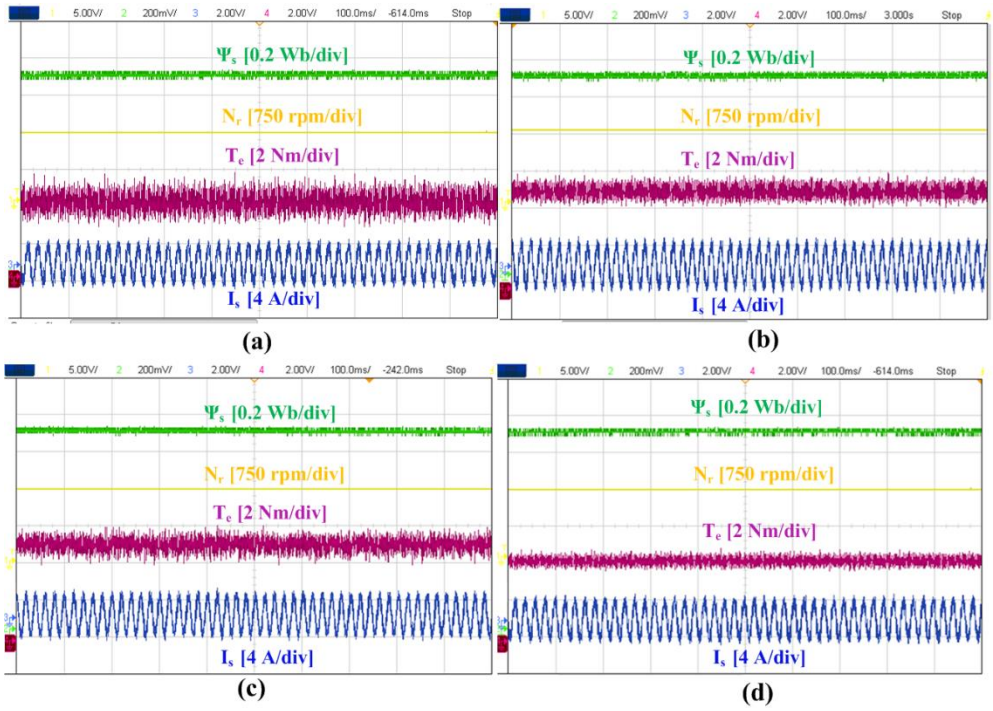

Figure 5.17 Response under steady-state condition at rated speed and 20% of rated load (a) C-MPCC, (b) DMPCC [56], (c) ECS-MPCC [77], (d) PMPCC.

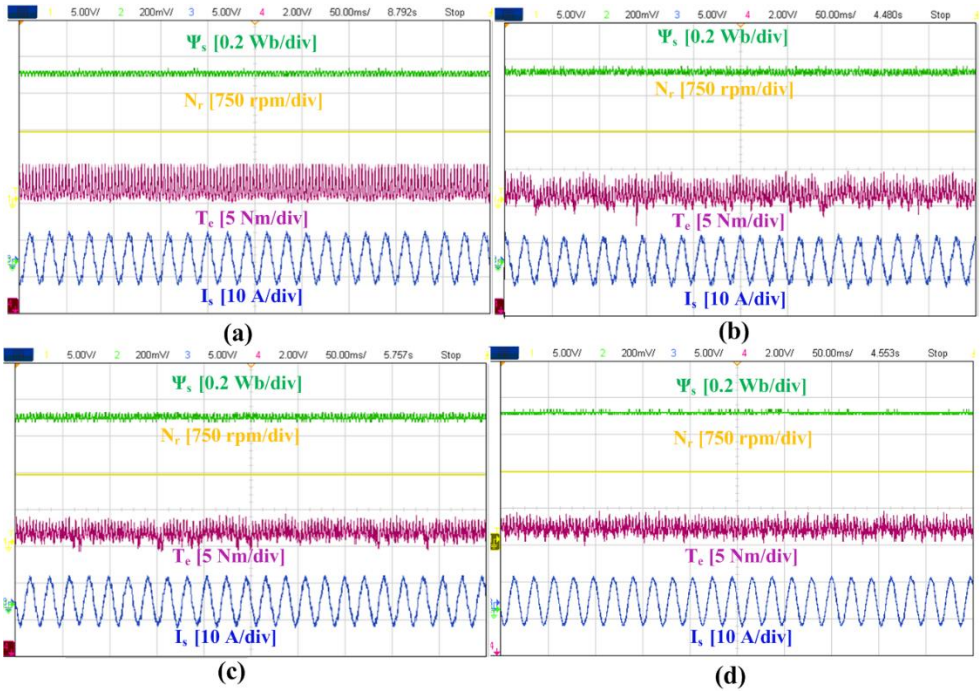

Figure 5.18 Response under steady-state condition at rated speed and rated load (a) C-MPCC, (b) DMPCC [56], (c) ECS-MPCC [77], (d) PMPCC.

The torque ripples (T_{e_rip}), and flux ripples (Ψ_{rip}) are calculated using standard deviation as,

$$T_{e\_rip} = \sqrt{\frac{1}{n}\sum_{i=0}^{n}(T_e(i) - T_e^*)^2)} \tag{5.18}$$

$$\psi_{rip} = \sqrt{\frac{1}{n}\sum_{i=0}^{n}(\psi_s(i) - \psi_s^*)^2)} \tag{5.19}$$

The PMPCC scheme is thus evaluated at low, medium, and high-speed conditions as well as different load conditions ranging from light to rated load. The ripples, switching frequency (f_{sw}), and stator current THD calculated are shown in Table 5.4 and Table 5.5. From Table 5.4 and Table 5.5, it can be observed that the torque ripples, flux ripples, and stator current THDs obtained for the PMPCC scheme is better than C-MPCC, DMPCC [56], and ECS-MPCC [77]. Thus, the PMPCC scheme is efficient in reducing the ripples in torque and flux in steady-state conditions and improves the stator current response due to the application of multiple VVs effectively in a sample time. This ascertains the applicability of the proposed scheme for different speeds, as well as load conditions.

Table 5.4 Performance evaluation under different load conditions

Control	**C-MPCC**		**DMPCC [56]**		**ECS-MPCC [77]**		**PMPCC**	
Speed(rpm), load (Nm)	**T_{e_rip} (Nm)**	**Ψ_{rip} (mWb)**	**T_{e_rip} (Nm)**	**Ψ_{rip} (mWb)**	**T_{e_rip} (Nm)**	**Ψ_{rip} (mWb)**	**T_{e_rip} (Nm)**	**Ψ_{rip} (mWb)**
250 rpm, 5 Nm	0.376	2.51	0.224	2.36	0.194	2.19	0.175	1.44
500 rpm, 5 Nm	0.419	2.48	0.281	1.49	0.255	1.42	0.212	1.31
500 rpm, 10 Nm	0.441	2.44	0.231	1.92	0.248	1.59	0.198	1.47
750 rpm,18 Nm	0.432	2.55	0.228	2.21	0.211	1.54	0.176	1.38
1000 rpm, 12 Nm	0.351	2.43	0.223	1.45	0.191	1.34	0.166	1.29
1000 rpm, 24 Nm	0.369	2.76	0.288	2.27	0.247	1.62	0.211	1.49
1500 rpm, 5 Nm	0.439	2.61	0.354	2.28	0.248	1.61	0.192	1.41
1500 rpm, 24 Nm	0.442	2.52	0.344	2.39	0.256	1.55	0.189	1.23

Table 5.5 Performance evaluation under different speeds and loads

Control	**C-MPCC**		**DMPCC [56]**		**ECS-MPCC [77]**		**PMPCC**	
Speed(rpm), load (Nm)	**f_{sw} (Hz)**	**THD (%)**	**f_{sw} (Hz)**	**THD (%)**	**f_{sw} (Hz)**	**THD (%)**	**f_{sw} (Hz)**	**THD (%)**
250 rpm, 5 Nm	2566	17.39	3655	12.92	4633	11.05	4641	8.54
500 rpm, 10 Nm	2488	16.52	3896	9.81	4513	9.12	4438	8.69
750 rpm,18 Nm	2376	17.54	3569	10.22	4341	8.89	4275	7.45
1000 rpm, 24 Nm	2554	18.41	3247	10.91	4079	9.87	4198	8.71
1500 rpm, 24 Nm	2607	17.39	3450	12.92	4065	11.05	3937	5.92

The experimental results obtained using the PMPCC scheme are further compared with the simulation results to quantify the deviation between the results. The torque ripples are deduced using (5.18) in both simulated and experimental results. The plot obtained for experimental results is shown to follow the trend of simulated results. An average error of 17% is obtained between the simulated and experimental results. Figure 5.19 shows the comparison of torque ripples under different operating speeds for all the methods.

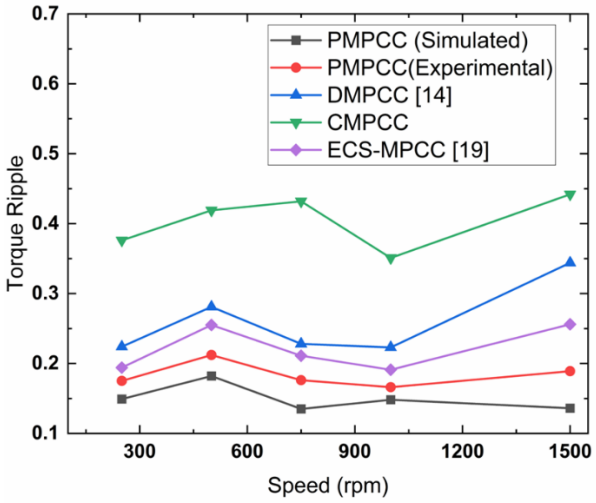

Figure 5.19 Comparison of Simulated and Experimental results of torque ripples in PMPCC under different operating speeds.

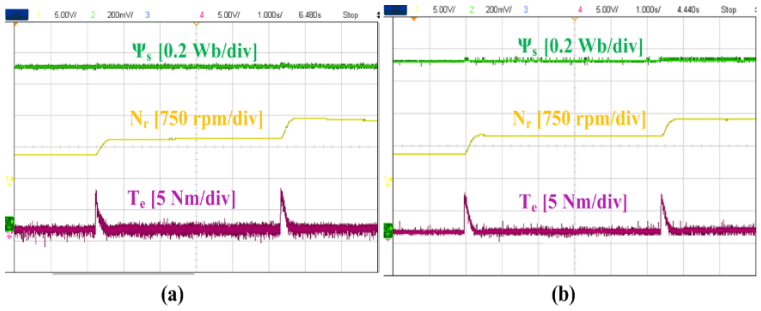

Figure 5.20 Dynamic response when speed is varied from 500 rpm to 1000 rpm to 1500 rpm (a) C-MPCC, (b) PMPCC.

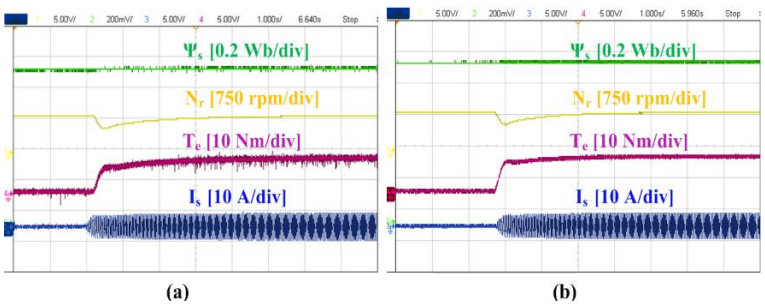

Figure 5.21 Dynamic response when the load is varied from 0 to 12 Nm at 1000 rpm. (a) C-MPCC, (b) PMPCC.

The dynamic performance of the drive is analyzed to ensure that the PMPCC scheme does not affect the dynamic capability offered by the C-MPCC scheme. The speed reference is varied from 500 rpm to 1000 rpm and further to 1500 rpm, to analyze the performance of the algorithm under sudden step-change in speed. The dynamic responses obtained are shown in Figure 5.20. The capability of the algorithm to track a sudden load change is in Figure 5.21. For this, a load of 12 Nm is suddenly applied to the motor operating at a speed of 1000 rpm. It can be observed in Figure 5.20 and Figure 5.21 that the dynamic performances of both schemes are similar.

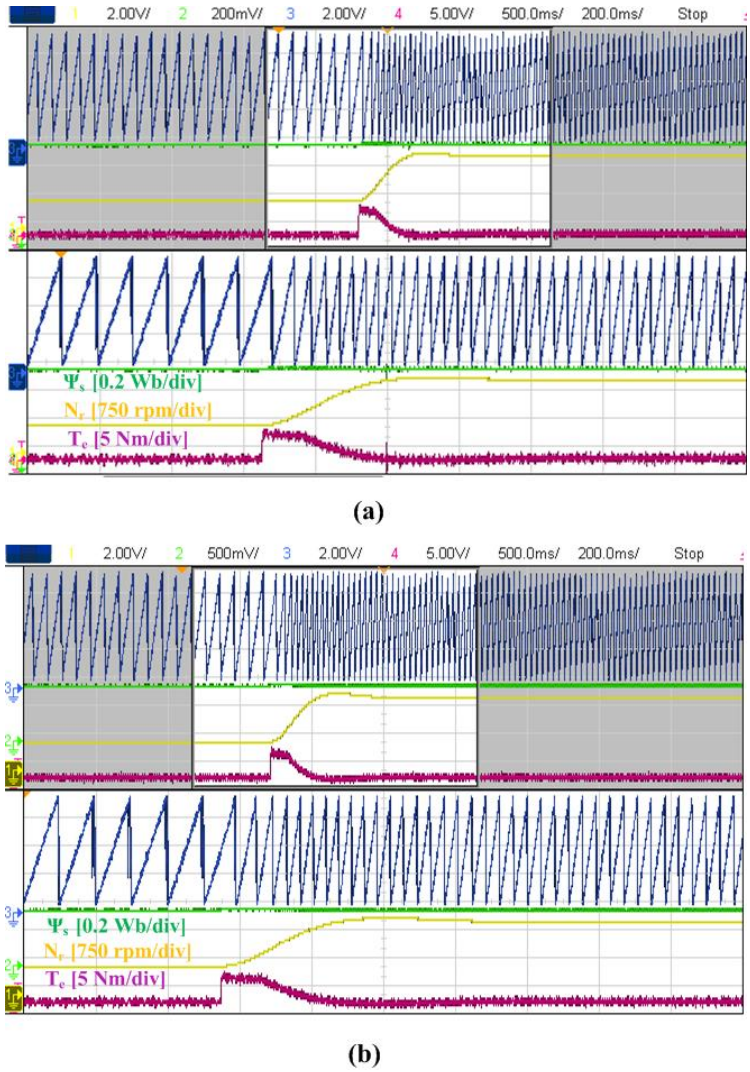

Figure 5.22 Dynamic response when speed command is changed from 250 rpm to 750 rpm (a) Proposed method with 26 VVs (b) PMPCC.

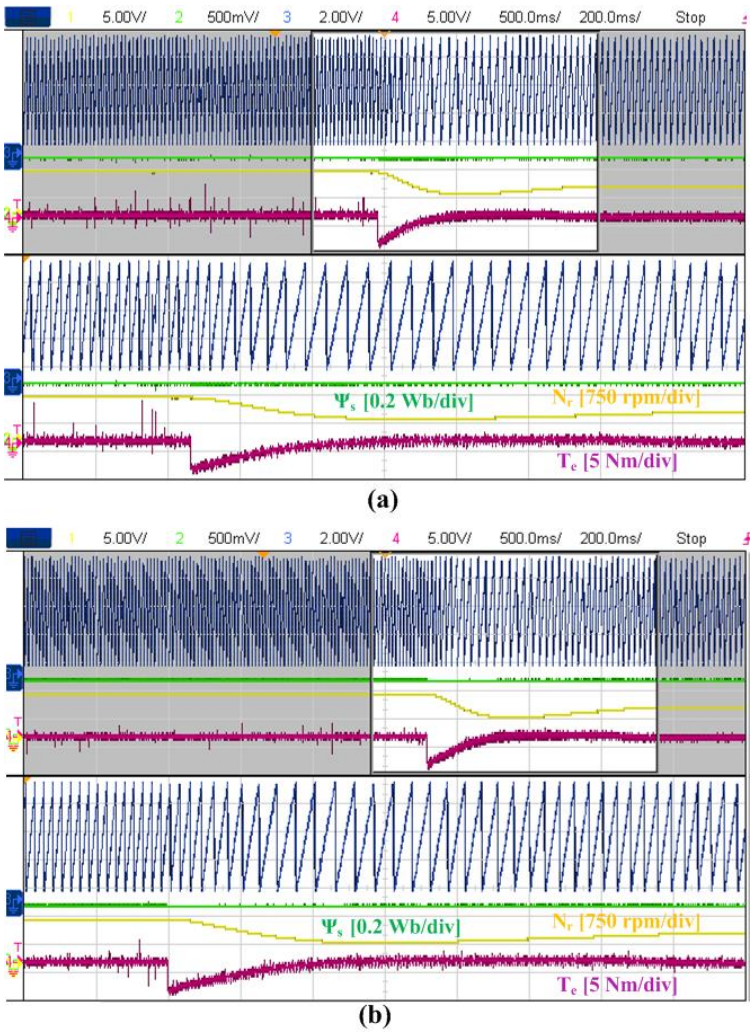

Figure 5.23 Dynamic response when speed is changed from 1200 rpm to 750 rpm (a) Proposed method with 26 VVs (b) PMPCC.

To verify the effect of reduced no. of VVs on the dynamic performance, a comparison of the dynamic performance of the proposed method and the method with 26 VVs and PMPCC is performed. Figure 5.22 shows the performance when the motor is accelerated from 250 rpm to 750 rpm. Similarly, Figure 5.23 shows the dynamic response during braking, i.e., speed reduction from 1200 rpm to 750 rpm. Thus, even with the reduced number of VVs, a similar dynamic response can be obtained. The meticulous grouping of VVs in PMPCC assures the dynamic and steady-state performance to be similar to the Proposed method with 26 VVs.

The computational time required for DMPCC [56] is 38 µs. ECS-MPCC [77] requires 44.5 µs and the proposed scheme with all 26 VVs requires 60.5 µs for the computations, while the PMPCC requires 43 µs. Thus, the operations involved are

reduced using the PMPCC VV grouping. Moreover, PMPCC reduces at least 50% of the ripples in output torque present in the C-MPCC scheme. The torque ripples are at least 18% and 12% lower than DMPCC [56] and ECS-MPCC [77], respectively. As the PMPCC method has more VVs in its CS, it is more efficient than DMPCC [56] and ECS-MPCC [77]. However, the average switching frequency of the PMPCC scheme is 4.3 kHz, which is higher than the C-MPCC due to the multi-vector application. In the present work, all methods are operated at the same sampling frequency. However, for a fair comparison, the frequency of the PMPCC scheme must be compared with a multivector-based approach. To achieve this, the frequency of the ECS-MPCC [77] scheme is compared with the PMPCC scheme, and the results prove that the switching frequency is not elevated in the proposed scheme as the frequency ranges of both schemes are similar. The computational time required for PMPCC is more than DMPCC [56] but less than ECS-MPCC [77]. In the PMPCC scheme, there is an effective enumeration of the VVs based on $\Delta$is. Instead, if the predicted current is larger than the reference current, two active VVs generating a negative slope along with the null VV, aid in reducing the error. However, if the predicted current is higher than the reference current with a small initial current error, the VV 'V_{prin}' along with a null VV is applied to reduce the ripples. However, in DMPCC [56], an active VV and a null VV is applied in all cases. Moreover, in ECS-MPCC [77], the number of additional VVs in the CS is less than that in the PMPCC scheme. In PMPCC, the duration of optimal VV is also obtained based on the optimum error between the reference and predicted stator currents. Thus, an effective reduction in steady-state torque and flux ripples can be obtained.

5.4 Effect of L_s and R_s variation

The performance of the PMPCC schemes when subjected to variation in machine parameters is investigated. For this, the stator resistance and inductance in the control algorithm are increased by 50%. As the effect of stator resistance variation becomes prominent at low speed, the response of the drive, when the machine is operated at a low speed of 100 rpm with the erroneous parameters fed to the algorithm is analyzed.

Figure 5.24. shows the performance under stator resistance variation for all the methods. It can be observed that when erroneous parameters are employed in the

algorithm, the performances of the MPCC methods are not affected as the current predictions are less affected by stator resistance variation. Thus, the MPCC schemes are robust towards stator resistance variations. However, the effect of variation in stator inductance affects the stator current predictions as per the stator current equation.

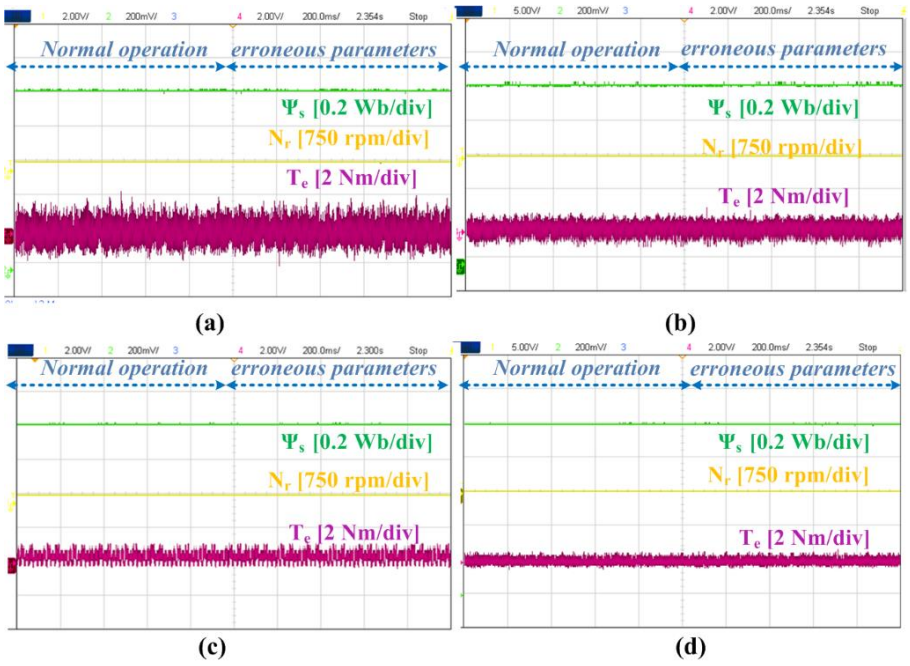

Figure 5.24 Performance under stator resistance variation at 100 rpm speed (a) C-MPCC, (b) DMPCC [56], (c) ECS-MPCC [77], (d) PMPCC.

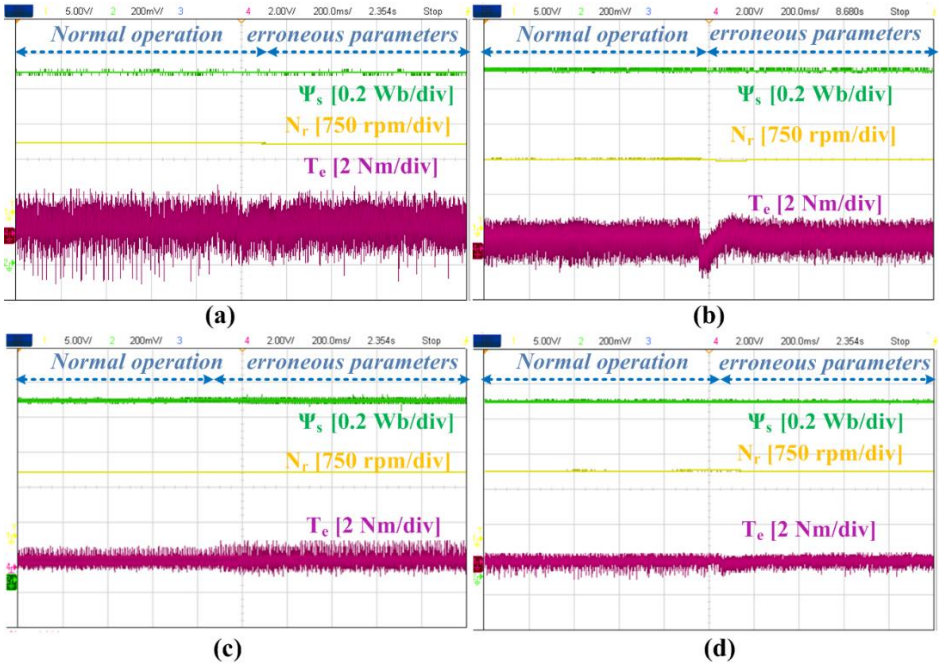

Figure 5.25 Performance under stator inductance variation at 1500 rpm speed (a) C-MPCC, (b) DMPCC [56], (c) ECS-MPCC [77], (d) PMPCC.

The effect of stator inductance variation is obvious at very high speeds. The machine is operated at a speed of 1500 rpm to analyze the effect of stator inductance variation. As shown in Figure 5.25., due to the inductance variation, the C-MPCC scheme response becomes slightly perturbed, and within a certain period, it regains its stability. However, DMPCC [56] employs a duty scheme with the optimum duration of active VV inversely proportional to the stator inductance, and in the ECS-MPCC [77] scheme, duty ratio calculation is based on the parameter-dependent reference VV. This causes the DMPCC [56] scheme and ECS-MPCC [77] to be affected more by the stator inductance variation. The torque ripples are increased in ECS-MPCC [77] due to the stator inductance variation. Conversely, the calculation of the duration of ECS-VV in the PMPCC scheme does not directly involve the stator inductance term. Hence, the variations are similar to the C-MPCC scheme and the system quickly regains stability. Thus, the PMPCC offers robustness with less sensitivity toward parameter variations.

5.5 Summary

In this chapter, a multi-vector-based MPCC scheme is proposed for the two-level VSI-operated PMSM drive in the present work. The torque control precision is enhanced due to the augmented CS and a look-up table is developed for reducing the number of operations involved in every sample time. The VV groups are selected based on the stator current error and effectively replicate the control scheme with all ECS-VVs. In PMPCC, the amplitude of the optimum ECS-VV is brought close to the reference. Therefore, the PMPCC method offers the flexibility to apply either two or three VVs in a sample time, for enhanced drive performance. The limitation of PMPCC is the increase in the switching frequency as compared to the C-MPCC scheme. Nevertheless, the switching frequency is less than the ECS-MPCC [77] scheme. Moreover, compared to the advantages offered by the proposed scheme, the increase in switching frequency can be considered trivial. The dynamic response of the drive is retained in the PMPCC and offers robustness against parameter variations. Thus, the proposed method offers better performance than the independent control offered by the duty-modulated scheme as well as the ECS-based MPCC scheme.

Chapter 6

A Multivector-Based Low-Complex Model Predictive Current Control of PMSM drive for Improved Torque and Flux Performance

6. A Multivector-Based Low-Complex Model Predictive Current Control of PMSM drive for Improved Torque and Flux Performance

6.1 Introduction

In the previous chapter, multivector operation was achieved using an extended control set consisting of virtual voltage vectors. The proposed scheme offers excellent steady-state performance at the expense of increased computational burden. Even though the computational time was limited using an effective voltage vector preselection scheme, the complex sector determination would take up some processor memory. In this chapter, a multivector-based MPCC scheme using a simplified voltage vector (VV) preselection is analyzed for improved torque performance of PMSM drives.

The prediction and optimization operations in the conventional MPCC (C-MPCC) scheme increase the computational burden of the processor. The proposed method aims to reduce the complexity of the control scheme with a VV-preselection based on an effective position estimation using the gradient concept. This helps to directly determine the optimal VV without evaluating cost-function using all the VVs. However, the application of a single VV in C-MPCC leads to large undulations in the torque and flux responses. This necessitates the application of multiple VVs in each control period to ensure improved torque response. To achieve this, the duration of application of the VVs is determined using the cost-function ratio of the different VVs chosen in the proposed scheme. Moreover, the need for the space vector modulation scheme for the estimation of the application time of the optimal VVs is also eliminated. Further, the proposed scheme maintains the dynamic performance of the drive as offered by the C-MPCC scheme with improved steady-state performance and lower computational complexity.

The chapter has the following organization: Section-6.2 describes the proposed MPCC. Section 6.3 comprises of experimental results. Section-6.4 presents the summary.

6.2 Proposed multivector-based MPCC scheme for PMSM drive

In the C-MPCC scheme, the cost-function is determined using the eight VVs, and the vector that yields the least error is applied to the VSI. Nevertheless, the single VV application for the whole control interval when the error is small results in large fluctuations in torque response. To address this limitation, dual VVs are employed, where the optimum active VV is applied for a determined time period and a null VV for the rest of the control period. Figure 6.1. shows the stator current waveform during one control interval. It should be noted that Figure 6.1. is merely used for illustration and the slopes of the current may not be precise.

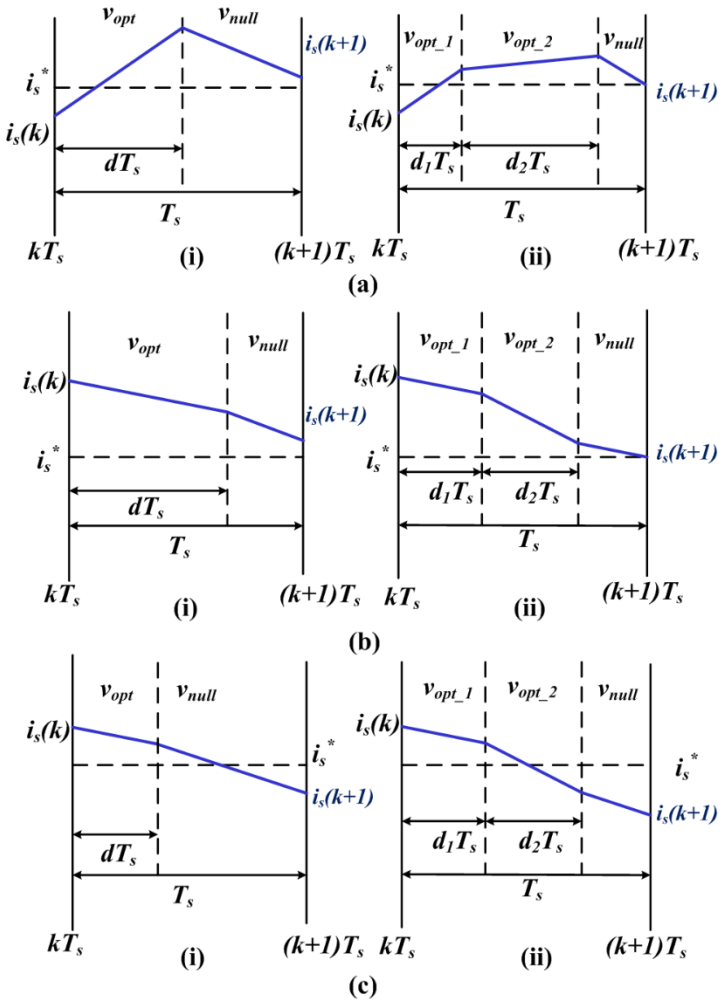

Figure 6.1 Waveform of stator current when: (a) the current reference is higher than assessed value (i) with two VVs (ii) with three VVs, (b) the current reference is smaller than the assessed value and the initial error is large (i) with two VVs (ii) with three VVs.

It can be seen from Figure 6.1 that the two VV-based control is insufficient

to improve the performance in certain operating conditions. For instance, when the reference current is larger than the assessed current as in Figure 6.1 (a), the application of the two optimum VVs (v_{opt1} and v_{opt2}) with an increasing slope along with a null VV (v_{null}) helps to reduce the error more effectively than dual VVs. Similarly, when the initial error is large and the reference value of the current is less than the assessed current, the combination of two active VVs with a decreasing slope and a null VV can yield a better current response as shown in Figure 6.1 (b). However, Figure 6.1 (c) shows that applying three VVs simultaneously in a control period leads to enlarged current errors when the reference value of the current is less than the assessed current. This is more obvious when the initial error is small. This condition demands the dual-VV application for improved performance.

As the predictive algorithm on its own is computationally intensive, the application of multiple vectors further contributes to the increased number of operations. This necessitates an enhanced VV preselection-based MPCC scheme applying multiple VVs in a control period while limiting the computational complexity. The block diagram of the proposed scheme is shown in Figure 6.2.

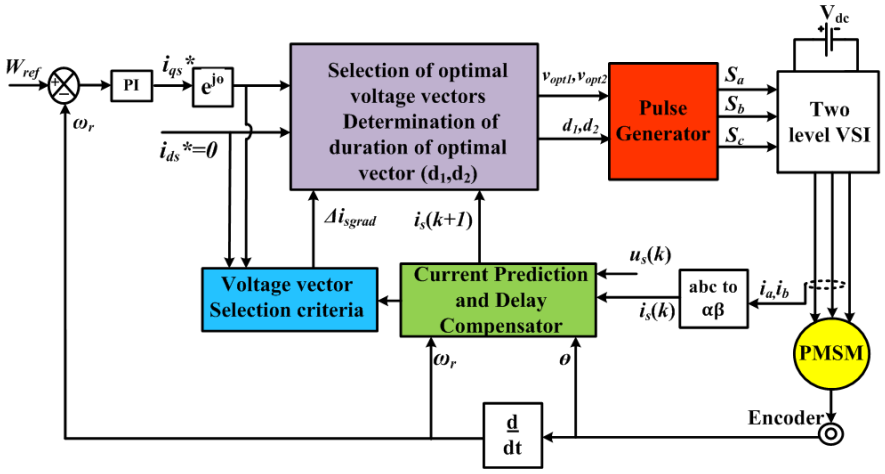

Figure 6.2 Proposed MPCC scheme block diagram.

6.2.1 Proposed Voltage Vector Preselection Scheme

The proposed MPCC scheme employs a VV preselection scheme derived from the simple concept of gradients. The proposed method achieves a modified position determination that avoids the tedious angle calculation using tangent inverse estimation.

The existing switching states in a two-level VSI can be represented in terms of eight VVs that are spatially displaced at 60^o in the α-β plane. Assuming that each

VV is confined within a sector, it can be observed from Fig. 4. that two symmetrically opposite sectors are bounded by two identical straight lines. Moreover, the lines possess a certain gradient, which is common to both sectors. For instance, the sector I and sector IV are assumed to be bounded within lines l_1 and l_2. The gradient of line l_1 is 0.5774 (i.e., *tan* 30^o), while that of line l_2 is -0.5774 (i.e., *tan* (-30^o)) as shown in Figure 6.3. Thus, if the reference vector lies within a certain sector, it is very convenient to select the VVs within those two symmetrically opposite sectors without actually estimating the position using the tangent inverse calculation.

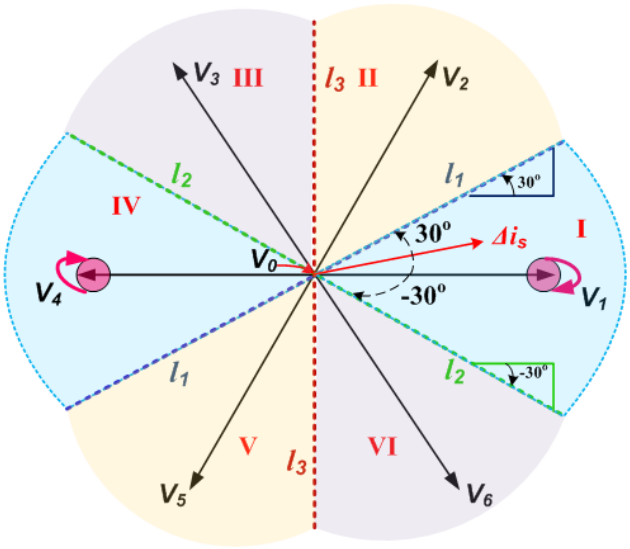

Figure 6.3 Proposed VV selection

The criteria for preselecting the VVs is based on the concept of conventional DTC (CDTC). In the CDTC scheme, the error in stator flux in any control period, T_s, can be attained as,

$$\Delta\psi_s = \psi_s^* - \psi_s(k) = U_s^* T_s \tag{6.1}$$

where, U_s^* is the reference VV. The stator current possesses a linear relationship with the stator flux as per (2). (8) can be thus modified using (2) neglecting stator resistance as (9).

$$\Delta i_s = i_s^* - i_s(k+1) = (U_s^* - e(k+1))\frac{T_s}{L_s} \tag{6.2}$$

where stator current error, $\Delta i_s = \Delta i_{\alpha s}(k+1) + j\Delta i_{\beta s}(k+1)$. Thus, the current error can be observed to be linearly co-related to U_s^*. Hence, the determination of the location of Δi_s is indirectly similar to the assessment of the U_s^* position. This helps to avoid the increase in parameter sensitivity caused by the U_s^* calculation while retaining the

control action offered by U_s^*.

In the proposed scheme, the criteria used for the VV preselection scheme is the estimation of real and imaginary components of Δi_s. A simple look-up table can be framed using the concept of the gradient of straight lines, which easily identifies the candidate VVs using a modified position estimation approach. For instance, if the stator current error is positioned in the first sector of the stationary-αβ plane as shown in Fig. 4, the ratio of $\Delta i_{\beta s}/\Delta i_{\alpha s}$ (i.e., the gradient of Δi_s) must be greater than the gradient of line l_2 and should be less than the gradient of line l_1.

Based on this inference, the following expression for the gradient of Δi_s in the sector-I is obtained as,

$$-0.5774 < \Delta i_{s\_grad} \leq 0.5774 \tag{6.3}$$

where, $i_{s\_grad} = \Delta i_{\beta s}/\Delta i_{\alpha s}$. From (6.3), the condition for VV selection in the Ist sector can be obtained. If this condition is satisfied, the shortlisted VVs are V_1 and V_4. This expression is valid for sectors I and IV, as they are bounded by the same straight lines. However, in sector-I, $\Delta \boldsymbol{i}_{\alpha s} \geq 0$, and the optimal VV can be directly obtained as V_1. Similarly, in sectors II and V, the condition to be satisfied is,

$$0.5774 < \Delta i_{s\_grad} \leq \infty \tag{6.4}$$

However, (6.4) is complicated to implement and can be modified as,

$$\Delta i_{s\_grad} > 0.5774, |\Delta i_{\alpha s}| \geq 0 \tag{6.5}$$

The absolute value of $\Delta \boldsymbol{i}_{\alpha s}$ is utilized for VV selection as $\Delta \boldsymbol{i}_{\alpha s}$ takes a positive value in sector II and a negative value in sector V. This further helps to shortlist the optimum VV as V_2 or V_5 based on the polarity of $\Delta \boldsymbol{i}_{\alpha s}$. Hence, using expressions based on relational operators, we can estimate the position of VVs and formulate the look-up table for VV preselection. Table I shows the proposed VV selection. It can be observed from Table 6.1 that the number of operations is reduced in the proposed scheme as one out of the two VVs positioned in the opposite sectors can be easily assigned as the optimal VV.

Table 6.1 Proposed voltage vector selection

Condition	Optimum VV
$-0.5774 < \Delta \boldsymbol{i}_{s\_grad} \leq 0.5774, \Delta \boldsymbol{i}_{\alpha s} \geq 0$	V_1
$\Delta \boldsymbol{i}_{s\_grad} > 0.5774, \lvert\Delta \boldsymbol{i}_{\alpha s}\rvert \geq 0, \Delta \boldsymbol{i}_{\alpha s} \geq 0$	V_2
$\Delta \boldsymbol{i}_{s\_grad} \leq -0.5774, \lvert\Delta \boldsymbol{i}_{\alpha s}\rvert \geq 0, \Delta \boldsymbol{i}_{\alpha s} \leq 0$	V_3
$-0.5774 < \Delta \boldsymbol{i}_{s\_grad} \leq 0.5774, \Delta \boldsymbol{i}_{\alpha s} < 0$	V_4
$\Delta \boldsymbol{i}_{s\_grad} > 0.5774, \lvert\Delta \boldsymbol{i}_{\alpha s}\rvert \geq 0, \Delta \boldsymbol{i}_{\alpha s} < 0$	V_5
$\Delta \boldsymbol{i}_{s\_grad} \leq -0.5774, \lvert\Delta \boldsymbol{i}_{\alpha s}\rvert \geq 0, \Delta \boldsymbol{i}_{\alpha s} > 0$	V_6

It can be thus seen from Table 6.1 that the proposed VV preselection scheme reduces the VVs required for the computations from 8 to 1. The advantage of the proposed scheme is the direct shortlisting of optimal VV without cost-function evaluation and optimization stages. The position of the stator current error precisely helps to shortlist the optimum VV required for the control action. Further, sector determination using tangent inverse angle calculation is avoided in this method. This further reduces the computational complexity. However, as the application of a single VV contributes to larger fluctuations in torque and flux, an amplitude optimization scheme is proposed that applies three VVs in a control period based on the stator current error.

6.2.2 Proposed multi-vector scheme and VV duration determination

The optimum VV offers the best torque and flux control, generating a minimum deviation between the reference and the control variable. Subsequently, the addition of a null VV to the optimum VV modifies the length of the optimal VV to decrease the steady-state torque ripples. However, the addition of null VV may not be sufficient to bring down the steady-state ripples in all operating conditions as pointed out in Figure 6.1. The present work focuses on applying multiple VVs considering the magnitude of Δi_s. It is evident from Figure 6.1 that if the current reference is more than the initial current, it is required to apply two VVs with an increasing current slope and a null VV to bring the error closer to the reference. Similarly, when the stator current error is more than the reference value, two VVs with a decreasing current slope and a null VV are chosen as the optimum VVs. This again depends upon the magnitude of the predicted error. In order to avoid an increased number of switching, adjacent VVs are chosen as the second VV.

Similar to the preselection of the first optimum VV, the second optimum VV is chosen according to the position of Δi_s and its gradient. However, the only difference is that the gradient of the first optimum VV is considered for the choice of the second optimum VV. If the gradient of the first optimum VV group is greater than Δi_s, the VV to the counter-clockwise direction of the first optimum VV group is chosen as the second optimum VV and vice-versa. The proposed VV grouping is shown in Figure 6.4 for more clarity. Assume that Δi_s is positioned in sector II of the stationary α-β plane. The first optimum VV is chosen as V_2 and it can be observed

that the gradient of Δi_s is more than V_2 (i.e., $tan\ 60^0$ = 1.732). Thus, the second optimum VV is chosen as V_3. The selection of the second optimum VV is shown in Table 6.2.

Table 6.2 Proposed second optimum VV selection

1st optimum VV	Condition	2nd optimum VV
V_1	$\Delta i_{s\_grad} \geq 0$ $\Delta i_{s\_grad} \leq 0$	V_2 V_6
V_2	$\Delta i_{s\_grad} \geq 1.732$ $\Delta i_{s\_grad} \leq 1.732$	V_3 V_1
V_3	$\Delta i_{s\_grad} \geq -1.732$ $\Delta i_{s\_grad} \leq -1.732$	V_4 V_2
V_4	$\Delta i_{s\_grad} \geq 0$ $\Delta i_{s\_grad} \leq 0$	V_5 V_3
V_5	$\Delta i_{s\_grad} \geq 1.732$ $\Delta i_{s\_grad} \leq 1.732$	V_6 V_4
V_6	$\Delta i_{s\_grad} \geq -1.732$ $\Delta i_{s\_grad} \leq -1.732$	V_1 V_5

.

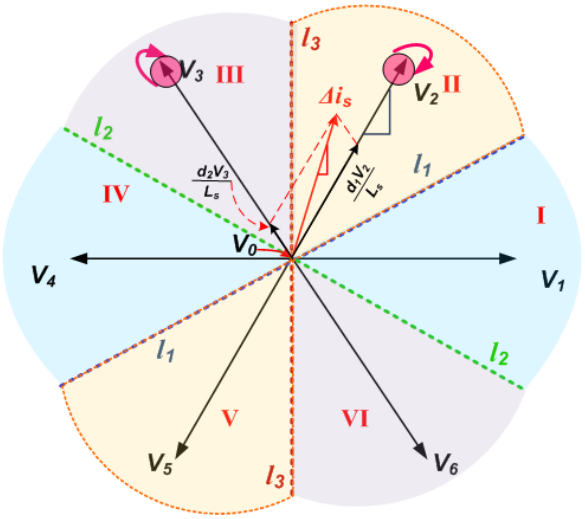

Figure 6.4 Proposed second VV selection.

Table 6.2 can be simplified using the expression given below.

$$V\_opt\ 2 = \begin{cases} V\_opt1 + 1, \ if\ \Delta i_{s\_grad} \geq (imag\ (V\_opt1)/real\ (V\_opt1)) \\ V\_opt1 - 1, \ if\ \Delta i_{s\_grad} < (imag\ (V\_opt1)/real\ (V\_opt1)) \end{cases} \quad (6.5)$$

Generally, as the control schemes employing two VVs do not offer improved steady-state torque response, two active VVs, and a null VV are applied in each sample time in the proposed scheme. This increases the precision of the control algorithm. Figure 6.5 shows the effect of multiple VVs on the stator current error.

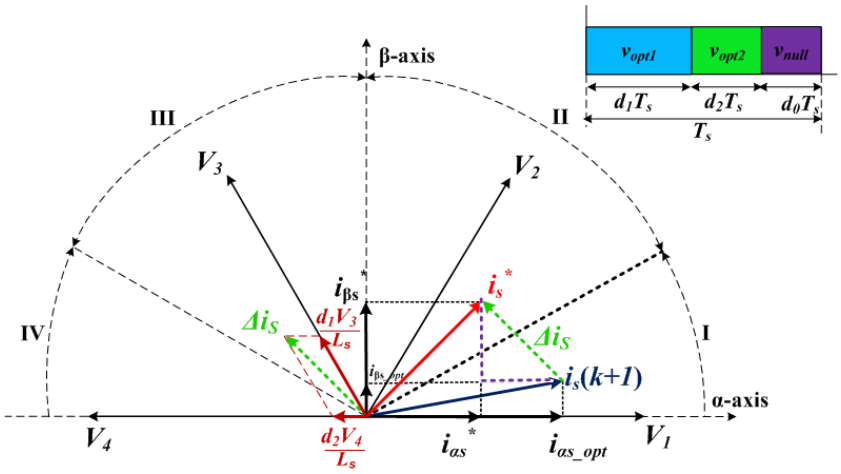

Figure 6.5 Effect of proposed multiple VV application based on stator current error.

For instance, assume that $i_s(k+1)$ is located in the first sector of the stationary α-β plane. It can be observed from Fig.6 that Δi_s has a negative gradient and is directed towards sector III of the stationary plane. Thus, the first optimal VV is chosen as V_3. Moreover, Δi_s has more gradient than V_3 and this helps to identify the second optimal VV as V_4.

To achieve multiple VV application, the proposed method determines the duration of optimum VVs using the ratio of cost-function evaluated using the optimum VVs. The duration of the optimum VVs is estimated using the concept of the weighted average of stator current errors.

Considering the duty ratios of $V_{\_opt1}$, $V_{\_opt2,}$ and null VV as d_1, d_2, and d_0, respectively, the following expression holds true.

$$d_1 + d_2 + d_0 = 1 \tag{6.6}$$

To find the duration of optimum VVs, the cost-function is modified by incorporating the duty ratios as given below.

$$G = d_1G_1 + d_2G_2 + d_0G_0 \tag{6.7}$$

For C-MPCC, $G = |i_{\alpha s}^* - i_{\alpha s}(k+2)|^2 + |i_{\beta s}^* - i_{\beta s}(k+2)|^2$, where, G_1, G_2, and G_0 are the cost functions evaluated using $V_{\_opt1}$, $V_{\_opt2,}$ and null VV, respectively. (6.7) represents a convex combination of error vectors with non-negative coefficients (or weights) that sum up to a value of 1. Using the concept of normalization of weights, the optimum durations can be obtained as per (6.8)-(6.10), assuming that the duty ratios are inversely proportional to the respective cost-function.

$$d_1 = \frac{k}{G_1} \tag{6.8}$$

$$d_2 = \frac{k}{G_2} \tag{6.9}$$

$$d_0 = \frac{k}{G_0} \tag{6.10}$$

where, k is the normalizing constant. Substituting (6.8) -(6.10) in (6.6) gives,

$$\frac{k}{G_1} + \frac{k}{G_2} + \frac{k}{G_0} = 1 \tag{6.11}$$

$$k = \frac{G_1 G_2 G_0}{G_1 G_2 + G_0 G_2 + G_1 G_0} \tag{6.12}$$

$$d_1 = \frac{\frac{G_1 G_2 G_0}{G_1 G_2 + G_0 G_1 + G_2 G_0}}{G_1} \tag{6.13}$$

$$d_2 = \frac{\frac{G_1 G_2 G_0}{G_1 G_2 + G_0 G_1 + G_2 G_0}}{G_2} \tag{6.14}$$

$$d_0 = \frac{\frac{G_1 G_2 G_0}{G_1 G_2 + G_0 G_1 + G_2 G_0}}{G_0} \tag{6.15}$$

$$d_1 = \frac{G_2 G_0}{G_1 G_0 + G_2 G_0 + G_1 G_2} \tag{6.16}$$

$$d_2 = \frac{G_1 G_0}{G_1 G_0 + G_2 G_0 + G_1 G_2} \tag{6.17}$$

$$d_0 = 1 - d_1 - d_2 \tag{6.18}$$

Thus, the cost-function is evaluated using the optimum VVs obtained using preselection criteria and the durations of VV application are estimated using (6.16)-(6.18).

The advantage of the proposed duty ratio scheme is that the parameter sensitivity of the algorithm is not further elevated as the cost-function itself is evaluated for obtaining the application duration. The implementation of the proposed control algorithm involves the following steps.

i. Measure the speed, currents, and DC link voltage at the k^{th} instant.
ii. Predict the stator current at the $(k+1)^{th}$ instant.
iii. Calculate the stator current error, Δi_s using (6.2) and estimate the gradient of Δi_s, i.e., Δi_{s_grad}.
iv. Access Table 6.1 using the value of Δi_{s_grad} and determine the first optimal VV, $V_{\_opt1}$.

v. Using (6.5), find the second optimal VV, $V_{\_opt2}$.

vi. Determine the duration of application of the active and null VVs using (6.16) -(6.18).

vii. The three optimum VVs and their application time are combined to determine the inverter's switching state.

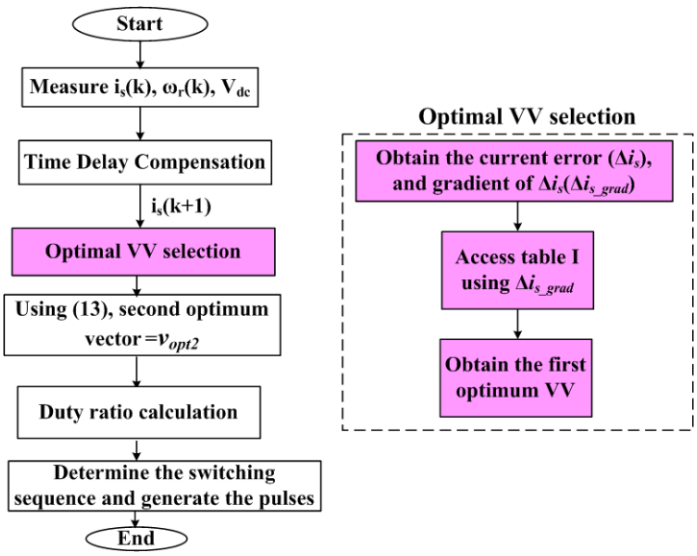

Figure 6.6 Flow diagram of the proposed scheme.

The flow diagram of the proposed scheme is shown in Figure 6.6.

The advantages of the proposed scheme are listed below.

i. The proposed MPCC scheme directly determines the optimum VVs without cost-function evaluation and optimization stages based on the modified position determination. This reduces the number of operations involved and hence, the computational burden of the processor.

ii. The proposed scheme eludes the determination of sector using conventional angle calculation and this alleviates the complexity of the algorithm.

iii. The determination of reference VV is also evaded in the proposed scheme and an indirect approach with the stator current error as the criteria for selection is deployed to improve the control technique. This benefits the algorithm to be robust against machine parameter variations compared to the reference VV-based approach.

iv. The drive torque response under steady-state conditions is improved owing to the application of three VVs in one control period. The amplitude optimization scheme proposed is based on the cost-function of the C-MPCC scheme. The

calculation is simple and effective.

v. The dynamic performance of the PMSM drive is not compromised while improving the steady-state response.

6.3 Experimental Results

For experimentation, a PMSM machine rated 5 HP, 415 V, 4 poles, and 1500 rpm is used. A dSPACE 1104 controller is used to implement the control algorithm. LEM hall sensors are used for sensing DC-link voltage and currents. A 1024-point-based incremental encoder is used to feedback the speed signal. The external load is applied through the resistor bank connected to the DC generator coupled to the motor shaft. To validate the effectiveness of the proposed scheme, the steady-state and dynamic performances of the drive are compared with C-MPCC, a duty-based MPC scheme (DMPC [101]), and a multivector-based MPC (MVMPC [99]) scheme to affirm its effectiveness. All the methods have a 10 kHz sampling frequency and are subjected to the same operating conditions. DMPC [99] scheme utilizes dual VV application and the computational burden is reduced using the reference VV-based sector determination method. This method also reduces the number of candidate VVs from eight to two. The second VV used in this scheme can either be a null VV or an active VV, which can be determined using the position of the reference VV. In MVMPC [97], two adjacent active VVs and a null VV are applied in each control interval to reduce the fluctuations in torque. This scheme shortlists three VVs for the computational operations. However, the duty-ratio calculation in this scheme involves more computations.

6.3.1 Steady state and Dynamic Responses

To verify the performance of the control algorithm, the motor is subjected to different loading conditions at different operating speeds. Figure 6.7 shows the performance of the drive when a load of 5 Nm (20% of the rated load) is applied to the machine at 300 rpm. Further, the steady-state performance at 750 rpm and 12 Nm load is shown in Figure 6.8. Similarly, Figure 6.9 and Figure 6.10 show the responses at 1000 rpm, 15 Nm load, and rated speed, 18 Nm load, respectively. The responses shown from Figure 6.7 to Figure 6.10 incorporate the flux, speed, current, and torque waveforms.

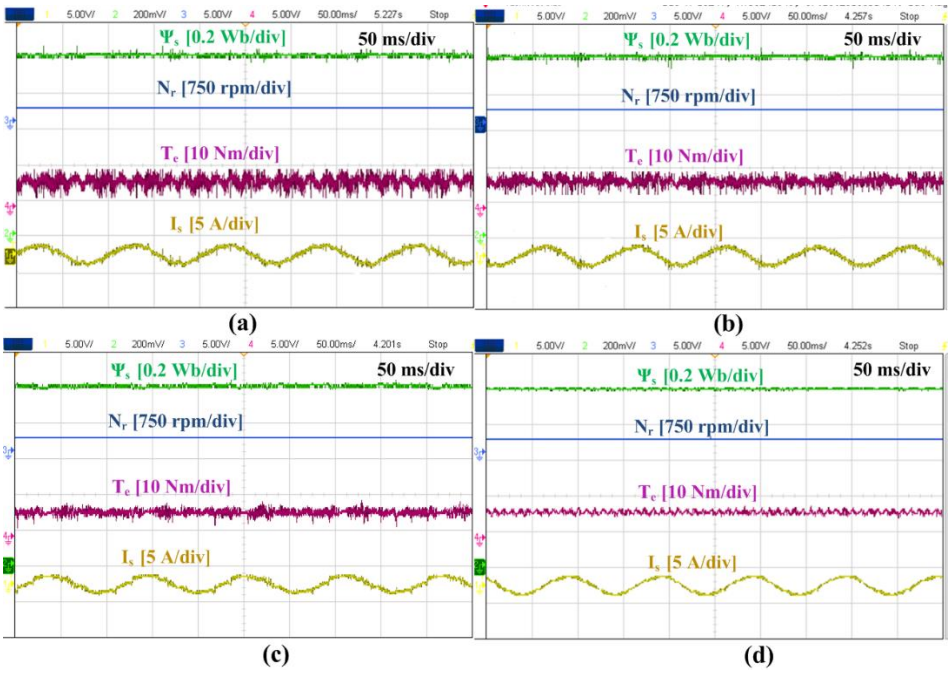

Figure 6.7 Response at 300 rpm, 5 Nm load under steady-state condition (a) C-MPCC, (b) DMPC [99], (c) MVMPC [97], (d) Proposed scheme.

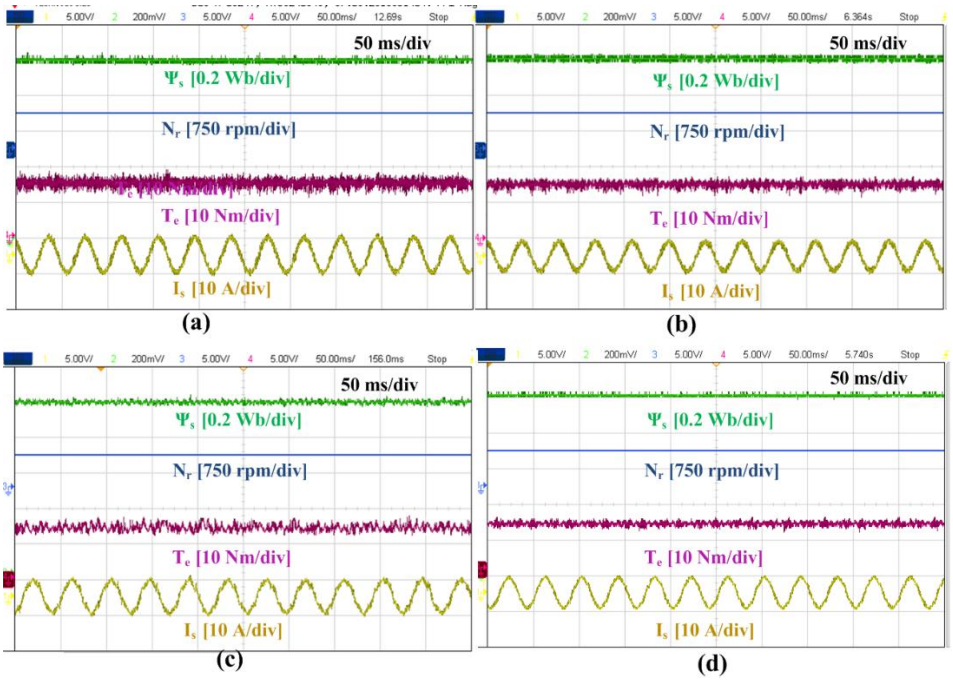

Figure 6.8 Response at 750 rpm, 12 Nm load under steady-state condition (a) C-MPCC, (b) DMPC [99], (c) MVMPC [97], (d) Proposed scheme.

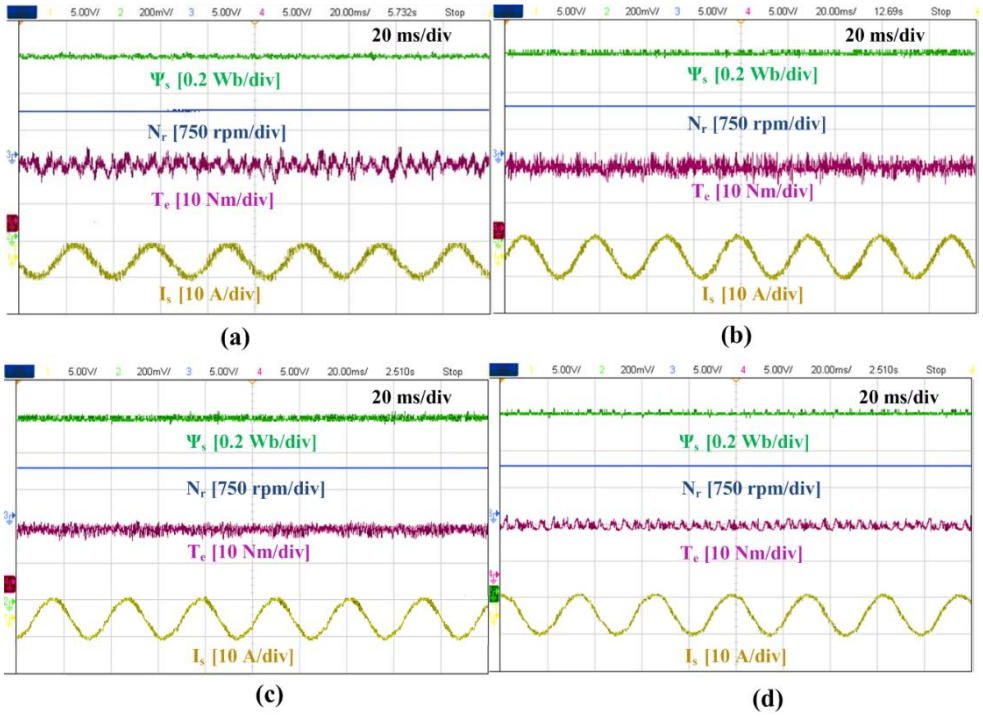

Figure 6.9 Response at 1000 rpm, 15 Nm load under steady-state condition (a) C-MPCC, (b) DMPC [99], (c) MVMPC [97], (d) Proposed scheme.

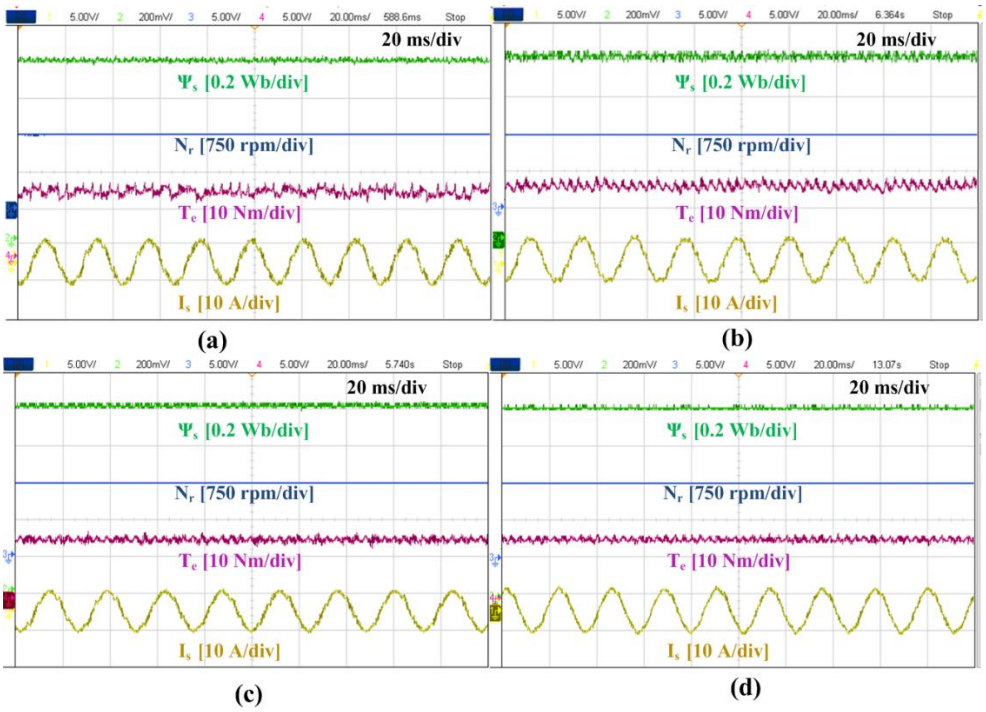

Figure 6.10 Response at 1500 rpm, 18 Nm load under steady-state condition (a) C-MPCC, (b) DMPC [99], (c) MVMPC [97], (d) Proposed scheme.

Table 6.3 Evaluation of performance indices under different speed and load conditions

Control scheme	300 rpm, 5 Nm		750 rpm, 12 Nm		1500 rpm, 18 Nm	
	T_{e_rip} (Nm)	Ψ_{rip} (mWb)	T_{e_rip} (Nm)	Ψ_{rip} (mWb)	T_{e_rip} (Nm)	Ψ_{rip} (mWb)
C-MPCC	0.392	2.1	0.374	2.3	0.341	1.9
DMPC [99]	0.318	1.9	0.289	1.3	0.249	1.4
MVMPC [97]	0.281	1.5	0.187	1.8	0.388	1.6
Proposed MPCC	0.197	1.2	0.168	1.1	0.232	1.2

Table 6.4 Evaluation of performance indices under different speed and load conditions

Control scheme	300 rpm, 5 Nm		750 rpm, 12 Nm		1500 rpm, 18 Nm	
	f_{sw}(Hz)	%THD	f_{sw}(Hz)	%THD	f_{sw}(Hz)	%THD
C-MPCC	2833	16.82	2665	15.47	2345	14.92
DMPC [99]	3899	13.78	3763	11.94	3431	10.87
MVMPC [97]	4782	9.23	4611	8.09	4329	7.66
Proposed MPCC	4673	7.93	4652	7.61	4265	6.98

The proposed scheme performance is thus validated at different speeds ranging from low to high and at different loads.

The torque ripples (T_{e_rip}), and flux ripples (Ψ_{rip}) are calculated based on standard deviation as,

$$T_{e\_rip} = \sqrt{\frac{1}{n}\sum_{i=0}^{n}(T_e(i) - T_e^*)^2)} \tag{6.19}$$

$$\psi_{rip} = \sqrt{\frac{1}{n}\sum_{i=0}^{n}(\psi_s(i) - \psi_s^*)^2)} \tag{6.20}$$

The performance indices like torque ripples, flux ripples, Total Harmonic Distortion (THD) of stator current, and switching frequency (f_{sw}) are evaluated and presented in Table 6.3 and Table 6.4. It can be observed from Table 6.3 and Table 6.4 that the proposed scheme offers improved steady-state performance with lower torque and flux ripple.

The stator current THD value is also less for the proposed scheme compared to C-MPCC, MVMPC [97], and DMPC [99] schemes. Thus, it can be validated that an improved performance is obtained for the proposed scheme owing to the application of three VVs in a control period.

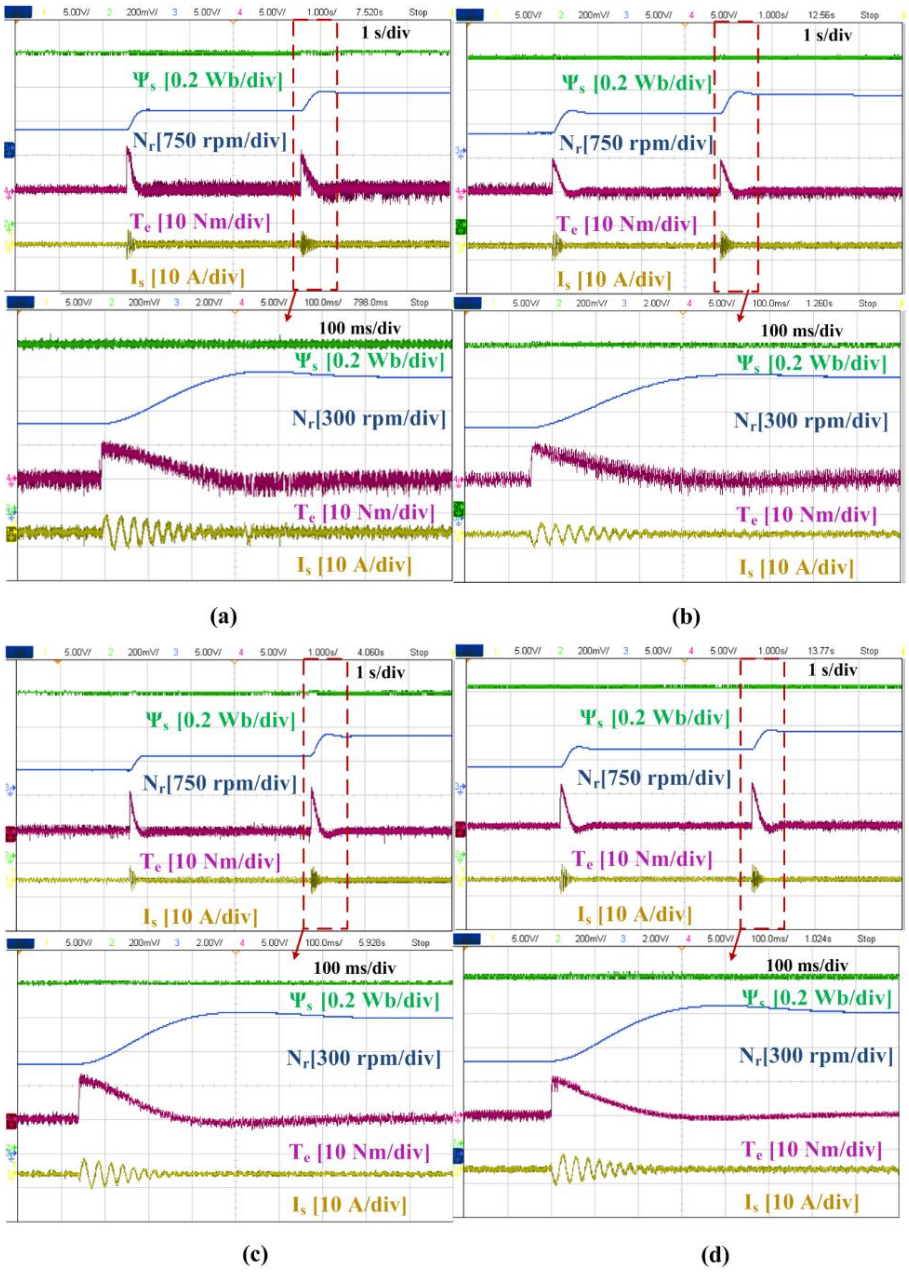

Figure 6.11 Dynamic acceleration for reference speed variation from 400 rpm to 800 rpm to 1200 rpm (a) C-MPCC, (b) DMPC [99], (c) MVMPC [97], (d) Proposed scheme.

Further, the dynamic response is investigated to verify the effectiveness of the proposed control technique. To achieve this, the motor is accelerated from an initial reference speed of 400 rpm to 800 rpm to 1200 rpm. The response during acceleration is shown in Figure 6.11. Similarly, the deceleration response, when the speed reference command is changed from 1000 rpm to 500 rpm, is shown in Figure 6.12.

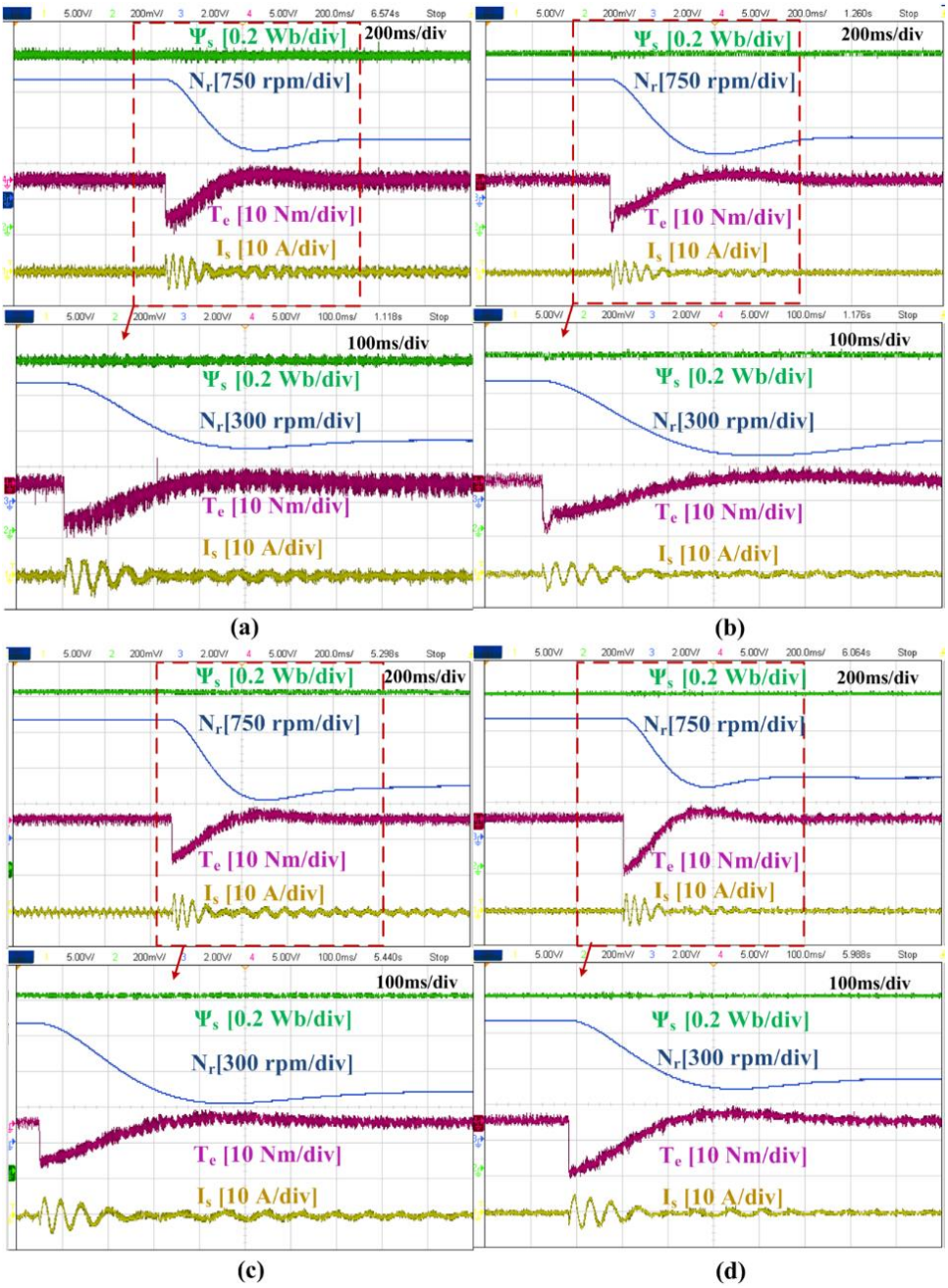

Figure 6.12 Dynamic deceleration for reference speed variation from 1000 rpm to 500 rpm (a) C-MPCC, (b) DMPC [99], (c) MVMPC [97], (d) Proposed scheme.

The response of the drive when a load of 12 Nm is supplied at 1000 rpm is given in Figure 6.13. It can be perceived from the responses that the proposed scheme offers a similar dynamic performance as that of the C-MPCC scheme with the added advantage of improved steady-state performance.

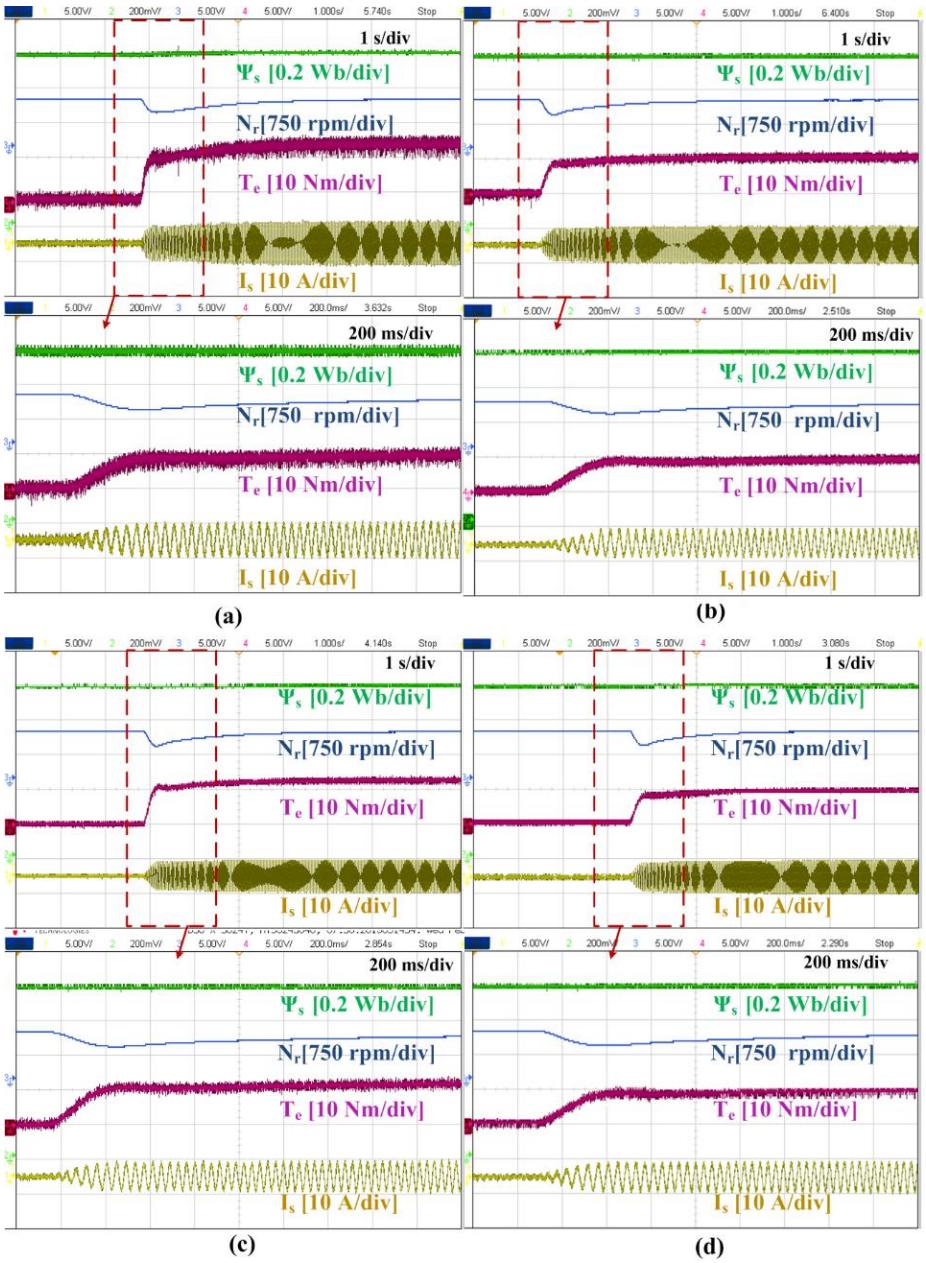

Figure 6.13 Dynamic load response after 12 Nm load is suddenly supplied at 1000 rpm. (a) C-MPCC, (b) DMPC [99], (c) MVMPC [97], (d) Proposed scheme.

The VV preselection scheme is framed in such a way as to choose the optimum VV directly without any prediction, cost-function evaluation, and optimization steps. However, it does not affect the drive performance due to the determination of the position of the current error using a modified position estimation approach. The proposed amplitude optimization is based on the cost-function ratio. This leads to reduced machine parameter dependence contributed by the reference VV calculation using the deadbeat solution. Further, the determination of optimum VVs and duty calculation does not upsurge the computational complexity of the algorithm.

6.3.2 Computational Time

The criteria used to evaluate the computational burden and algorithm complexity is the turnaround time, which can be directly obtained from the control desk as shown in Table 6.5. The C-MPCC scheme requires a computational time of 42 µs for its implementation. The dual VV-based DMPC [99] scheme requires 39 µs, whereas MVMPC [97] takes up 34 µs for the control algorithm evaluation. Conversely, the proposed scheme has a turnaround time of 30 µs. Therefore, the proposed scheme has the least computational time compared to the other three schemes. It can be observed from Table 6.5 that in DMPC [99], the calculation of the deadbeat-based reference VV and sector determination almost nullifies the advantage of the preselection for reduced computations. The determination of the sector inevitably requires tangent inverse angle calculations. Moreover, the cost-function must be evaluated two times to obtain the optimal VVs.

Similarly, in the MVMPC [97] scheme, only three VVs are shortlisted for the numerical computations. Nevertheless, the duty ratio calculation in this scheme allocates additional computational time. Compared to other schemes, the advantage offered by the proposed scheme is the direct estimation of the optimal VVs based on the modified position estimation. This scheme avoids the prediction and optimization stages and simple relational operations help to choose the optimal VVs effectively. The amplitudes of the three VVs are also optimized based on the cost-function ratios, which require fewer computations compared to MVMPC [97].

Table 6.5 Determined computational time (tc)

Terms	**C-MPCC**	**DMPC [99]**	**MVMPC [97]**	**Proposed**
	t_c **(µs)**	t_c **(µs)**	t_c **(µs)**	t_c **(µs)**
Measurement and estimation	8.12	8.12	8.12	8.12
Reference VV determination	-	1.46	-	-
Identification of sector or criteria for VV selection	-	13.07	7.06	8.15
VV grouping	-	5.96	1.01	-
Prediction of currents, Cost function Evaluation	24.23	4.57	6.61	2.95
Optimum VVs determination	9.33	4.27	2.56	5.31
Duty calculation	-	1.33	8.68	5.29
Total	**42**	**39**	**34**	**30**

6.3.3 Effect of R_s and L_s variation

The performance of the proposed scheme is analyzed for machine parameter variations. To achieve this, the machine parameters R_s and L_s used in the predictive scheme are incremented by 30%.

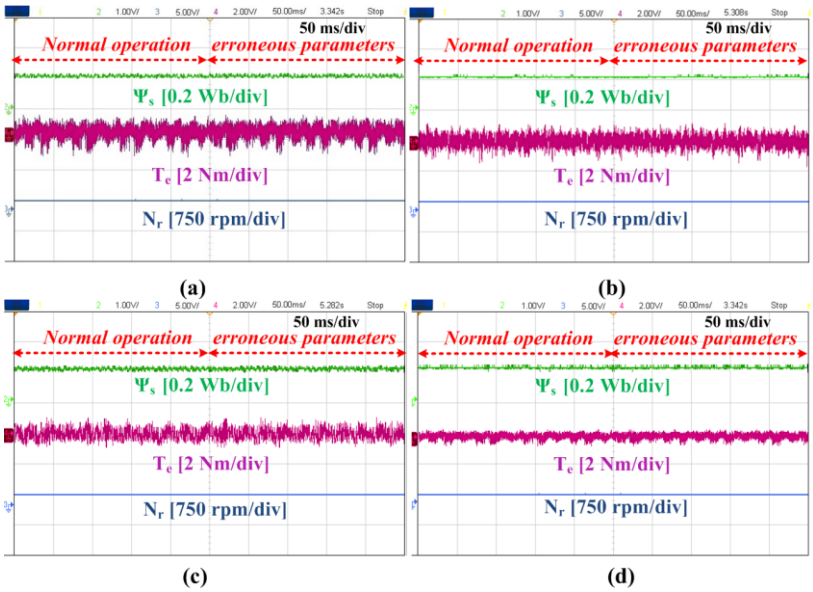

Figure 6.14 Response of drive at a speed of 100 rpm under a change in Rs (a) C-MPCC, (b) DMPC [99], (c) MVMPC [97], (d) Proposed scheme.

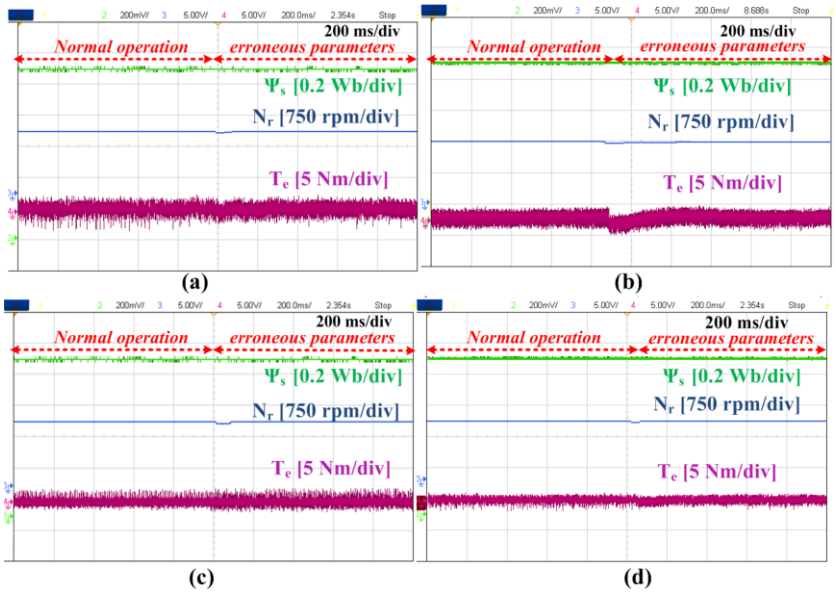

Figure 6.15 Response of the drive at rated speed under a change in Ls (a) C-MPCC, (b) DMPC [99], (c) MVMPC [97], (d) Proposed scheme.

The effect of change in R_s can be observed prominently in the low-speed region. Thus, with the incremented value of resistance fed to the algorithm, the drive performance is assessed at 100 rpm speed. The performances obtained for all the

control schemes are shown in Figure 6.14. It is apparent that the change in R_s value does not affect the effectiveness of the control techniques as the prediction of stator current is less dependent on R_s. Nonetheless, the effect of L_s variation has a significant influence on the drive performance at high speeds. The motor is run at the rated speed and the erroneous L_s value is used in the algorithm to evaluate the effect. As shown in Figure 6.15., the MPCC schemes are slightly perturbed due to the variation in L_s. The effect of L_s variation is more on reference VV-based MPCC scheme using the deadbeat solution. Hence, the performance of the DMPC [99] scheme is disturbed more than the other schemes. On the other hand, MVMPC [97] shows slightly increased torque ripples due to the variation in L_s and the response of the proposed scheme is analogous to the C-MPCC scheme. The disturbance caused by the sudden change in L_s is easily stabilized. Thus, the proposed scheme is robust and offers less sensitivity toward machine parameter variations.

6.4 Summary

In this chapter, a low-complex multivector-based MPCC scheme is proposed for the two-level VSI-based PMSM drive. In the proposed scheme, the optimum VVs are directly obtained using a modified position estimation approach. This eliminates the operations involving cost-function evaluation and optimizations. Thus, the VVs involved in the computations are confined to 1. However, the steady-state response of the drive can be improved when multiple VVs are applied in a control period. To achieve this, the proposed scheme applies two active and a null VV based on the stator current error. The second optimal VV is also obtained using simple relational operations based on the gradient of the first optimal VV. To limit the increase in the switching transitions, the adjacent VVs are selected as optimal VVs. The duration of application of the optimal VVs is obtained by the weighted average error-based duty calculation method. The cost-function-based duty ratio calculation is simple and does not elevate the complexity of the control algorithm. Moreover, the proposed scheme is devoid of reference VV estimation and does not contribute to additional parameter sensitivity. Thus, the proposed scheme offers improved steady-state torque performance and lower computational burden, while maintaining the dynamic drive performance.

Chapter 7

Conclusions and Future Scope

7. Conclusions and Future Scope

The research works in this thesis have explored several duty-based MPCC strategies of a PMSM drive and focused on the enhancement of steady-state torque and flux responses. The highlighted contributions from the research works conducted are the development of simple, reduced parameter sensitive, low-complex duty-based MPCC schemes with a reduction in the computational time of the predictive algorithm. This contributes to the pertinence of the control algorithm for real-time applications. The outcomes of the research work incorporated in this thesis are summarized in the following section.

7.1 Conclusion

A dual voltage vector-based MPCC has been proposed for a two-level Voltage Source Inverter (VSI) based PMSM drive to improve the steady-state performance. In the proposed method, two voltage vectors (one active and one null) are applied in every control interval. The proposed method aims to retain the simplicity of the C-MPCC method while addressing the demerits of large torque and flux ripples due to the application of a single voltage vector for the entire control period. The duty ratio calculation is obtained from the deadbeat principle, where the predicted current is forced to reach the reference values at the end of the sample time. The proposed duty ratio is obtained as the ratio of the error between the reference and predicted current values and a constant. Thus, the control of quadrature-axis current error would minimize the torque variations and the direct-axis current error control aids in reducing the flux variations. In the proposed method, the calculations involving current slopes are eliminated and thus, establish a parameter-insensitive duty calculation. The steady-state performance is improved due to the dual voltage vector application and the computational burden is maintained within its limit. Moreover, the dynamic performance is unaltered.

A low complex dual voltage vector-based MPCC scheme is proposed to address the limitation of increased computational burden due to the duty implementation. The application of dual voltage vectors enhances the steady-state torque and flux responses at the expense of increased computational time. The C-MPCC scheme employs seven voltage vectors in every control period for the

prediction and optimization stages, which necessitates the deployment of a fast processor with a large data handling capacity. The algorithm gets updated every sample time and increases the processor burden. To address this, a voltage vector preselection scheme is proposed which chooses three voltage vectors in every sample time for the prediction, cost function evaluation, and optimization steps. This considerably reduces the number of operations involved in every sample time and the computational time. The proposed voltage vector grouping requires only the direction of rotation of the motor and the previous sample time voltage vector. The proposed scheme does not require any sector or angle determination to achieve this aim. Further, the C-MPCC method is confined to the use of only a single voltage vector during the entire control period, which inversely affects the steady-state drive performance. Thus, an effective duty modulation based on the rms-current ripple minimization technique is proposed to attain a better steady-state response of the drive. The proposed duty scheme aids in altering the magnitude of the voltage vectors suitably according to the stator current error with the addition of a null voltage vector. The duty calculation does not require any complex calculations while retaining the dynamic drive performance.

In certain operating conditions, the addition of a null voltage vector alone cannot achieve improvement in the steady-state performance. Thus, a multivector-based MPCC scheme is proposed to enhance the control precision and improve the steady-state response of the drive. The multi-vector operation is obtained using an effective virtual voltage vector synthesis, which augments the control set to yield an improvement in the control precision. The burden on the processor is limited with the help of a predefined look-up table-based voltage vector selection scheme using the stator current error. The optimum voltage vector amplitude is optimized to further enhance the steady-state performance. Thus, the average error minimization technique is used to obtain the duration of application of the optimum extended control set-based voltage vector. The proposed method offers the feasibility of applying two or three voltage vectors in a sample time based on the magnitude of the error. The dynamic response of the drive is retained and duty ratio calculation is less sensitive against parameter variations. Thus, the proposed method offers better performance than the independent control offered by the duty-modulated scheme as well as the extended control set-based MPCC scheme.

The multiple voltage vector application improves the steady-state performance of the drive at the expense of increased computational complexity. Thus, a low-complex multivector-based MPCC scheme is proposed for the PMSM drive. The proposed scheme aims to alleviate the number of operations associated with the C-MPCC scheme according to an improved position assessment approach using the gradient concept. The voltage vector preselection scheme considers the magnitude of the error in the stator current and avoids the parameter-sensitive reference voltage vector determination. The novel voltage vector preselection scheme utilized decreases the number of candidate voltage vectors used for computation from 8 to 1. Further, the torque performance of the drive is improved under steady-state conditions using a simple cost-function ratio-based duty modulation scheme. In the proposed scheme, three voltage vectors (two active and a null) are applied in each sample time considering the magnitude of the error between the control variables. The proposed duty modulation scheme estimates the duration of application of the optimal voltage vectors using the cost-function ratio of the chosen voltage vectors. This eliminates the need for the space vector modulation scheme for the estimation of the application time of voltage vectors. Further, the proposed scheme maintains the dynamic performance of the drive as offered by the C-MPCC scheme with improved steady-state performance and lower computational complexity.

The proposed schemes in this thesis are suitable for controlling PMSM used in electric and hybrid electric vehicle applications in the transportation sector, robotic applications in manufacturing industries, offshore and onshore wind energy applications, etc.

7.2 Future Scope

The research works in this thesis evaluated duty-based MPCC schemes for PMSM drives. Based on the techniques used, the future scope of these works includes the following.

1. The proposed works can be extended to multi-level or multi-phase PMSM drives for enhanced steady-state responses.
2. All the proposed works are implemented for the surface-mounted PMSMs. The proposed works can be extended to evaluate the performance of

interior PMSM. Thus, wide-speed operation capability can also be assessed for all the schemes. It can be also used for three-phase Induction motors.

3. The constant frequency operation can be analyzed for all the proposed schemes.
4. The proposed schemes can be extended for speed sensorless operations using sophisticated speed observers. Further, the parameter sensitivity of the control algorithms can be reduced using the design of suitable observers.

Appendix-1 Experimental Setup

The proposed MPCC schemes presented in this thesis were experimentally tested on the PMSM drive employed with a dSPACE controller. The schematic of the experimental set up of the two-level inverter-fed PMSM used is shown in the following Figure A.1. A 5 HP surface-mounted PMSM is used for all the experimentation. The PMSM is mechanically coupled to the 3.7 kW DC generator which is used as an electrical load when connected to the variable resistance load. The DC supply for the inverter is obtained using a three-phase rectifier circuit. The DC link voltage ripples are further eliminated after rectification using the DC link capacitor.

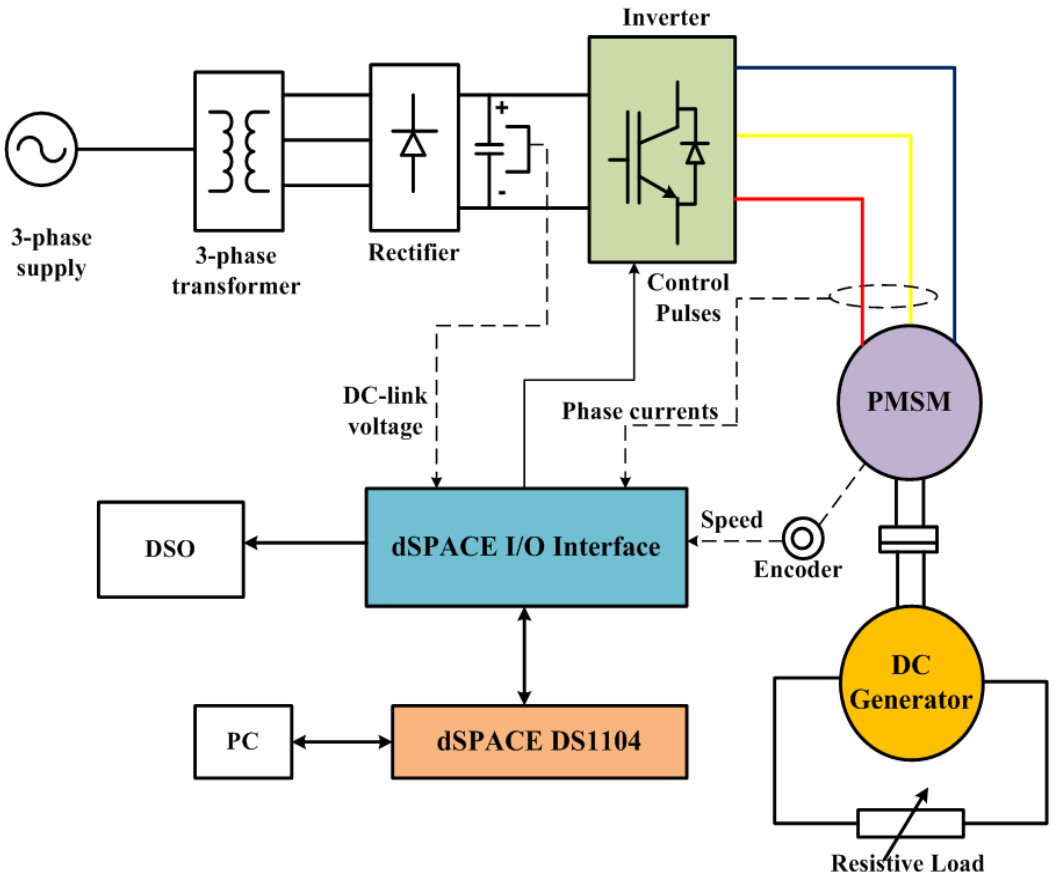

Figure A.1 Block diagram of two-level three-phase VSI fed PMSM drive.

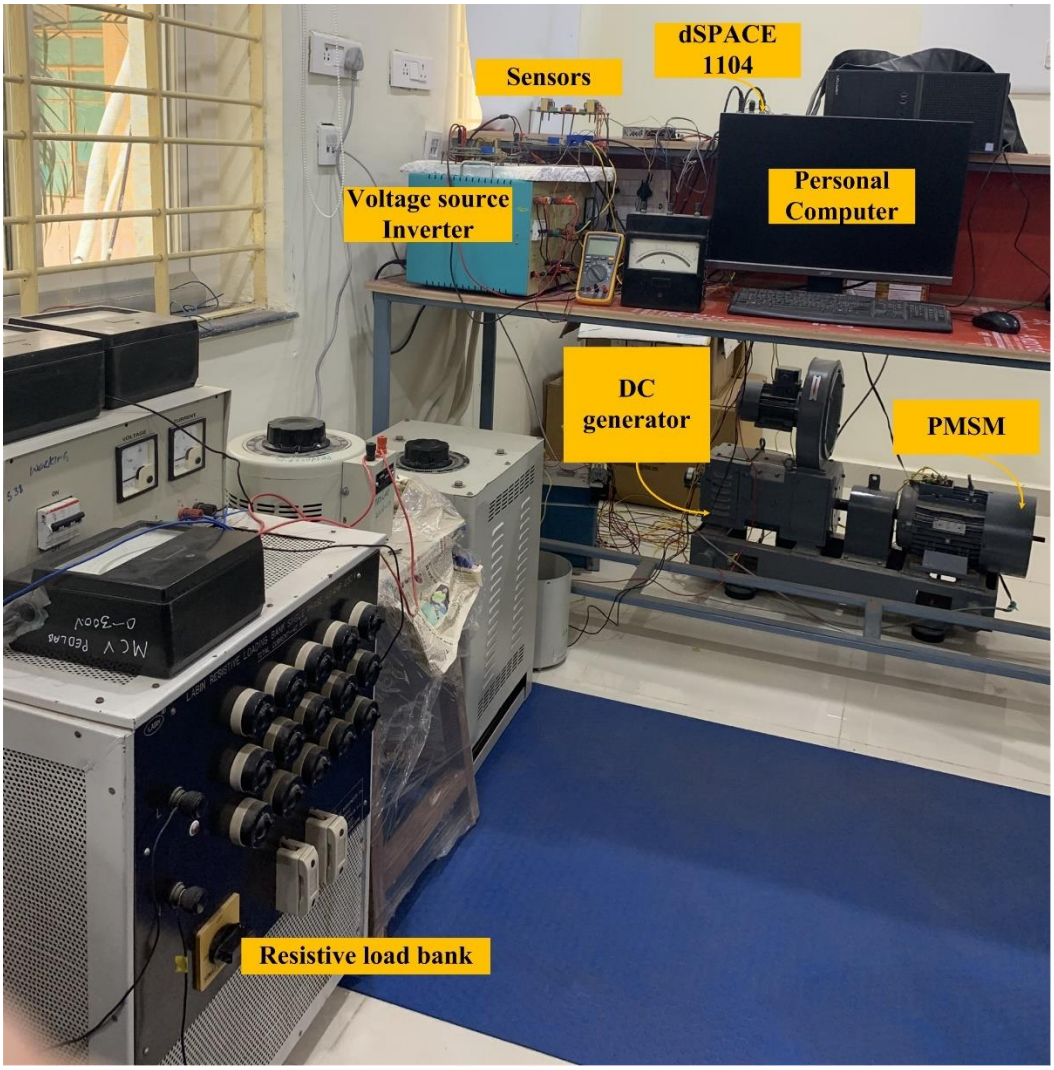

Figure A.2 Test bench setup for the MPCC operated PMSM drive.

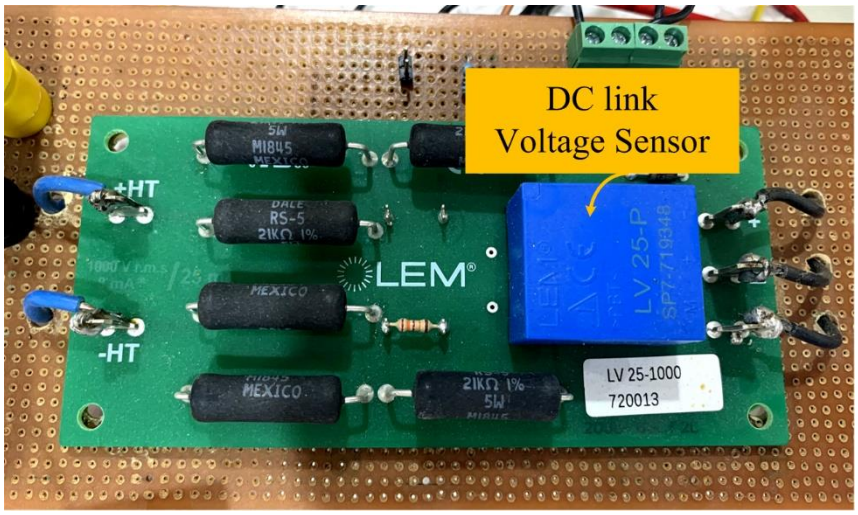

Figure A.3 Voltage sensor

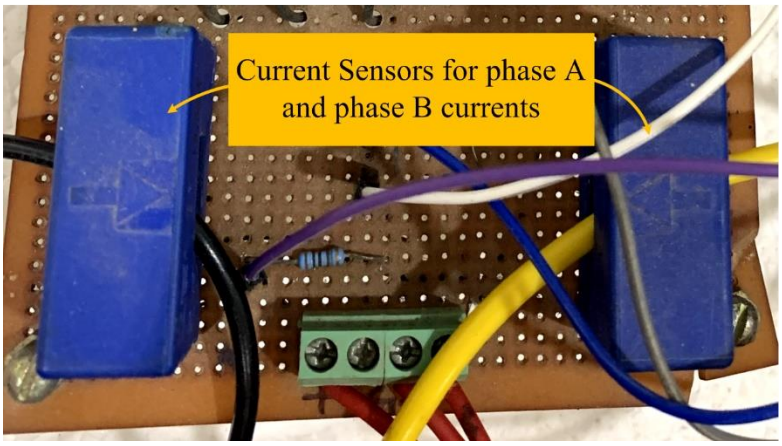

Figure A.4 Current sensors

The DS 1104 controller is used for the real-time implementation of all the control algorithms. It requires an MPC8240 CPU which has a clock frequency of 250 MHz. A slave processor TMS320F240 is also used along with the main processor. The dSPACE 1104 processor I/O interface has 8 Analog to Digital Conversion (ADC) channels and 8 Digital to Analog Conversion (DAC) channels. The voltage range of these channels is within ±10V. Further, it has 20 digital I/O pins that can be operated individually. There are 10 PWM channels supported by the slave processor, which can be programmed independently.

The dSPACE 1004 controller also has a provision to directly interface the incremental encoder. The control algorithms can be programmed using the MATLAB/Simulink software and the online optimizations as well as control of different parameters can be performed using the integrated Control Desk software. The ratings of the equipment and machines used for experimentation are included in the following Table A.1.

The DC voltage along with the phase currents are sensed and fed to the ADC channels of the dSPACE DS-1104 controller. The control algorithms are executed at a sampling time that is greater than the execution time of the algorithm. The control pulses generated at the end of every sample time during the program execution are applied to the inverter. The estimated torque and the stator flux response are observed on the digital signal oscilloscope (DSO) through the DAC channel output of dSPACE DS-1104.

Table A.1 Parameters of equipment in the experimental test setup

PMSM	
Motor Parameter	**Quantity**
Rated Power	3.7 kW
Rated Torque	23.5 N m
Rated Speed	1500 rpm
Rated current	6A
Stator Resistance (R_s)	1.12 Ω
Stator Inductance (L_s)	10.5 mH
Rotor flux(ψ_f)	1 Wb
Poles (P)	4
Inertia (J)	0.061 kg-m^2
Load (DC machine)	
Rated power	3.7 kW
Rated speed	1500 RPM
Rated torque	23.5 Nm
VSI	
Voltage rating	1200 V
Current rating	75 A
DC link capacitor	4700 μF
LV-25 Voltage sensing board	
Supply voltage	± 15 V
Maximum voltage	1000 V
LA-25 Current sensing board	
Supply voltage	± 15 V
Maximum current	25 A

References

[1] T. Li, X. Sun, G. Lei, Y. Guo, Z. Yang, and J. Zhu, "Finite-Control-Set Model Predictive Control of Permanent Magnet Synchronous Motor Drive Systems—An Overview," *IEEE/CAA Journal of Automatica Sinica*, vol. 9, no. 12, pp. 2087–2105, Dec. 2022, doi: 10.1109/JAS.2022.105851.

[2] H. Abu-Rub, A. Iqbal, and J. Guzinski, *High Performance Control of AC Drives with MATLAB®/Simulink*. Wiley, 2021. doi: 10.1002/9781119591313.

[3] V. R. Ivanova and I. Yu. Ivanov, "Efficiency of Introduction of Variable Frequency Drive," in *2020 International Multi-Conference on Industrial Engineering and Modern Technologies (FarEastCon)*, IEEE, Oct. 2020, pp. 1–7. doi: 10.1109/FarEastCon50210.2020.9271325.

[4] A. T. de Almeida, F. J. T. E. Ferreira, and G. Baoming, "Beyond induction motors — Technology trends to move up efficiency," in *49th IEEE/IAS Industrial & Commercial Power Systems Technical Conference*, IEEE, Apr. 2013, pp. 1–13. doi: 10.1109/ICPS.2013.6547330.

[5] Krishnan R, *Electric motor drives: modelling, analysis, and control*. Prentice Hall, 2001.

[6] Sen P. C, *Principles of Electric Machines and Power Electronics*. Wiley, 1988.

[7] Sang-Hoon Kim, *Electric Motor Control DC, AC, and BLDC Motors*. Elsevier, 2017.

[8] Bose Bimal K, *Modern power electronics and AC drives*. Prentice Hall, 2002.

[9] B. Asaei and B. Rahrovi, "Minimum-copper-loss control over full speed range of an IPMSM drive for hybrid electric vehicle application," in *2010 IEEE Vehicle Power and Propulsion Conference*, IEEE, Sep. 2010, pp. 1–6. doi: 10.1109/VPPC.2010.5728999.

[10] Z. Song, J. Yang, X. Mei, T. Tao, and M. Xu, "Deep reinforcement learning for permanent magnet synchronous motor speed control systems," *Neural Comput Appl*, vol. 33, no. 10, pp. 5409–5418, 2021, doi: 10.1007/s00521-020-05352-1.

[11] R Krishnan, *Permanent Magnet Synchronous and Brushless DC Motor Drives*. CRC Press, 2010.

[12] S. Meier, "Theoretical design of surface-mounted permanent magnet motors with field weakening capabilit," Royal Institute of Technology, Stockholm, 2001.

[13] L. V. Iyer *et al.*, "A novel MTPA theory based bottom-up approach towards parametric and structural design of interior PMSM for electric vehicles," *International Transactions on Electrical Energy Systems*, vol. 28, no. 2, p. e2489, Feb. 2018, doi: 10.1002/etep.2489.

[14] Z. Tang, X. Li, S. Dusmez, and B. Akin, “A New V/f-Based Sensorless MTPA Control for IPMSM Drives,” *IEEE Trans Power Electron*, vol. 31, no. 6, pp. 4400–4415, Jun. 2016, doi: 10.1109/TPEL.2015.2470177.

[15] S. Datta, A. Chandra, and S. Chowdhuri, “High performance sensor-less V/f control of surface PMSM in voltage vector plane with ZVV injection and SMO-based position estimation method,” *Electrical Engineering*, vol. 104, no. 2, pp. 657–666, Apr. 2022, doi: 10.1007/s00202-021-01325-2.

[16] W. Tu, G. Xiao, C. Suo, and K. Yang, “A design of sensorless permanent magnet synchronous motor drive based on V/f control,” in *2017 20th International Conference on Electrical Machines and Systems (ICEMS)*, IEEE, Aug. 2017, pp. 1–5. doi: 10.1109/ICEMS.2017.8056032.

[17] S. Agarlita, C. Coman, G. Andreescu, and I. Boldea, “Stable V/f control system with controlled power factor angle for permanent magnet synchronous motor drives,” *IET Electr Power Appl*, vol. 7, no. 4, pp. 278–286, Apr. 2013, doi: 10.1049/iet-epa.2012.0392.

[18] Peter Vas, *Sensorless vector and direct torque control*. Oxford University Press, 1998.

[19] Z. Daboussi and N. Mohan, “Digital simulation of field-oriented control of induction motor drives using EMTP,” *IEEE Transactions on Energy Conversion*, vol. 3, no. 3, pp. 667–673, 1988, doi: 10.1109/60.8083.

[20] A. D. Alexandrou, N. Adamopoulos, and A. Kladas, “Development of a Constant Switching Frequency Deadbeat Predictive Control Technique for Field-Oriented Synchronous Permanent-Magnet Motor Drive,” *IEEE Transactions on Industrial Electronics*, vol. 63, no. 8, pp. 5167–5175, Aug. 2016, doi: 10.1109/TIE.2016.2559419.

[21] D. Casadei, F. Profumo, G. Serra, and A. Tani, “FOC and DTC: two viable schemes for induction motors torque control,” *IEEE Trans Power Electron*, vol. 17, no. 5, pp. 779–787, Sep. 2002, doi: 10.1109/TPEL.2002.802183.

[22] I. Takahashi and T. Noguchi, “A New Quick-Response and High-Efficiency Control Strategy of an Induction Motor,” *IEEE Trans Ind Appl*, vol. IA-22, no. 5, pp. 820–827, Sep. 1986, doi: 10.1109/TIA.1986.4504799.

[23] L. Zhong, M. F. Rahman, W. Y. Hu, and K. W. Lim, “Analysis of direct torque control in permanent magnet synchronous motor drives,” *IEEE Trans Power Electron*, vol. 12, no. 3, pp. 528–536, May 1997, doi: 10.1109/63.575680.

[24] F. Niu, B. Wang, A. S. Babel, K. Li, and E. G. Strangas, “Comparative Evaluation of Direct Torque Control Strategies for Permanent Magnet Synchronous Machines,” *IEEE Trans Power Electron*, vol. 31, no. 2, pp. 1408–1424, Feb. 2016,

doi: 10.1109/TPEL.2015.2421321.

[25] J. Maciejowski, *Predictive Control*. Pearson, 2002.

[26] E. Camacho and C. Bordons, *Model Predictive Control*. Springer Verlag, 2007.

[27] J. Rawlings and D. Mayne, *Model Predictive Control: Theory and Design*. Nob Hill Publishing , 2009.

[28] and P. C. J. Rodriguez, *Predictive Control of Power Converters and Electrical Drives*. New York, NY, USA: Wiley, 2012.

[29] A. Linder and R. Kennel, "Model Predictive Control for Electrical Drives," in *IEEE 36th Conference on Power Electronics Specialists, 2005.*, IEEE, pp. 1793–1799. doi: 10.1109/PESC.2005.1581874.

[30] F. Wang, S. Li, X. Mei, W. Xie, J. Rodriguez, and R. M. Kennel, "Model-Based Predictive Direct Control Strategies for Electrical Drives: An Experimental Evaluation of PTC and PCC Methods," *IEEE Trans Industr Inform*, vol. 11, no. 3, pp. 671–681, Jun. 2015, doi: 10.1109/TII.2015.2423154.

[31] J. H. Lee, "Model predictive control: Review of the three decades of development," *Int J Control Autom Syst*, vol. 9, no. 3, pp. 415–424, Jun. 2011, doi: 10.1007/s12555-011-0300-6.

[32] M. A. Perez, J. Rodriguez, E. J. Fuentes, and F. Kammerer, "Predictive Control of AC–AC Modular Multilevel Converters," *IEEE Transactions on Industrial Electronics*, vol. 59, no. 7, pp. 2832–2839, Jul. 2012, doi: 10.1109/TIE.2011.2159349.

[33] P. Correa and J. Rodriguez, "A predictive control scheme for current source rectifiers," in *2008 13th International Power Electronics and Motion Control Conference*, IEEE, Sep. 2008, pp. 699–702. doi: 10.1109/EPEPEMC.2008.4635346.

[34] P. Cortes, G. Ortiz, J. I. Yuz, J. Rodriguez, S. Vazquez, and L. G. Franquelo, "Model Predictive Control of an Inverter With Output LC Filter for UPS Applications," *IEEE Transactions on Industrial Electronics*, vol. 56, no. 6, pp. 1875–1883, Jun. 2009, doi: 10.1109/TIE.2009.2015750.

[35] M. Rivera *et al.*, "A Comparative Assessment of Model Predictive Current Control and Space Vector Modulation in a Direct Matrix Converter," *IEEE Transactions on Industrial Electronics*, vol. 60, no. 2, pp. 578–588, Feb. 2013, doi: 10.1109/TIE.2012.2206347.

[36] J. Guzinski and H. Abu-Rub, "Speed Sensorless Induction Motor Drive With Predictive Current Controller," *IEEE Transactions on Industrial Electronics*, vol. 60, no. 2, pp. 699–709, Feb. 2013, doi: 10.1109/TIE.2012.2205359.

[37] Z. Zhang, F. Wang, T. Sun, J. Rodriguez, and R. Kennel, "FPGA-Based

Experimental Investigation of a Quasi-Centralized Model Predictive Control for Back-to-Back Converters," *IEEE Trans Power Electron*, vol. 31, no. 1, pp. 662–674, Jan. 2016, doi: 10.1109/TPEL.2015.2397695.

[38] T. Atalik *et al.*, "Multi-DSP and -FPGA-Based Fully Digital Control System for Cascaded Multilevel Converters Used in FACTS Applications," *IEEE Trans Industr Inform*, vol. 8, no. 3, pp. 511–527, Aug. 2012, doi: 10.1109/TII.2012.2194160.

[39] W. Xie *et al.*, "Finite-Control-Set Model Predictive Torque Control With a Deadbeat Solution for PMSM Drives," *IEEE Transactions on Industrial Electronics*, vol. 62, no. 9, pp. 5402–5410, Sep. 2015, doi: 10.1109/TIE.2015.2410767.

[40] F. Wang, Z. Zhang, X. Mei, J. Rodríguez, and R. Kennel, "Advanced Control Strategies of Induction Machine: Field Oriented Control, Direct Torque Control and Model Predictive Control," *Energies (Basel)*, vol. 11, no. 1, p. 120, Jan. 2018, doi: 10.3390/en11010120.

[41] T. Geyer, G. Papafotiou, and M. Morari, "Model Predictive Direct Torque Control—Part I: Concept, Algorithm, and Analysis," *IEEE Transactions on Industrial Electronics*, vol. 56, no. 6, pp. 1894–1905, Jun. 2009, doi: 10.1109/TIE.2008.2007030.

[42] Y. Zhou, H. Li, R. Liu, and J. Mao, "Continuous Voltage Vector Model-Free Predictive Current Control of Surface Mounted Permanent Magnet Synchronous Motor," *IEEE Transactions on Energy Conversion*, vol. 34, no. 2, pp. 899–908, Jun. 2019, doi: 10.1109/TEC.2018.2867218.

[43] S. A. Davari, D. A. Khaburi, and R. Kennel, "An Improved FCS–MPC Algorithm for an Induction Motor With an Imposed Optimized Weighting Factor," *IEEE Trans Power Electron*, vol. 27, no. 3, pp. 1540–1551, Mar. 2012, doi: 10.1109/TPEL.2011.2162343.

[44] R. Vargas, U. Ammann, J. Rodriguez, and J. Pontt, "Predictive Strategy to Control Common-Mode Voltage in Loads Fed by Matrix Converters," *IEEE Transactions on Industrial Electronics*, vol. 55, no. 12, pp. 4372–4380, Dec. 2008, doi: 10.1109/TIE.2008.2007016.

[45] J. Rodriguez, J. Pontt, P. Cortes, and R. Vargas, "Predictive Control of a Three-Phase Neutral Point Clamped Inverter," in *2005 IEEE 36th Power Electronics Specialists Conference*, IEEE, 2005, pp. 1364–1369. doi: 10.1109/PESC.2005.1581807.

[46] F. Wang, X. Mei, J. Rodriguez, and R. Kennel, "Model predictive control for electrical drive systems-an overview," *CES Transactions on Electrical Machines*

and Systems, vol. 1, no. 3, pp. 219–230, Sep. 2017, doi: 10.23919/TEMS.2017.8086100.

[47] E. Kusuma, K. M. R. Eswar, and T. Vinay Kumar, "An Effective Predictive Torque Control Scheme for PMSM Drive Without Involvement of Weighting Factors," *IEEE J Emerg Sel Top Power Electron*, vol. 9, no. 3, pp. 2685–2697, Jun. 2021, doi: 10.1109/JESTPE.2020.2989429.

[48] F. Morel, Xuefang Lin-Shi, J.-M. Retif, B. Allard, and C. Buttay, "A Comparative Study of Predictive Current Control Schemes for a Permanent-Magnet Synchronous Machine Drive," *IEEE Transactions on Industrial Electronics*, vol. 56, no. 7, pp. 2715–2728, Jul. 2009, doi: 10.1109/TIE.2009.2018429.

[49] H. Miranda, P. Cortes, J. I. Yuz, and J. Rodriguez, "Predictive Torque Control of Induction Machines Based on State-Space Models," *IEEE Transactions on Industrial Electronics*, vol. 56, no. 6, pp. 1916–1924, Jun. 2009, doi: 10.1109/TIE.2009.2014904.

[50] Z. Ma, S. Saeidi, and R. Kennel, "FPGA Implementation of Model Predictive Control With Constant Switching Frequency for PMSM Drives," *IEEE Trans Industr Inform*, vol. 10, no. 4, pp. 2055–2063, Nov. 2014, doi: 10.1109/TII.2014.2344432.

[51] Y. Zhang, L. Huang, D. Xu, J. Liu, and and J. Jin, "Performance evaluation of two-vector-based model predictive current control of PMSM drives," *Chinese Journal of Electrical Engineering*, vol. 4, no. 2, pp. 65–81, Jun. 2018, doi: 10.23919/CJEE.2018.8409352.

[52] Yongchang Zhang and Jianguo Zhu, "Direct Torque Control of Permanent Magnet Synchronous Motor With Reduced Torque Ripple and Commutation Frequency," *IEEE Trans Power Electron*, vol. 26, no. 1, pp. 235–248, Jan. 2011, doi: 10.1109/TPEL.2010.2059047.

[53] Yuan Ren, Z. Q. Zhu, and Jiaming Liu, "Direct Torque Control of Permanent-Magnet Synchronous Machine Drives With a Simple Duty Ratio Regulator," *IEEE Transactions on Industrial Electronics*, vol. 61, no. 10, pp. 5249–5258, Oct. 2014, doi: 10.1109/TIE.2014.2300070.

[54] Y. Zhang and H. Yang, "Model Predictive Torque Control of Induction Motor Drives With Optimal Duty Cycle Control," *IEEE Trans Power Electron*, vol. 29, no. 12, pp. 6593–6603, Dec. 2014, doi: 10.1109/TPEL.2014.2302838.

[55] S. A. Davari, D. A. Khaburi, and R. Kennel, "An Improved FCS–MPC Algorithm for an Induction Motor With an Imposed Optimized Weighting Factor," *IEEE Trans Power Electron*, vol. 27, no. 3, pp. 1540–1551, Mar. 2012, doi: 10.1109/TPEL.2011.2162343.

[56] A. M. Bozorgi, M. Farasat, and S. Jafarishiadeh, “Model predictive current control of surface-mounted permanent magnet synchronous motor with low torque and current ripple,” *IET Power Electronics*, vol. 10, no. 10, pp. 1120–1128, Aug. 2017, doi: 10.1049/iet-pel.2016.0850.

[57] X. Zhang, L. Zhang, and Y. Zhang, “Model Predictive Current Control for PMSM Drives With Parameter Robustness Improvement,” *IEEE Trans Power Electron*, vol. 34, no. 2, pp. 1645–1657, Feb. 2019, doi: 10.1109/TPEL.2018.2835835.

[58] J. Chen, Y. Qin, A. M. Bozorgi, and M. Farasat, “Low Complexity Dual-Vector Model Predictive Current Control for Surface-Mounted Permanent Magnet Synchronous Motor Drives,” *IEEE J Emerg Sel Top Power Electron*, vol. 8, no. 3, pp. 2655–2663, Sep. 2020, doi: 10.1109/JESTPE.2019.2917865.

[59] S. G. Petkar, K. Eshwar, and V. K. Thippiripati, “A Modified Model Predictive Current Control of Permanent Magnet Synchronous Motor Drive,” *IEEE Transactions on Industrial Electronics*, vol. 68, no. 2, pp. 1025–1034, Feb. 2021, doi: 10.1109/TIE.2020.2970671.

[60] Y. Zhang and S. Gao, “Simultaneous optimization of voltage vector and duty cycle in model predictive torque control of PMSM drives,” in *2014 17th International Conference on Electrical Machines and Systems (ICEMS)*, IEEE, Oct. 2014, pp. 3338–3344. doi: 10.1109/ICEMS.2014.7014068.

[61] F. Niu, K. Li, and Y. Wang, “Direct Torque Control for Permanent-Magnet Synchronous Machines Based on Duty Ratio Modulation,” *IEEE Transactions on Industrial Electronics*, vol. 62, no. 10, pp. 6160–6170, Oct. 2015, doi: 10.1109/TIE.2015.2426678.

[62] Y. Zhang, H. Yang, and B. Xia, “Model predictive torque control of induction motor drives with reduced torque ripple,” *IET Electr Power Appl*, vol. 9, no. 9, pp. 595–604, Nov. 2015, doi: 10.1049/iet-epa.2015.0138.

[63] A. M. Bozorgi, M. Farasat, and S. Jafarishiadeh, “Model predictive current control of surface-mounted permanent magnet synchronous motor with low torque and current ripple,” *IET Power Electronics*, vol. 10, no. 10, pp. 1120–1128, Aug. 2017, doi: 10.1049/iet-pel.2016.0850.

[64] Y. Zhang, D. Xu, J. Liu, S. Gao, and W. Xu, “Performance Improvement of Model-Predictive Current Control of Permanent Magnet Synchronous Motor Drives,” *IEEE Trans Ind Appl*, vol. 53, no. 4, pp. 3683–3695, Jul. 2017, doi: 10.1109/TIA.2017.2690998.

[65] D. Su, C. Zhang, and Y. Dong, “Finite-State Model Predictive Current Control for Surface-Mounted Permanent Magnet Synchronous Motors Based on Current Locus,” *IEEE Access*, vol. 5, pp. 27366–27375, 2017, doi:

10.1109/ACCESS.2017.2771418.

[66] X. Chen, Z. Zhang, L. Yu, and Z. Bian, “Model Predictive Current Control of Doubly Salient Electromagnetic Machine for Current Ripple Suppression,” in *2019 IEEE International Symposium on Predictive Control of Electrical Drives and Power Electronics (PRECEDE)*, IEEE, May 2019, pp. 1–5. doi: 10.1109/PRECEDE.2019.8753359.

[67] C. A. Agustin, J. Yu, C.-K. Lin, and X.-Y. Fu, “A Modulated Model Predictive Current Controller for Interior Permanent-Magnet Synchronous Motors,” *Energies (Basel)*, vol. 12, no. 15, p. 2885, Jul. 2019, doi: 10.3390/en12152885.

[68] Hyung-Tae Moon, Hyun-Soo Kim, and Myung-Joong Youn, “A discrete-time predictive current control for PMSM,” *IEEE Trans Power Electron*, vol. 18, no. 1, pp. 464–472, Jan. 2003, doi: 10.1109/TPEL.2002.807131.

[69] O. Sandre-Hernandez, J. de J. Rangel-Magdaleno, and R. Morales-Caporal, “Modified model predictive torque control for a PMSM-drive with torque ripple minimisation,” *IET Power Electronics*, vol. 12, no. 5, pp. 1033–1042, May 2019, doi: 10.1049/iet-pel.2018.5525.

[70] C. Xia, S. Wang, X. Gu, Y. Yan, and T. Shi, “Direct Torque Control for VSI-PMSM Using Vector Evaluation Factor Table,” *IEEE Transactions on Industrial Electronics*, vol. 63, no. 7, pp. 4571–4583, Jul. 2016, doi: 10.1109/TIE.2016.2535958.

[71] Y. Zhang, D. Xu, and L. Huang, “Generalized Multiple-Vector-Based Model Predictive Control for PMSM Drives,” *IEEE Transactions on Industrial Electronics*, vol. 65, no. 12, pp. 9356–9366, Dec. 2018, doi: 10.1109/TIE.2018.2813994.

[72] T. Geyer, “Low complexity model predictive control in power electronics and power systems,” Ph.D. dissertation, Swiss Federal Inst. Technol., , Z¨urich, Switzerland, 2005.

[73] W. Zhao, T. Tao, J. Zhu, H. Tan, and Y. Du, “A Novel Finite-Control-Set Model Predictive Current Control for Five-Phase PM Motor With Continued Modulation,” *IEEE Trans Power Electron*, vol. 35, no. 7, pp. 7261–7270, Jul. 2020, doi: 10.1109/TPEL.2019.2954285.

[74] M. S. R. Saeed, W. Song, B. Yu, and X. Wu, “Low-Complexity Deadbeat Model Predictive Current Control With Duty Ratio for Five-Phase PMSM Drives,” *IEEE Trans Power Electron*, vol. 35, no. 11, pp. 12085–12099, Nov. 2020, doi: 10.1109/TPEL.2020.2983048.

[75] T. Tao, W. Zhao, Y. He, J. Zhu, H. Tan, and R. Xue, “Multivector Predictive Current Control for Five-Phase PM Motor by Using Hybrid Duty Modulation

Technology," *IEEE Transactions on Transportation Electrification*, vol. 6, no. 4, pp. 1603–1612, Dec. 2020, doi: 10.1109/TTE.2020.2991080.

[76] D. Xiao, K. S. Alam, and M. F. Rahman, "Modulated predictive current control for a two-level grid-connected converter with over-modulation capability," *IET Power Electronics*, vol. 13, no. 7, pp. 1466–1476, May 2020, doi: 10.1049/iet-pel.2019.0781.

[77] L. Chen, H. Xu, X. Sun, and Y. Cai, "Three-Vector-Based Model Predictive Torque Control for a Permanent Magnet Synchronous Motor of EVs," *IEEE Transactions on Transportation Electrification*, vol. 7, no. 3, pp. 1454–1465, Sep. 2021, doi: 10.1109/TTE.2021.3053256.

[78] X. Wang and D. Sun, "Three-Vector-Based Low-Complexity Model Predictive Direct Power Control Strategy for Doubly Fed Induction Generators," *IEEE Trans Power Electron*, vol. 32, no. 1, pp. 773–782, Jan. 2017, doi: 10.1109/TPEL.2016.2532387.

[79] M. Xiao, T. Shi, Y. Yan, W. Xu, and C. Xia, "Predictive Torque Control of Permanent Magnet Synchronous Motors Using Flux Vector," *IEEE Trans Ind Appl*, vol. 54, no. 5, pp. 4437–4446, Sep. 2018, doi: 10.1109/TIA.2018.2833817.

[80] T. Tao, W. Zhao, Y. He, J. Zhu, H. Tan, and R. Xue, "Multivector Predictive Current Control for Five-Phase PM Motor by Using Hybrid Duty Modulation Technology," *IEEE Transactions on Transportation Electrification*, vol. 6, no. 4, pp. 1603–1612, Dec. 2020, doi: 10.1109/TTE.2020.2991080.

[81] Z. Zhou, C. Xia, Y. Yan, Z. Wang, and T. Shi, "Torque Ripple Minimization of Predictive Torque Control for PMSM With Extended Control Set," *IEEE Transactions on Industrial Electronics*, vol. 64, no. 9, pp. 6930–6939, Sep. 2017, doi: 10.1109/TIE.2017.2686320.

[82] B. Yu, W. Song, Y. Guo, J. Li, and M. S. R. Saeed, "Virtual Voltage Vector-Based Model Predictive Current Control for Five-Phase VSIs With Common-Mode Voltage Reduction," *IEEE Transactions on Transportation Electrification*, vol. 7, no. 2, pp. 706–717, Jun. 2021, doi: 10.1109/TTE.2020.3030793.

[83] S. Suresh and P. P. Rajeevan, "Virtual Space Vector-Based Direct Torque Control Schemes for Induction Motor Drives," *IEEE Trans Ind Appl*, vol. 56, no. 3, pp. 2719–2728, May 2020, doi: 10.1109/TIA.2020.2978447.

[84] Yongchang Zhang and Jianguo Zhu, "A Novel Duty Cycle Control Strategy to Reduce Both Torque and Flux Ripples for DTC of Permanent Magnet Synchronous Motor Drives With Switching Frequency Reduction," *IEEE Trans Power Electron*, vol. 26, no. 10, pp. 3055–3067, Oct. 2011, doi: 10.1109/TPEL.2011.2129577.

[85] Y. Zhang, Y. Bai, and H. Yang, "A Universal Multiple-Vector-Based Model

Predictive Control of Induction Motor Drives," *IEEE Trans Power Electron*, vol. 33, no. 8, pp. 6957–6969, Aug. 2018, doi: 10.1109/TPEL.2017.2754324.

[86] Y. Wang, H. Li, R. Liu, L. Yang, and X. Wang, "Modulated Model-Free Predictive Control With Minimum Switching Losses for PMSM Drive System," *IEEE Access*, vol. 8, pp. 20942–20953, 2020, doi: 10.1109/ACCESS.2020.2968379.

[87] O. Sandre-Hernandez, J. de J. Rangel-Magdaleno, and R. Morales-Caporal, "Modified model predictive torque control for a PMSM-drive with torque ripple minimisation," *IET Power Electronics*, vol. 12, no. 5, pp. 1033–1042, May 2019, doi: 10.1049/iet-pel.2018.5525.

[88] M. Xiao, T. Shi, X. Gu, and C. Xia, "Simplified predictive torque control for permanent magnet synchronous motor with discrete duty cycle control," *IET Electr Power Appl*, vol. 13, no. 3, pp. 294–301, Mar. 2019, doi: 10.1049/iet-epa.2018.5086.

[89] A. Dahlmann, V. Yaramasu, A. Dekka, and K. Yadlapati, "Modulated Model Predictive Control of a Two-Level Inverter with Even-Order Harmonic Elimination," in *2020 International Conference on Power Electronics & IoT Applications in Renewable Energy and its Control (PARC)*, IEEE, Feb. 2020, pp. 508–513. doi: 10.1109/PARC49193.2020.236665.

[90] Y. Xu, X. Ding, J. Wang, and C. Wang, "Robust three-vector-based low-complexity model predictive current control with supertwisting-algorithm-based second-order sliding-mode observer for permanent magnet synchronous motor," *IET Power Electronics*, vol. 12, no. 11, pp. 2895–2903, Sep. 2019, doi: 10.1049/iet-pel.2018.5750.

[91] Y. Xu, X. Ding, J. Wang, and Y. Li, "Three-vector-based low-complexity model predictive current control with reduced steady-state current error for permanent magnet synchronous motor," *IET Electr Power Appl*, vol. 14, no. 2, pp. 305–315, Feb. 2020, doi: 10.1049/iet-epa.2019.0108.

[92] Y. Xu, H. Li, J. Ren, and Y. Zhang, "Three-vector-based model predictive current control with disturbance feedforward compensation," *Journal of Power Electronics*, vol. 20, no. 3, pp. 687–697, May 2020, doi: 10.1007/s43236-020-00056-0.

[93] J. Eyre and J. Bier, "The evolution of DSP processors," *IEEE Signal Process Mag*, vol. 17, no. 2, pp. 43–51, Mar. 2000, doi: 10.1109/79.826411.

[94] W. Chen, X. Zhang, X. Gu, Y. Yan, and T. Shi, "Band-Based Multi-Step Predictive Torque Control Strategy for PMSM Drives," *IEEE Access*, vol. 7, pp. 171411–171422, 2019, doi: 10.1109/ACCESS.2019.2955956.

[95] K. M. R. Eswar, K. V. P. Kumar, and T. V. Kumar, "A Simplified Predictive

Torque Control Scheme for Open-End Winding Induction Motor Drive," *IEEE J Emerg Sel Top Power Electron*, vol. 7, no. 2, pp. 1162–1172, Jun. 2019, doi: 10.1109/JESTPE.2018.2832240.

[96] X. Yuan, C. Zhang, and S. Zhang, "Torque Ripple Suppression for Open-End Winding Permanent-Magnet Synchronous Machine Drives With Predictive Current Control," *IEEE Transactions on Industrial Electronics*, vol. 67, no. 3, pp. 1771–1781, Mar. 2020, doi: 10.1109/TIE.2019.2907506.

[97] T. Geyer, "Computationally Efficient Model Predictive Direct Torque Control," *IEEE Trans Power Electron*, vol. 26, no. 10, pp. 2804–2816, Oct. 2011, doi: 10.1109/TPEL.2011.2121921.

[98] M. Mamdouh and M. A. Abido, "Efficient Predictive Torque Control for Induction Motor Drive," *IEEE Transactions on Industrial Electronics*, vol. 66, no. 9, pp. 6757–6767, Sep. 2019, doi: 10.1109/TIE.2018.2879283.

[99] X. Li, Z. Xue, X. Yan, L. Zhang, W. Ma, and W. Hua, "Low-Complexity Multivector-Based Model Predictive Torque Control for PMSM With Voltage Preselection," *IEEE Trans Power Electron*, vol. 36, no. 10, pp. 11726–11738, Oct. 2021, doi: 10.1109/TPEL.2021.3073137.

[100] J. Chen, Y. Qin, A. M. Bozorgi, and M. Farasat, "Low Complexity Dual-Vector Model Predictive Current Control for Surface-Mounted Permanent Magnet Synchronous Motor Drives," *IEEE J Emerg Sel Top Power Electron*, vol. 8, no. 3, pp. 2655–2663, Sep. 2020, doi: 10.1109/JESTPE.2019.2917865.

[101] X. Zhang and B. Hou, "Double Vectors Model Predictive Torque Control Without Weighting Factor Based on Voltage Tracking Error," *IEEE Trans Power Electron*, vol. 33, no. 3, pp. 2368–2380, Mar. 2018, doi: 10.1109/TPEL.2017.2691776.

[102] Y. Zhang and H. Yang, "Two-Vector-Based Model Predictive Torque Control Without Weighting Factors for Induction Motor Drives," *IEEE Trans Power Electron*, vol. 31, no. 2, pp. 1381–1390, Feb. 2016, doi: 10.1109/TPEL.2015.2416207.

[103] Z. Zhang, H. Fang, F. Gao, J. Rodriguez, and R. Kennel, "Multiple-Vector Model Predictive Power Control for Grid-Tied Wind Turbine System With Enhanced Steady-State Control Performance," *IEEE Transactions on Industrial Electronics*, vol. 64, no. 8, pp. 6287–6298, Aug. 2017, doi: 10.1109/TIE.2017.2682000.

[104] M. Xiao, T. Shi, Y. Yan, W. Xu, and C. Xia, "Predictive Torque Control of Permanent Magnet Synchronous Motors Using Flux Vector," *IEEE Trans Ind Appl*, vol. 54, no. 5, pp. 4437–4446, Sep. 2018, doi: 10.1109/TIA.2018.2833817.

[105] Z. Chen and J. Qiu, "Adjacent-Vector-Based Model Predictive Control for Permanent Magnet Synchronous Motors with Full Model Estimation," *IEEE J*

Emerg Sel Top Power Electron, pp. 1–1, 2022, doi: 10.1109/JESTPE.2022.3172714.

[106] H. Yang, Y. Zhang, and M. Li, "Duty-Cycle Correction-based Model Predictive Current Control for PMSM Drives Fed by a Three-level Inverter with Low Switching Frequency," *IEEE Trans Power Electron*, pp. 1–10, 2023, doi: 10.1109/TPEL.2023.3250480.

[107] C. Xia, S. Wang, Z. Wang, and T. Shi, "Direct Torque Control for VSI–PMSMs Using Four-Dimensional Switching-Table," *IEEE Trans Power Electron*, vol. 31, no. 8, pp. 5774–5785, Aug. 2016, doi: 10.1109/TPEL.2015.2498207.

[108] C. Xia, Z. Zhou, Z. Wang, Y. Yan, and T. Shi, "Computationally efficient multi-step direct predictive torque control for surface-mounted permanent magnet synchronous motor," *IET Electr Power Appl*, vol. 11, no. 5, pp. 805–814, May 2017, doi: 10.1049/iet-epa.2016.0221.

Publications

1. **Parvathy M.L.**, Kusuma Eshwar and T. Vinay Kumar, “A Modified Duty-Modulated Predictive Current Control for Permanent Magnet Synchronous Motor drive,” ***IET Electric Power Applications***, vol.15, pp. 25-38, 2021.

2. **Parvathy M.L.** and T. Vinay Kumar, “An Effective Modulated Predictive Current Control of PMSM drive with Low Complexity,”, ***IEEE Journal of Emerging and Selected Topics in Power Electronics***, vol. 10, no. 4, pp. 4565-4575, Aug. 2022.

3. **Parvathy M.L.** and T. Vinay Kumar, “A Multivector-based Model Predictive Current Control of PMSM Drive with Enhanced Torque and Flux Response”, ***IEEE Journal of Emerging and Selected Topics in Power Electronics***, vol. 10, no. 6, pp. 7527-7538, Dec. 2022.

4. **Parvathy M.L.** and T. Vinay Kumar, “An Enhanced Predictive Current Control Scheme for Common Mode Voltage Alleviation and Improvement of Torque Response of PMSM Drive”, ***IEEE Journal of Emerging and Selected Topics in Power Electronics***, vol. 11, no.2, pp. 2139-2150, April 2023.

5. **Parvathy M.L.** and T. Vinay Kumar, “A Simplified Voltage Vector Preselection based Multivector Predictive Current Control for Improved Torque Performance of PMSM Drive,” ***IEEE Transactions on Power Electronics***, vol. 38, no. 7, pp. 8775-8785, July 2023, doi: 10.1109/TPEL.2023.3267107.

Curriculum-Vitae

Name	:	Parvathy
M.L. Date of Birth	:	25th May,1992
Gender	:	Female
Contact Number	:	+91-8848964827
Email Id	:	parvathy4218@gmail.com

Academic Qualifications

Program	University	%/CGPA	Year of completion
M. Tech. (Electrical Machines)	APJ Abdul Kalam Kerala Technological University	9.28	2017
B. Tech. (Electrical and Electronics Engineering)	University of Kerala	8.76	2014